

Alma Mater Studiorum Università di Bologna  
Archivio istituzionale della ricerca

A review of cretaceous smooth-slopes extensional basins along the Iberia-Eurasia plate boundary: How pre-rift salt controls the modes of continental rifting and mantle exhumation

This is the final peer-reviewed author's accepted manuscript (postprint) of the following publication:

*Published Version:*

A review of cretaceous smooth-slopes extensional basins along the Iberia-Eurasia plate boundary: How pre-rift salt controls the modes of continental rifting and mantle exhumation / Yves Lagabriele; Riccardo Asti; Thibault Duretz; Camille Clerc; Serge Fourcade; Antonio Teixell; Pierre Labaume; Benjamin Corre; Nicolas Saspiturry. - In: EARTH-SCIENCE REVIEWS. - ISSN 0012-8252. - ELETTRONICO. - 201:103071(2020), pp. 1-24. [10.1016/j.earscirev.2019.103071]

*Availability:*

This version is available at: <https://hdl.handle.net/11585/943166> since: 2023-09-27

*Published:*

DOI: <http://doi.org/10.1016/j.earscirev.2019.103071>

*Terms of use:*

Some rights reserved. The terms and conditions for the reuse of this version of the manuscript are specified in the publishing policy. For all terms of use and more information see the publisher's website.

This item was downloaded from IRIS Università di Bologna (<https://cris.unibo.it/>).  
When citing, please refer to the published version.

(Article begins on next page)

This is the final peer-reviewed accepted manuscript of:

Yves Lagabrielle; Riccardo Asti; Thibault Duretz; Camille Clerc; Serge Fourcade; Antonio Teixell; Pierre Labaume; Benjamin Corre; Nicolas Saspiturry: *A review of cretaceous smooth-slopes extensional basins along the Iberia-Eurasia plate boundary: How pre-rift salt controls the modes of continental rifting and mantle exhumation*

EARTH-SCIENCE REVIEWS VOL. 201 ISSN 0012-8252

DOI: 10.1016/j.earscirev.2019.103071

The final published version is available online at:

<https://dx.doi.org/10.1016/j.earscirev.2019.103071>

Terms of use:

Some rights reserved. The terms and conditions for the reuse of this version of the manuscript are specified in the publishing policy. For all terms of use and more information see the publisher's website.

This item was downloaded from IRIS Università di Bologna (<https://cris.unibo.it/>)

**When citing, please refer to the published version.**

7  
8 **A review of Cretaceous smooth-slopes extensional basins along the Iberia-**  
9 **Eurasia plate boundary: how pre-rift salt controls the modes of continental**  
10 **rifting and mantle exhumation**  
11  
12

13  
14  
15 by :

16  
17  
18 9 Yves Lagabriele<sup>1</sup>, Riccardo Asti<sup>1</sup>, Thibault Duretz<sup>1</sup>, Camille Clerc<sup>2</sup>, Serge Fourcade<sup>1</sup>, Antonio  
19  
20 Teixell<sup>4</sup>, Pierre Labaume<sup>3</sup>, Benjamin Corre<sup>1</sup>, Nicolas Saspiturry<sup>5</sup>  
21

22  
23  
24  
25 13 Addresses

26 14 1. Université de Rennes, CNRS, UMR 6118 Géosciences Rennes, Campus de Beaulieu, 35000 Rennes, France  
27

28  
29 16 2. ISEA, Université de la Nouvelle Calédonie, 98800 Nouméa, Nouvelle Calédonie  
30

31  
32 18 3. Géosciences Montpellier, CNRS-Université de Montpellier-Université des Antilles, 34095 Montpellier, France  
33

34  
35 20 4. Dept. de Geologia, Universitat Autònoma de Barcelona, 08193 Bellaterra, Spain  
36

37  
38 22 5. EA4592 Géoressources & Environnement, Bordeaux INP, Université Bordeaux Montaigne, 1 Allée Daguin,  
39 33607 Pessac, France  
40

41  
42 25 Riccardo Asti [riccardo.asti@univ-rennes1.fr](mailto:riccardo.asti@univ-rennes1.fr), Duretz Thibault [thibault.duretz@univ-rennes1.fr](mailto:thibault.duretz@univ-rennes1.fr), Camille Clerc  
43 [camille.clerc@univ-nc.nc](mailto:camille.clerc@univ-nc.nc), "Serge Fourcade; [sg.fourcade@orange.fr](mailto:sg.fourcade@orange.fr)" [sg.fourcade@orange.fr](mailto:sg.fourcade@orange.fr), Antonio Teixell  
44 [antonio.teixell@uab.cat](mailto:antonio.teixell@uab.cat), "Pierre Labaume" [labauame@gm.univ-montp2.fr](mailto:labauame@gm.univ-montp2.fr), "Benjamin Corre"  
45 [benjcorre@hotmail.fr](mailto:benjcorre@hotmail.fr), Saspiturry Nicolas [saspiturry.nicolas@gmail.com](mailto:saspiturry.nicolas@gmail.com),  
46  
47  
48  
49  
50

51 31 *Corresponding author: Yves Lagabriele. [yves.lagabriele@univ-rennes1.fr](mailto:yves.lagabriele@univ-rennes1.fr)*  
52  
53  
54  
55  
56  
57  
58  
59  
60

61  
62  
63 **34 Key words** : Smooth-slopes basins; symmetrical profile; Iberia; Eurasia; Triassic evaporites;  
64  
65 décollement layer; thermal anomaly; sedimentary burial; dominating-ductile tectonic  
66  
67 regime.

68 **37 Short abstract (for submission)**

69 We enhance a striking correlation between the paleogeography of Upper Triassic deposits  
70 and the mode of crustal stretching of the north Iberia plate during the Cretaceous  
71 transtensional event. The basins which opened during the mid-Cretaceous times along the  
72 Iberia-Eurasia plate boundary (like the emblematic Parentis basin) exhibit a peculiar  
73 synclinal-shaped profile and are devoid of prominent block faulting. The top of the basement  
74 is characterized by gentle slopes dipping symmetrically towards the basin center. Based on a  
75 comparison with rifting models established from the North Pyrenean Zone, this architecture  
76 appear to result from the thinning of the central basin continental crust under dominating-  
77 ductile deformation in greenschist facies conditions. The common character shared by all  
78 the pre-rift sequences of the studied basins is the presence of a thick low-strength Upper  
79 Triassic evaporites and clays layer belonging to the Keuper group and forming a thick pre-rift  
80 low-strength unit. Efficient décollement along this layer triggers mechanical decoupling and  
81 gliding of the pre-rift cover remaining in the basin center as the continental crust is laterally  
82 extracted. Using recent paleogeographic reconstructions, we show that the distribution of  
83 the Keuper sediments remarkably matches the distribution of the Pyrenean and peri-  
84 Pyrenean, Parentis-type basins. This allows for the first time to propose a genetic link  
85 between the distribution of evaporite-bearing pre-rift sedimentary formations and the  
86 development of smooth-slopes rift basins.  
87  
88  
89

90  
91 56

92 57

93 **58 Abstract**

94 59

95 This article enhances for the first time a striking correlation between the paleogeography of  
96  
97 Upper Triassic deposits and the mode of crustal stretching around and inside the Iberia plate  
98 during the Cretaceous transtensional event. In a first step, we propose a review of the  
99 architecture of the basins which opened during the mid-Cretaceous times along the Iberia-  
100 Eurasia plate boundary. Like the emblematic Parentis basin, all these basins exhibit a  
101 peculiar synclinal-shaped profile and are devoid of prominent block faulting. The top of the  
102 basement is characterized by gentle slopes, which dip symmetrically towards the center of  
103 the basins. Based on a comparison with recent geologically-based rifting models established  
104 from the North Pyrenean Zone, we propose that this architecture results from the thinning  
105 of the central basin continental crust under dominating-ductile deformation in greenschist  
106 facies conditions. The common character shared by all the pre-rift sequences of the studied  
107 basins is the presence of a thick low-strength Upper Triassic evaporites and clays layer  
108 belonging to the Keuper group and forming a specific pre-rift salt unit. In the studied basins,  
109  
110  
111  
112  
113  
114  
115  
116  
117  
118  
119  
120

121  
122  
123 73 efficient décollement along the Keuper evaporites and clays triggers mechanical decoupling  
124  
125 74 and gliding of the pre-rift cover that remains in the center of the basin as the continental  
126  
127 75 crust is laterally extracted. Thus, during the early rifting phase, the basement undergoes  
128  
129 76 thinning while the pre-rift cover remains preserved in the basin center. In response to hyper-  
130  
131 77 thinning and horizontal extraction of the continental crust, hot mantle material approaches  
132  
133 78 the detached pre-rift cover. The major consequences of this central basin thermal anomaly  
134  
135 79 are twofolds: (i) the ductile deformation of the thinned continental crust beneath the  
136  
137 80 detached pre-rift units, and (ii) the development of HT-LP metamorphic conditions in the  
138  
139 81 pre-rift sediments and at the base of the syn-rift flysch levels. This thermal event is well  
140  
141 82 recorded in the axial portion of the Pyrenean realm (future North Pyrenean Zone) as well as  
142  
143 83 in the pre-rift sediments of the Cameros basin (northern Spain). Continental stretching is  
144  
145 84 accommodated by shearing in the bulk upper and middle crust leading to the formation of  
146  
147 85 thin tectonic lenses of mylonitic crustal material remaining welded on the exhuming mantle.  
148  
149 86 The architecture of the smooth-slopes, Parentis-type basins studied in this article thus  
150  
151 87 contrasts with the structure of the Iberia-Newfoundland Atlantic margins which are  
152  
153 88 characterized by (i) top-basement detachment faults accommodating crustal extension  
154  
155 89 through rotation and translation of undeformed basement blocks, and (ii) by the  
156  
157 90 individualization of continental extensional allochthons lying tectonically over exhumed  
158  
159 91 lower crust or mantle rocks. Finally, using recent paleogeographic reconstructions, we show  
160  
161 92 that the distribution of the Keuper evaporites and clays remarkably matches the distribution  
162  
163 93 of the Pyrenean and peri-Pyrenean, Parentis-type basins. This allows for the first time to  
164  
165 94 propose a genetic link between the distribution of evaporite-bearing pre-rift sedimentary  
166  
167 95 formations and the development of smooth-slopes rift basins.  
168  
169  
170  
171  
172  
173  
174  
175  
176  
177  
178  
179  
180

181  
182  
183 **97 Introduction**

184 98

185 99 More than 30 years ago, important steps in our understanding of the mechanisms of  
186  
187 100 continental rifting were achieved through the acquisition and interpretation of ECORS  
188  
189 101 seismic reflection profiles (1983-1994) (Damotte et al., 1998). New images of crustal and  
190  
191 102 Moho geometries beneath stretched continental crusts were obtained, shading light on  
192  
193 103 important discrepancies between structural patterns at the base of rift systems. In  
194  
195 104 particular, ECORS profiles from the Rhine graben and the Parentis basin displayed  
196  
197 105 contrasting images of the thinned upper lithosphere. In the first case, the upper crust  
198  
199 106 appears clearly rifted and offset by stepping normal faults (Brun et al., 1991) whilst, despite  
200  
201 107 slight tectonic inversion, the second case exhibits a smooth basement top, with gentle  
202  
203 108 slopes dipping symmetrically towards the basin center (Bois et al., 1997). Because only few  
204  
205 109 cases of Parentis-type architecture were observed worldwide, little attention has been paid  
206  
207 110 to this symmetrical, smooth-slopes type of continental rift, which apparently lacks major  
208  
209 111 upper crustal faulting and block tilting. Rather, most of the current models of rift-related  
210  
211 112 crustal thinning generally point to the individualization of a series of tilted continental blocks  
212  
213 113 indicating that the upper crustal levels behave in a dominant brittle mode in the proximal (or  
214  
215 114 continentward) as well as in the distal (or oceanward) margin domains. In such models,  
216  
217 115 shallow detachment faults accommodate the upper crustal extension through the rotation  
218  
219 116 and the translation of undeformed basement blocks. In the distal margin, these blocks,  
220  
221 117 referred to as extensional allochthons, are covered by syn-rift and post-rift sediments and  
222  
223 118 may lie tectonically over exhumed lower levels, including subcontinental mantle (Reston et  
224  
225 119 al., 1995; Manatschal et al., 2001; Jammes et al., 2010c; Osmundsen and Peron-Pinvidic,  
226  
227 120 2018, and references therein).

228  
229 121 Recent geological investigations in the northern units of the Pyrenean belt forming the  
230  
231 122 North Pyrenean Zone (NPZ) as well as in the Basque-Cantabrian basin (fig. 1) show that  
232  
233 123 Parentis-type basins of mid-Cretaceous age were distributed all along the boundary between  
234  
235 124 the northern Iberia and southern Eurasia plates, thus introducing doubts regarding the  
236  
237 125 ubiquitous character of Iberia-Newfoundland-type margins (Lagabrielle et al., 2010 ; Clerc  
238  
239 126 and Lagabrielle, 2014; Teixell et al., 2016; 2018; Asti et al., 2019). In this article, we first list  
240  
127 the main characteristics of these Parentis-type basins, based on the analysis of detailed  
128 geological reconstructions from areas exposed all along the northern flank of the Pyrenean

241  
242  
243 129 belt. Then we review the distribution of such basins at the scale of the Iberia and Eurasia  
244  
245 130 plates. We finally discuss some of the key-factors controlling the evolution of smooth-slopes  
246  
247 131 basins and we evaluate how such information increases our understanding of the  
248  
249 132 mechanisms of continental rifting and passive margin formation.

250 133

252 134 **I. Symmetrical, smooth-slopes basins of the north Iberia margin: insights from the North**  
253 135 **Pyrenean Zone (NPZ) and the Basque-Cantabrian range**

254  
255 136

256  
257 137 The Pyrenees and the Cantabrian mountain (fig. 1) form a narrow, N110 trending fold-and-  
258  
259 138 thrust belt resulting from the collision of the northern edge of the Iberia plate (north Iberia  
260  
261 139 margin) with the southern edge of the Eurasia plate during the Late Cretaceous-Tertiary  
262  
263 140 (Choukroune and ECORS team, 1989; Muñoz, 1992; Deramond et al., 1993; Roure and  
264  
265 141 Choukroune, 1998; Teixell, 1998; Vergés and Garcia-Senz, 2001; Pedrera et al., 2017; Teixell  
266  
267 142 et al., 2018). Convergence initiated ca. 83 Ma, following an almost 40 Ma long period of  
268  
269 143 transtensional motion in relation with the counterclockwise rotation of Iberia relative to  
270  
271 144 Eurasia, also leading to oceanic spreading in the Bay of Biscaye between Chron M0 and A33o  
272  
273 145 (ca. 125-83 Ma) (Le Pichon et al., 1971; Choukroune and Mattauer, 1978; Olivet, 1996;  
274  
275 146 Sibuet et al., 2004). Convergence led to the partial or complete tectonic inversion of  
276  
277 147 discontinuous Cretaceous rift basins opened along the Iberia-Eurasia plate boundary during  
278  
279 148 the transtensional episode (Puigdefàbregas and Souquet, 1986; Debroas, 1990). Rotation  
280  
281 149 was achieved just before the Albian according to paleomagnetic data collected onland (Gong  
282  
283 150 et al., 2008). Earlier Triassic and Jurassic rifting events preceded the development of the  
284  
285 151 Cretaceous rifts (Canérot, 2017, and references therein).

286  
287 152 Along the northern flank of the Pyrenees, more than forty, up to km-sized exposures of  
288  
289 153 subcontinental lherzolites are widespread within the Mesozoic pre-rift and syn-rift  
290  
291 154 sediments forming the NPZ (Monchoux, 1970; Vielzeuf and Kornprobst, 1984; Fabriès *et al.*,  
292  
293 155 1991, 1998). The NPZ is bounded by two major post-metamorphic thrusts, the North  
294  
295 156 Pyrenean Fault (NPF) to the South and the North Pyrenean Frontal Thrust (NPFT) to the  
296  
297 157 North. The NPF represents the tectonic boundary between the NPZ and the prominent axial  
298  
299 158 zone of the belt (AZ) constituted of a stack of Paleozoic basement units (Choukroune, 1976a;  
300 159 1976b; 1978b).

300 160 Based on field and geophysical evidence from the central and western NPZ, exhumation of

301  
302  
303 161 sub-continental mantle is shown to have occurred coevally with extreme thinning of the  
304 162 continental crust in the Pyrenean realm during the mid-Cretaceous (Lagabrielle and  
305 163 Bodinier, 2008; Jammes et al., 2009; Masini et al., 2014). Therefore, mantle exhumation  
306 164 (locally followed by peridotite exposure up to the floor of the Pyrenean basins) is now  
307 165 considered as a general mechanism accounting for the presence of ultramafic material  
308 166 within the NPZ. It is established that the well-known regional high temperature and low  
309 167 pressure (HT-LP) Pyrenean metamorphism (Ravier, 1957; Azambre & Rossy, 1976; Bernus-  
310 168 Maury, 1984) developed along the southern NPZ in relation with continental thinning during  
311 169 the major Cretaceous extensional event (Vielzeuf and Kornprobst, 1984; Dauteuil and Ricou,  
312 170 1989; Golberg & Leyreloup 1990; Clerc et al., 2015b; 2016). Following the early ECORS  
313 171 profiles (Choukroune and ECORS team, 1989), additional information on the architecture of  
314 172 the paleo-margin of Northern Iberia in the Pyrenees is provided by recent interpretation of  
315 173 tomographic data acquired during the temporary PYROPE and IBERARRAY experiments  
316 174 across the Pyrenees (Chevrot et al., 2015; 2018; fig. 1). Based on such data set, Wang et al.  
317 175 (2016) suggest the inversion of a northern Iberia margin characterized by a short necking  
318 176 domain and a large distal domain made of strongly attenuated crust (less than 10 km thick)  
319 177 overlying a large volume of subcontinental mantle. As discussed further in this article, this  
320 178 domain can be compared to large sheets of hyper-extended continental crust found in the  
321 179 distal portions of present-day passive continental margins (see section III C)

322  
323  
324  
325  
326  
327  
328  
329  
330  
331  
332  
333  
334  
335  
336 180

337 181 Various models of continental crust thinning and associated mantle exhumation have been  
338 182 proposed recently to account for geological constraints collected inside the metamorphic  
339 183 NPZ. In figure 2 (profiles a to e), we present a selection of reconstructions extracted from  
340 184 recent literature, which highlights numerous similarities between recently published models  
341 185 of Cretaceous NPZ basins structure (Lagabrielle et al., 2010; Clerc and Lagabrielle, 2014;  
342 186 Masini et al., 2014; Tugend et al., 2014; 2015; Clerc et al., 2016; Teixell et al., 2016, 2018;  
343 187 Corre et al., 2016; Lagabrielle et al., 2016; DeFelipe et al., 2017; Pedrera et al., 2017; Espurt  
344 188 et al., 2019; Saspiturry et al., 2019; Asti et al., 2019; Ducoux et al., in review). Most of these  
345 189 architecture models stress the role played by a major cover décollement layer during the  
346 190 Cretaceous crustal thinning. This weak layer corresponds to the Upper Triassic Keuper  
347 191 evaporites which contain clays and sands as well as minor carbonates and doleritic MORB  
348 192 basalts (ophites). Its maximum thickness in the Pyrenean realm reached 2.7 km, as deduced



361  
362  
363 193 from field data in the southern Pyrenees coupled to well data in the Mauléon and Aquitaine  
364  
365 194 basins and the Bay of Biscay region (James & Canérot, 1988; McClay et al., 2004; Biteau et  
366  
367 195 al., 2006; Jammes et al., 2010a; 2010b; 2010c; Roca et al., 2011; Saura et al., 2016; Orti et  
368  
369 196 al., 2017; Saspiturry et al., 2019). In the décollement layer now exposed in the metamorphic  
370  
371 197 NPZ, the Triassic clays were transformed into talc and chlorite, and the carbonates most  
372  
373 198 often suffered intense tectonic brecciation with talc, tremolite and dolomite  
374  
375 199 recrystallizations (Thiébaud et al., 1992; Lagabrielle et al., 2019a, 2019b). Pre-rift to syn-rift  
376  
377 200 salt diapirism was also frequently observed in the non-metamorphic NPZ and in the  
378  
379 201 Southern Pyrenees (e.g. Canérot, 1988; 1989; Lenoble and Canérot, 1992; Canérot and  
380  
381 202 Lenoble, 1989; 1993; James and Canérot, 1999; Canérot et al., 2005; Jammes et al., 2009;  
382  
383 203 Jammes et al., 2010a; 2010b; Roca et al., 2011; Saura et al., 2016; Teixell et al., 2016).

384  
385  
386  
387  
388  
389  
390  
391  
392  
393  
394  
395  
396  
397  
398  
399  
400  
401  
402  
403  
404  
405  
406  
407  
408  
409  
410  
411  
412  
413  
414  
415  
416  
417  
418  
419  
420

204  
205 As early stated by Clerc and Lagabrielle, (2014), the main consequence of the presence of  
206 the low-strength Keuper layer along the north Iberia margin is that during the Cretaceous  
207 rifting, the pre-rift Mesozoic cover was efficiently decoupled from the Paleozoic basement  
208 along the evaporites and thus remained on top of the stretched continental lithosphere in  
209 the center of the basin. It must be noted that in the external parts of the Pyrenean rift, the  
210 borders of the subsiding Cretaceous flysch basins remain at low temperature and display  
211 classical faulted and tilted blocks (e.g. half-grabens of Quillan basin, Camarade basin,  
212 Gensac-Bonrepos basin, western border of the Mauléon basin, edges of the Gran Rieu high  
213 and Lacq basin) (Debroas, 1978; 1990; Biteau et al., 2006; Lagabrielle et al., 2010; Masini et  
214 al., 2014; Grool et al., 2018; Espurt et al., 2019).

215

216 The Cinco Villas Paleozoic massif and the Le Danois Bank (fig. 1) respectively form the  
217 eastern and western boundary of the Basque-Cantabrian basin which develops to the west  
218 of the NPZ towards the northern Iberia Peninsula. It is filled by an up to 12.5 km thick  
219 succession of Upper Jurassic-Cretaceous sediments with interlayered Aptian to Santonian  
220 basic volcanic rocks (Azambre and Rossy, 1976; Rat et al., 1983; Rat, 1988; Castañares et al.,  
221 2001; García-Mondéjar et al., 1996; 2004; Floquet, 2004) (fig. 2f-h). This basin was floored by  
222 an extremely thinned lithosphere in its central parts (Biscay Synclinorium and Nappes des  
223 Marbres) and was also affected by a Late Cretaceous thermal metamorphism (Golberg and  
224 Leyreloup, 1990; Cuevas and Tubía, 1999; Pedrera et al., 2017). A peridotite outcrop close to

421  
422  
423 225 the Leiza fault shows that crustal thinning led to the exhumation of the upper mantle close  
424 226 to the floor of the basin (Mendia and Gil-Ibarguchi, 1991; deFelipe et al., 2017). The basin  
425 227 architecture deduced from field investigations in the eastern part of the Basque-Cantabrian  
426 228 basin (the “Nappe des Marbres” area) includes smooth-slopes margins with normal faults  
427 229 and tilted blocks restricted to the external domains (deFelipe et al., 2017; Pedrera et al.,  
430 230 2017; Ducoux et al., in review). These reconstructed geometries bear affinities with basin  
431 231 architectures deduced from geological observations in the NPZ (fig. 2f-h). Indeed, such  
432 232 architecture and the overall evolution deduced for this rift system implicate gliding of the pre-  
433 233 rift sequence over its basement during crustal extension with ductile crustal thinning in its  
434 234 central part in a way similar to models deduced from NPZ studies (e.g. Clerc and Lagabrielle,  
435 235 2014; Corre et al., 2016; Teixell et al., 2016). The Leiza detachment system of deFelipe et al.  
436 236 (2017) (fig. 2g) corresponds to the basal décollement allowing pre-rift sequence allochthony.  
437 237 The presence of a high-density mantle body beneath the Basque-Cantabrian basin has been  
438 238 established on the basis of lithospheric-scale gravity inversion (Pedrera et al., 2017). The  
439 239 association of this exhumed mantle body with rift and post-rift structural geometries  
440 240 suggests the activation of a major south-dipping ramp-flat-ramp extensional detachment  
441 241 between Valanginian and early Cenomanian times with horizontal extension of ~48 km.  
442 242 Interpretation of geophysical data shows that low-strength Triassic Keuper evaporites and  
443 243 mudstones above the basement favor the decoupling of the cover with formation of  
444 244 minibasins, expulsion rollovers, and diapirs (Pedrera et al., 2017).

445  
446  
447  
448  
449  
450  
451  
452  
453  
454  
455  
456  
457 245

458  
459 246 Finally, the presence of a thick pre-rift salt layer underlying the Mesozoic carbonates  
460 247 appears as an ubiquitous parameter to take into account when reconstructing the evolution  
461 248 of the Cantabrian-Pyrenean range. Recent models of rift development at the northern Iberia  
462 249 margin show that Triassic lithology controls the three intrinsic characteristics of the  
463 250 Pyrenean rifting which can be summarized as follows:

- 464  
465  
466  
467 251 i. Tectonic juxtaposition of exhumed peridotites and pre-rift sediments. This occurs  
468 252 when the lateral extraction of the thinned continental crust is completed. In  
469 253 response to plate separation, the stretched crust is removed horizontally from the  
470 254 center of the rift and decoupling of the pre-rift cover from its basement occurs along  
471 255 the Keuper décollement. As a consequence a tectonic contact is established between  
472 256 the decoupled pre-rift sediments and the uplifted sub-continental mantle rocks

481  
482  
483  
484  
485  
486  
487  
488  
489  
490  
491  
492  
493  
494  
495  
496  
497  
498  
499  
500  
501  
502  
503  
504  
505  
506  
507  
508  
509  
510  
511  
512  
513  
514  
515  
516  
517  
518  
519  
520  
521  
522  
523  
524  
525  
526  
527  
528  
529  
530  
531  
532  
533  
534  
535  
536  
537  
538  
539  
540

257 (Clerc and Lagabrielle, 2014) (fig. 2e). In some locations, due to subsequent complete  
258 removal of the pre-rift cover, mantle rocks may be in turn exposed to the seafloor as  
259 observed around the Lherz, Urdach and Bestiac Iherzolite bodies (Lagabrielle et al.  
260 2010; 2016; de Saint Blanquat et al., 2016).

261 ii. Crustal stretching under dominantly-ductile conditions. The geometry of the thinned  
262 crustal units in the distal domain of the rift margins does not correspond to a  
263 succession of triangular-shaped isolated undeformed blocks (extensional  
264 allochthons) as described along the Iberia-Newfoundland conjugate margins and  
265 along the reconstructed alpine paleomargins (Manatschal, 2001; Manatschal et al.,  
266 2001; 2006; Peron-Pinvidic and Manatschal, 2009; Mohn et al., 2010; 2012; 2015)  
267 (fig. 3). By contrast, it appears as an assemblage of very thin lenses of ductilely  
268 deformed pre-Mesozoic material, originating mainly from the middle crust,  
269 separated by anastomosing shear zones that developed in greenschist facies  
270 conditions at low pressure (e.g. Corre et al., 2016; Teixell et al., 2016; Asti et al.,  
271 2019; Espurt et al., 2019) (fig. 2b-d). This important feature occurs because stretching  
272 develops under the allochthonous pre-rift cover that maintains moderate  
273 temperature in the upper and middle crust. Microscopic study of crustal material  
274 welded on the Urdach Iherzolites demonstrates that the middle crust was extracted  
275 laterally from the rift axis and deformed ductilely at temperatures between 450°C  
276 and 350°C (Asti et al., 2019). Large strains in the greenschist facies are testified by  
277 strongly elongate quartz ribbons in ortho- and para-derived mylonites with bulging  
278 recrystallization and brittle fracturing of feldspar in cataclastic flows (fig. 4a-b).

279 iii. Dominantly ductile deformation of the pre-rift and syn-rift sediments under HT-LP  
280 conditions. All along the rifting phase, the decoupled pre-rift cover remains in the  
281 center of the rift where the rift-related rise of the isotherms is more pronounced and  
282 where it is progressively buried under thick flysch sequence deposits. Sedimentary  
283 burial first preserves heat acquired during early rifting stages and second trigger  
284 temperature increase in the pre-rift cover. As a result, the detached pre-rift cover  
285 locally undergoes drastic syn-metamorphic ductile thinning and boudinage during  
286 continental breakup (fig. 5a-d). Such peculiar mechanical behaviour is outlined in all  
287 published rifting models (i.e. base of Nappe des Marbres basins, Leiza detachment  
288 system, base of Mauléon and Chaînons Béarnais basin infills, base of Baronnies and

541  
542  
543  
544  
545  
546  
547  
548  
549  
550  
551  
552  
553  
554  
555  
556  
557  
558  
559  
560  
561  
562  
563  
564  
565  
566  
567  
568  
569  
570  
571  
572  
573  
574  
575  
576  
577  
578  
579  
580  
581  
582  
583  
584  
585  
586  
587  
588  
589  
590  
591  
592  
593  
594  
595  
596  
597  
598  
599  
600

289 Boucheville basins infill, fig. 2). Progressive rifting triggers the upward propagation of  
290 the brittle-ductile transition which may reach syn-rift sediments deposited at the  
291 early stage of the basin opening (Clerc et al., 2016). Brittle deformation dominated by  
292 cataclastic brecciation follows ductile shearing and flattening in sedimentary units  
293 accompanying final exposure of mantle rocks to the seafloor, as proposed from  
294 studies in the Lherz area (Lagabrielle et al., 2016). The ductile-brittle transition is  
295 frequently observed at the mesoscopic and microscopic scale with sets of normal  
296 faults offsetting the extensional HT foliation (fig. 5e-f, 5h). Finally, at the scale of the  
297 entire rift, extensional deformation in the lower margin is accompanied by tectonic  
298 denudation of the cover in the upper margin (Lagabrielle et al., 2010; Teixell et al.,  
299 2016, 2018).

300

301 To sum up, figure 6 presents the intrinsic characteristics of the Pyrenean rifting listed  
302 above, compiled along an idealized column of the NPZ lithologies with photographs  
303 illustrating the most emblematic deformed levels exposed along the NPZ.

304

## 305 **II. A review of smooth-slopes basins around the Pyrenees and Cantabrian ranges**

306

307 Seismic images of oceanic margins and intracontinental rifts in the close surroundings of the  
308 Pyrenees and Cantabrian ranges bear crucial information on the mode of crustal thinning  
309 along the northern Iberia margin and adjacent areas during the Cretaceous.

310

311 (1) Parentis basin (fig. 1 and 7a). First interpretations of the Parentis ECORS profile point to a  
312 symmetrical, syncline-shaped basin, with only few normal faults in the stretched crust, even  
313 in the proximal domain (Pinet et al., 1987; Bois et al., 1997). Beneath the Parentis basin fill,  
314 the crust is less than 10 km thick and decreases westward from 7 km (along the ECORS Bay  
315 of Biscay profile, fig. 1), to 6–5 km (along the MARCONI 3 profile, fig. 1) (Tomassino and  
316 Marillier, 1997; Gallart et al., 2004; Ruiz, 2007). More recently, Jammes et al. (2010a),  
317 proposed that the southern Parentis basin represents a lower plate sag basin floored by a  
318 top-basement detachment system with an asymmetrical mode of opening. These authors  
319 emphasize the presence of a thick pre-rift salt layer in the area undergoing extreme crustal  
320 thinning, forcing sub- and suprasalt layers to deform differently. Whatever the processes of

601  
602  
603 321 crustal thinning are favoured, both older and recent models of Parentis basin evolution  
604  
605 322 highlight three major features: (1) the occurrence of symmetrical smooth-slopes gently  
606  
607 323 dipping basinward; (2) the presence of a crust which thins regularly towards basin axis,  
608  
609 324 without discrete steeply dipping faults, and (3) the presence of a thick pre-rift salt layer  
610  
611 325 allowing décollement of the pre-rift cover from its basement (Jammes et al., 2010b, 2010c).

612  
613 326 (2) South Bay of Biscay margin (fig. 1, fig. 7b-c). Both the northern and southern margins of  
614  
615 327 the Bay of Biscay have been explored seismically. North-south transects of the Armorican  
616  
617 328 margin (Norgasis profiles, fig. 1: Thinon et al., 2003; Tugend et al., 2014) reveal a short  
618  
619 329 necking domain that concentrates most of the crustal deformation. Crustal thickness  
620  
621 330 decreases from 35 km at the shelf break to less than 10 km at the foot of the slope. Steep  
622  
623 331 rise of mantle implies the disappearance of the lower crust beneath the slope. Based on  
624  
625 332 results of gravity inversion combined with seismic interpretations, Tugend et al. (2014) map  
626  
627 333 a continuous domain of exhumed mantle from the Armorican basin toward the  
628  
629 334 hyperthinned Parentis basin where minimum crustal thickness occurs (fig. 7a) (Pinet et al.,  
630  
631 335 1987, Bois et al., 1996, Jammes et al., 2010a). According to Roca et al. (2011), the Bay of  
632  
633 336 Biscay Abyssal Plain itself consists of a transitional zone formed by a thin (4–9 km) crust with  
634  
635 337 riders of Mesozoic pre-rift and syn-rift sediments and continental crustal rocks that are  
636  
637 338 extensionally detached over an exhumed sub-continental mantle with seismic velocities  
638  
639 339 comprised between 7.2 and 8 km/s. The distal domain of the Bay of Biscay Abyssal Plain  
640  
641 340 bounds to the north the North Iberian margin, an extended continental margin with  
642  
643 341 Cretaceous basins (e.g. the Asturian basin, up to 10 km thick, fig. 1) and basement highs as  
644  
645 342 the Le Danois Bank (Cadenas and Fernández Viejo, 2016; Teixell et al., 2018), where  
646  
647 343 granulites have been dredged (Capdevila et al., 1980; Fügenschuh et al., 2003) (fig. 1).

648  
649 344 (3) North-eastern Iberia intra-crustal basins (Iberian Chain and Valencia trough) (fig 1 and fig.  
650  
651 345 7b-d). Helpful additional information regarding the thinning modes of the northern Iberia  
652  
653 346 crust can be obtained from seismic images of the Los Cameros, Maestrat and Columbrets  
654  
655 347 basins now partly inverted in the Iberian Chain (fig. 1). These basins result from the  
656  
657 348 distributed extension of the northern Iberia plate synchronously with the opening of the Bay  
658  
659 349 of Biscay-Pyrenees in the mid-Cretaceous (Verges and Garcia-Senz, 2001; Mas et al., 2011).  
660  
661 350 They represent a well-developed Mesozoic rift having similarities with the North Atlantic  
662  
663 351 margins (Salas and Casas, 1993; Salas et al., 2001). In their internal parts, reconstructed

661  
662  
663 352 Iberian Chain basin geometries point to simple troughs exhibiting gentle slopes devoid of  
664  
665 353 marked fault stepping, suggesting the absence of tilted blocks and a smooth basement top  
666  
667 354 (e.g. Guimerà et al., 1995; Casas-Sainz and Gil-Imaz, 1998; Omodeo et al., 2014). The Moho  
668  
669 355 generally shows an arched outline with a regular shallowing toward the basin center where  
670  
671 356 the crust is reduced to some kilometers only. The Triassic evaporites play an important role  
672  
673 357 during the Albian rifting in the basins of northeast Iberia. This role was recently well  
674  
675 358 illustrated by interpretation of seismic reflection profiles in the Valencia trough (Etheve et  
676  
677 359 al., 2018) (fig. 7b). These profiles reveal the presence of a large Albian basin, the Columbrets  
678  
679 360 basin (fig. 1), filled with up to 10 km thick Mesozoic sediments over a highly extended  
680  
681 361 continental basement locally only 3.5 km thick. The pre-rift and syn-rift successions form a  
682  
683 362 large-scale synclinal with thinned borders, in relation with displacement along local  
684  
685 363 extensional detachments. Whole deformation results of interaction between the thick pre-  
686  
687 364 rift Triassic salt layer and dominantly ductile crustal thinning (Etheve et al. 2018) leading to  
688  
689 365 the development of an abnormally thin continental crust (Gallart et al., 1990; Dañobeitia et  
690  
691 366 al., 1992; Ayala et al., 2015). In the Cameros basin (fig. 7c-d), the pre-rift cover is decoupled  
692  
693 367 on Triassic evaporites and is smeared all over the stretched domain. No major offset of the  
694  
695 368 top basement is attested by the syn-rift record (Casas-Sainz and Gil-Imaz, 1998; Casas-Sainz  
696  
697 369 et al., 2000). A striking feature is that like in the NPZ, HT-LP metamorphism associated with  
698  
699 370 crustal thinning is reported in the Cameros basin fill (Guiraud and Séguret, 1985; Goldberg et  
700  
701 371 al., 1988; Rat et al., 2019).

### 702 **III. Discussion**

703

#### 704 **A. Smooth-slopes basins: symmetrical geometries versus asymmetrical tectonic regime**

705

706 376 A common characteristic of the smooth-slopes basins described in this review is the lack of  
707  
708 377 tilted crustal blocks and related stepping fault scarps in their central part, thus defining a  
709  
710 378 dominant symmetrical smooth-slopes profile of the basement top (figs. 2 and 7). Based on  
711  
712 379 field data from the NPZ, we have shown that stretching of the crustal basement occurs in a  
713  
714 380 dominant ductile mode under greenschist facies conditions, since the central part of the  
715  
716 381 basin remains overlain by a permanent cover of detached pre- and syn-rift sediments . An  
717  
718 382 important question is now to determine whether such symmetrical shapes result from  
719  
720

721  
722  
723 383 symmetrical or asymmetrical stretching processes.  
724

725 384

726  
727 385 The symmetry or asymmetry of the processes of lithosphere stretching and continental  
728  
729 386 breakup has been largely debated over the last 30 years (i.e. Buck et al., 1988; Allemand et  
730  
731 387 al., 1989; Buck, 1991; Brun, 1999, with references therein). More recently, the symmetrical  
732  
733 388 character of the final architecture of passive margins has been discussed by many authors  
734  
735 389 (i.e. Michon and Merle, 2003; Huisman and Beaumont, 2007; Reston et al., 1995; Sutra et  
736  
737 390 al., 2013; Brune et al., 2014). Apparent symmetry does not imply dominant pure shear  
738  
739 391 thinning mechanisms but may result from asymmetrical tectonic processes involving large-  
740  
741 392 scale discrete extensional shear zones (simple shear) as discussed by Nagel and Buck (2004)  
742  
743 393 (fig. 8a).

744 394

745  
746 395 It is well admitted that architecture of extended crustal systems depends on the geometrical  
747  
748 396 and temporal associations between simple shear and pure shear regimes. In the pure shear  
749  
750 397 model of McKenzie (1978), designed to explain the evolution of sedimentary basins, the  
751  
752 398 lithosphere is stretched uniformly resulting in a symmetrical basin with faulting in the brittle  
753  
754 399 crust. By contrast, the simple shear model (Wernicke, 1981, 1985) points to one or few  
755  
756 400 detachment faults that originate at low-angle with dips less than 30° and concentrate the  
757  
758 401 entire deformation, so that, apart from the fault zones, the lithosphere is not deformed. The  
759  
760 402 simple shear model has been complicated with the adjonction of sequential detachments  
761  
762 403 faults (Lister and Davis, 1989). Combination of pure and simple shear model was further  
763  
764 404 proposed (Lister et al., 1991). In this combination model, crustal deformation is controlled  
765  
766 405 by low angle detachment faulting but thinning of the mantle lithosphere results from pure  
767  
768 406 shear. By introducing time-dependant rheological changes at the lithospheric scale, Reston  
769  
770 407 and Perez-Gussinye (2007) report a complex evolution from symmetric to asymmetric  
771  
772 408 extension, and back to symmetric, at margins displaying exhumed mantle in the hyper-  
773  
774 409 extended domain.

775 410

776  
777 411 A laboratory model combining simple and pure shear has been realized by Brun and Beslier  
778  
779 412 (1996) in order to account for the exhumation of mantle rocks at ocean-continent  
780  
413 boundaries (fig. 8b). This model applies easily to the case of rifts with exhumed mantle such  
414 as the Pyrenean and peri-Pyrenean smooth-slopes basins. This four-layer model is composed

781  
782  
783 415 of sand and silicone putty layers, regarded as analogues of the brittle and ductile layers of  
784 416 both crust and mantle. However, it does not discriminate a mid-crustal level. The lower crust  
785 417 deforms ductilely and the upper mantle is strong. Necking of the whole lithosphere model is  
786 418 nearly symmetrical (pure shear) but asymmetrical structures (simple shear) develop  
787 419 internally, due to boudinage and/or faulting of brittle layers. This model explains the  
788 420 occurrence of shear zones in the mantle lithosphere as described by Vissers et al. (1995) in  
789 421 the Pyrenean mantle and accounts for the ductile deformation of the crust as demonstrated  
790 422 by Asti et al. (2019).

796 423

797 424 In contrast with the Brun and Beslier (1996) symmetrical model, recent models of margin  
798 425 evolution based on the Iberian or Alpine examples have put forward asymmetric  
799 426 architectures resulting from the development of few major detachment faults, and  
800 427 promoted the use of “lower-” and “upper-plate” terminology (Manatschal, 2004; Mohn et  
801 428 al., 2010, 2012, 2015; Sutra et al., 2013). Mohn et al. (2012) propose a model of three-layer  
802 429 continental crust where the brittle upper and lower crusts are strongly decoupled by a  
803 430 ductile middle crust (fig. 3b). Crustal thinning, accommodated through a so-called necking  
804 431 zone, is the result of interplay between detachment faulting in the brittle layers and  
805 432 decoupling in ductile quartzo-feldspatic mid-crustal levels along localized ductile  
806 433 décollements. The excision of ductile mid-crustal layers and the progressive embrittlement  
807 434 of the crust by coupling the lower and upper crusts enable major detachment faults to cut  
808 435 into the underlying mantle, exhuming it to the seafloor.

809 436 In the Iberian and Alpine examples, authors envision the presence of one or few large-scale  
810 437 discrete detachment faults controlling the entire crustal thinning and the basin subsidence.  
811 438 This is also applied by Masini et al. (2014) in their model for the western NPZ where a major  
812 439 north-dipping detachment fault accomodates the denudation of the sub-Eurasian mantle to  
813 440 form the basement of the Mauléon basin (fig. 9a). Interpretation involving single  
814 441 detachment faults has also been retained in the preliminary reconstructions of the NPZ  
815 442 basins by Lagabrielle and Bodinier (2008), Lagabrielle et al. (2010) and Vauchez et al. (2013)  
816 443 (fig.9b, c), as well as in the reconstructed S-N transect from the Basque – Cantabrian to the  
817 444 Armorican margin by Roca et al. (2011) (fig. 9d). Similarly, few detachment faults are used in  
818 445 the Espurt et al. (2019), Saspiturry et al. (2019) and Ducoux et al. (in review) models for the  
819 446 Barronies, Mauléon and “Nappe des Marbres” basins respectively (fig. 2). Others models



841  
842  
843 447 invoke deep-seated staircase extensional faults accounting for large-scale ramp-synclinal  
844  
845 448 folding as documented in the Cameros and Columbrets basins (Guimerà et al., 1995; Roma  
846  
847 449 et al., 2018). By contrast, models from the western NPZ by Corre et al. (2016) and Teixell et  
848  
849 450 al. (2016, 2018) (fig. 2) do not favor the activation of single detachment faults alone. Rather,  
850  
851 451 they involve symmetrical tectonic processes triggering a homogeneous thinning of the crust  
852  
853 452 during its lateral extraction from the rift axis.

854  
855 453 In their study of the evolution of the western Betics including the exhumation of the Ronda  
856  
857 454 subcontinental mantle, Frasca et al. (2016) identify three successive steps: (i) ductile crust  
858  
859 455 thinning and ascent of subcontinental mantle thanks to mid-crustal shear zone and crust-  
860  
861 456 mantle shear zones acting synchronously; (ii) disappearance of the ductile crust bringing the  
862  
863 457 upper crust in contact with the subcontinental mantle, (iii) complete exhumation of the  
864  
865 458 mantle in the zone of localized stretching and high-angle normal faulting cutting through the  
866  
867 459 Moho, with related block tilting. These steps do not completely apply to the Pyrenean case,  
868  
869 460 notably because field and geophysical studies of the metamorphic NPZ never evidenced  
870  
871 461 brittle faulting of the Moho during the Cretaceous rifting.

872  
873 462

874  
875 463 Based on these examples of recent interpretations of rifting evolution, we stress that both  
876  
877 464 Alpine and Betic examples do not refer to a décollement level at the base of the pre-rift  
878  
879 465 cover. They promote evolutionary models lacking allochthony of the detached pre-rift  
880  
881 466 sediments, in contradiction with the examples detailed in section I and II. In addition, both  
882  
883 467 Alpine and Betic models refer to a progressive embrittlement in the rift axis resulting in the  
884  
885 468 complete elimination of ductile crustal layers. Again, this contrasts with the NPZ examples  
886  
887 469 where thin ductile crustal layers are extracted in the distal domain and remain welded on  
888  
889 470 the exhumed mantle.

890  
891 471

892  
893 472 **B. Smooth-slopes basins: crustal shear zones and lenticular fabrics at the mesoscale.**

894  
895 473

896  
897 474 Petrological studies of continental units exposed around the Urdach and Sarailé lherzolite  
898  
899 475 bodies (western NPZ) provide information on the deformation mode associated with crustal  
900  
476 thinning and mantle exhumation (Corre et al., 2016; Asti et al., 2019). Reconstruction of  
477 sections across the NPZ Cretaceous basins by Clerc et al. (2015b), Teixell et al. (2016), Corre  
478 et al. (2016) and Asti et al. (2019) use such ductile deformation mode having affinities with a

901  
902  
903 479 regional-scale, uniform pure shear mechanism. It is shown that extension in the Paleozoic  
904  
905 480 basement was achieved through lenticular deformation and pervasive ductile flattening with  
906  
907 481 anastomosing extensional mylonitic shear zones developing at temperatures of 350-450°C.  
908  
909 482 Here, during its lateral extraction from the rift axis, the crust thinned ductilely under  
910  
911 483 greenschist facies P-T conditions. Stretching occurred by the mean of undulating shear  
912  
913 484 contacts between tectonic lenses of flattened crustal material as described in figure 10. At  
914  
915 485 the final step of the continental breakup, very thin continental crustal lenses remained  
916  
917 486 welded on the exhumed mantle.

918  
919 487 A very similar lenticular mode of deformation derives from investigations in the Basin and  
920  
921 488 Range province. Hamilton (1987) describes tectonic lenses of middle crustal rocks that  
922  
923 489 normally lie at separate levels in the crust with undulating shear contacts between them (fig.  
924  
925 490 8c). This deformation mode allows the juxtaposition of different lithologies by uplifting  
926  
927 491 deeper lenses during the extensional deformation. In a different way, Gartrell (1997)  
928  
929 492 propose a large scale crustal boudinage involving successive necking regions where the  
930  
931 493 ductile middle crust is extremely sheared (fig. 8d). The resulting architecture is a succession  
932  
933 494 of tectonic lenses that may evolve toward a large-scale lenticular geometry as proposed by  
934  
935 495 Espurt et al. (2019) for the evolution of the North Pyrenean massifs (fig. 2d).

936  
937 496 In their recent detailed study of the tectonic and metamorphic evolution of the Urdach and  
938  
939 497 Sarailé mantle bodies and associated units, Lagabrielle et al. (2019a; 2019b) describe two  
940  
941 498 types of low-angle shear zones that accommodated part of extension of the distal domain of  
942  
943 499 the Iberia passive margin during the mid-Cretaceous (fig. 10a, b). The deepest shear zone is  
944  
945 500 the crust-mantle detachment. It separates the ultramafic mantle rocks from strongly thinned  
946  
947 501 continental Paleozoic rocks. It is composed of a basal 20-50 m thick lenticular layer of  
948  
949 502 sheared serpentinites followed by a 10 m thick damage zone. The lenticular layer consists of  
950  
951 503 ultramafic symmetrical tectonic lenses, a few meters long, separated by anastomosing  
952  
953 504 serpentine-rich shear zones. The damage zone consists of an assemblage of centimeter-sized  
954  
955 505 symmetrical lenses of a soft, talc-rich, sheared material, separated by conjugate shear zones.  
956  
957 506 The shallowest shear zone is the cover sole décollement. It corresponds to the tectonic  
958  
959 507 boundary separating the base of the detached pre-rift Mesozoic metasedimentary cover  
960  
961 508 from either mantle lherzolites or continental basement rocks. It consists of a thick  
962  
963 509 deformation zone (some meters to tens of meters thick) that was the locus of important  
964  
965 510 metasomatic crystallizations involving notably fluids of Triassic origin (Corre et al., 2016).

961  
962  
963 511 Detailed structural study of the basement and mantle rocks shows that it is not easy to  
964  
965 512 discriminate between dominant pure shear and dominant simple shear processes at the  
966  
967 513 outcrop and regional scales (Lagabrielle et al. 2019a; 2019b). Indeed, a major detachment  
968  
969 514 fault zone (typically related to regional simple shear) may contain abundant symmetrical  
970  
971 515 lenses suggesting locally dominant pure shear.

972 516 Finally, in the studied smooth-slopes basins, dominant pure shear mechanisms concentrate  
973  
974 517 into the strongly thinned continental tectonic lenses whereas simple shear mechanism  
975  
976 518 characterize the main detachments. Pure shear mechanisms associated with overall  
977  
978 519 flattening of the syn-rift and pre-rift sedimentary pile progressively develop into the basin  
979  
980 520 center as represented in figure 10a. Chronological constraints have to be integrated in order  
981  
982 521 to establish possible succession from simple shear-dominant toward pure shear-dominant  
983  
984 522 deformation mechanisms at the scale of the entire system.

985  
986  
987  
988  
989 523

985 524 **C. Smooth-slopes basins formation, insights for the evolution of passive, magma-poor**  
986  
987 525 **continental margins.**

988  
989  
990  
991  
992  
993  
994  
995  
996  
997  
998  
999  
1000  
1001  
1002  
1003  
1004  
1005  
1006  
1007  
1008  
1009  
1010  
1011  
1012  
1013  
1014  
1015  
1016  
1017  
1018  
1019  
1020

990 526 We deduce from section B above that dominant pure shear deformation concentrates into  
991  
992 527 anastomosed tectonic lenses forming the strongly stretched continental in the central region  
993  
994 528 of smooth-slopes basins. In the following, we review examples of comparable uniform  
995  
996 529 modes of ductile deformation worldwide.

997 530 A lenticular mode of deformation devoid of any steep normal fault is proposed at the scale  
998  
999 531 of an entire passive margin by Gernigon et al., (2014) to account for the symmetrical  
1000  
1001 532 stretching of the continental crust during the formation of the Barents margin (fig. 11a). This  
1002  
1003 533 geometry recalls the structures proposed by Gartrell (1997) (fig. 8d). Lenticular fabric is also  
1004  
1005 534 suggested for deep crustal units connected to tilted blocks through listric faults along the  
1006  
1007 535 Norway margin (Osmundsen and Ebbing, 2008; fig. 11b). These structures accommodate  
1008  
1009 536 crustal thinning to only a few kilometer thicknesses through dominant ductile mode. The  
1010  
1011 537 symmetrical mode of stretching implying ductile thinning or boudinage of some crustal layer  
1012  
1013 538 can be compared to processes of depth-dependent stretching or thinning (DDT and DDS)  
1014  
1015 539 envisioned by Reston and McDermott (2014) in order to account for extensional  
1016  
1017 540 discrepancies at some passive margins. It must be noted that according to an interpretation  
1018  
1019 541 of deep seismic reflection profiles by Reston (1988), lens-shaped low-strain lozenges  
1020

1021  
1022  
1023 543 separated by high strain shear zones form the structural pattern of the lower crust beneath  
1024  
1025 544 the United Kingdom. This overall pattern seems to be possibly applied to numerous units of  
1026  
1027 545 stretched crust at a large scale.

1028 546 Several distal domains of North Atlantic passive margins display geometries that suggest the  
1029  
1030 547 presence of lens-shaped units of thinned to hyper-thinned continental crust detached along  
1031  
1032 548 anastomosing shear zones and now separated by large zones exposing exhumed mantle (e.g.  
1033  
1034 549 Labrador and West Greenland margins; Reston and Perez-Gussinyé, 2007) (fig. 11c, d). These  
1035  
1036 550 units do not resemble extensional allochthons of the West Iberia-type margins (figs. 2 and  
1037  
1038 551 11e) and show geometrical affinities with crustal boudins extracted during the Pyrenean  
1039  
1040 552 extension in the center of the Cretaceous rift (e.g. the Baronnies and Agly crustal boudins;  
1041  
1042 553 Espurt et al., 2019; Clerc et al., 2016) (fig. 2). Such large areas of hyper-thinned continental  
1043  
1044 554 crust possibly composed of an assemblage of heterogeneous boudins, can be viewed as  
1045  
1046 555 sheets representing considerable volumes of sheared and flattened continental material  
1047  
1048 556 (thickness less than 10 km, width of 100 km and length more that few 1000 km, along the  
1049  
1050 557 margin), formed through processes of uniform pure shear at a crustal scale. We infer that  
1051  
1052 558 the modes of deformation exhibited by the Pyrenean crustal units welded on the exhumed  
1053  
1054 559 mantle (although at a much smaller scale) can apply to the formation of these crustal sheets,  
1055  
1056 560 suggesting predominance of greenschists facies mylonites. Similar crustal sheets underlying  
1057  
1058 561 sag basins are well imaged in recent numerical models of margin evolution (Brune et al.,  
1059  
1060 562 2014 ; Huisman and Beaumont, 2011; 2014) as shown in figure 12a, b. Crustal sheets are  
1061  
1062 563 present along the Angola margin (fig. 12d), they may be present in the very distal domain of  
1063  
1064 564 the Gulf of Lion margin where they may originate by extraction of lower crustal material  
1065  
1066 565 (Jolivet et al., 2017) (fig. 11f). Similar long and thin sheets are typically imaged by Wang et al.  
1067  
1068 566 (2016) at the base of the reconstructed Iberia margin of the Mauléon basin, and by Roca et  
1069  
1070 567 al. (2011) in their reconstruction of the north Iberia margin north of the Cantabrian coast  
1071  
1072 568 (fig. 9d).

1073 569 In their compilation of high-quality and deep penetration seismic profiles of several passive  
1074  
1075 570 margins (Uruguay, Southern Namibia, Gabon, South China Sea and Barents Sea), Clerc et al.  
1076  
1077 571 (2015a; 2018) suggest that the lower crust of some margins is weaker than assumed and  
1078  
1079 572 accommodates a large part of extension by ductile shearing (fig. 8e). Boudinage appears as a  
1080  
573 recurrent deformation process accounting for the thinning of the continental crust at  
574 variable scales. This leads authors to an unorthodox vision of some type of passive margins

1081  
1082  
1083 575 where: (i) the lower crust is weak, (ii) boudinage controls a large part of the deformation and  
1084 576 localization of low-angle normal faults, and (iii) these normal faults often dip toward the  
1085 577 continent. This study highlights a crustal behavior dominated by boudinage and  
1088 578 lenticulation, implying interplay between ductile shear zones (boudin edges) and more  
1089 579 resistant crustal volumes (boudin cores). As discussed above in section B, this deformation  
1092 580 mode may apply to the thinned crustal levels in the axis of the Cretaceous Pyrenean rifts  
1093 581 (Teixell et al. 2016, 2018; Asti et al., 2019) (fig. 10) and is supported by recent numerical  
1095 582 models of lithospheric rifting incorporating macroscale anisotropy (Duretz et al., 2016).  
1097 583 In their interpretation of deep seismic profiles of the Gulf of Lion margin, Jolivet et al. (2015)  
1098 584 point to an intense stretching of the distal margin and reveal a 80 km-wide ocean-continent  
1100 585 transition zone that may consist of thin lower continental crust (the “Gulf of Lion  
1101 586 metamorphic core complex”) and exhumed mantle (fig. 11f). They infer an overall hot  
1102 587 geodynamic environment with a shallow lithosphere-asthenosphere boundary able to  
1105 588 weaken the upper mantle and the lower crust enough to make them flow south-eastward. In  
1107 589 this example, the lower crust bears an important role, which is not fully documented by field  
1108 590 data in the NPZ since evidence of exposure of lower crustal levels during the Cretaceous  
1110 591 rifting event has not yet been reported with confidence. Moreover, in most of the sections  
1111 592 of figures 3 and 7, the lower crust is considered as a high-strength layer that does not  
1113 593 deform ductilely but tends to break into large scale boudins and to remain at depth during  
1115 594 the rifting processes (e.g. figs. 2a, e, f, h).

1117 595

#### 1119 596 **D. Comparison with thermo-mechanical models of crustal hyper-extension.**

1120 597

1122 598 The examples discussed above lead us to emphasize the frequency of lenticular fabrics at  
1123 599 various scales reported from different studies in both the upper mantle and the crust. The  
1125 600 formation of lenticular fabrics, necking and lateral extraction during continental rifting have  
1127 601 been addressed in mechanical and thermo-mechanical numerical models (Duretz and  
1128 602 Schmalholz, 2015; Duretz et al., 2016). These models emphasize the role of a pre-existing  
1131 603 macroscopic mechanical anisotropy on the development of continental rifts. They illustrate  
1132 604 the interplay between necking and lateral extraction of strong layers along weak  
1133 605 décollements, thus defining a lenticular fabric and anastomosed shear zone networks at the  
1136 606 regional scale as envisioned in the NPZ case.

1141  
1142  
1143 607 Models of metamorphic core complexes (MCCs) formation generally involve a thick and hot  
1144  
1145 608 continental crust (Brun and van den Driessche, 1994). This does not apply to the Pyrenean  
1146  
1147 609 case but constructive inputs can be expected from a confrontation with the rheological  
1148  
1149 610 parameters used for MCCs modeling. For instance, Tirel et al. (2008) use initial Moho  
1150  
1151 611 temperatures of 800°C or higher, with crustal thicknesses of 45 km or greater. This is much  
1152  
1153 612 more than what can be retained for the post-Variscan crust in the Pyrenees (thicknesses  
1154  
1155 613 between 30 and 20 km) (Teixell et al., 2018, and references therein) and Moho  
1156  
1157 614 temperatures lower than 800°C. In the Tirel et al. (2008) experiment, the exhumation  
1158  
1159 615 process of the metamorphic dome results in the progressive development of a detachment  
1160  
1161 616 zone and the Moho remains flat because the lower crust has a low viscosity and the upper  
1162  
1163 617 mantle is weak enough. With Moho temperatures lower than 800°C, the sub-Moho mantle  
1164  
1165 618 has high strength and effective viscosity resulting in strong Moho deflection and crustal-  
1166  
1167 619 scale necking. These conditions (relatively cold mantle and thin crust) are reached in the  
1168  
1169 620 Pyrenean rift explaining why the Pyrenean mantle rapidly reached the surface when it was  
1170  
1171 621 passively mobilized in response to the drift of the Iberia plate.

1168  
1169 622 A former numerical model that applies to the formation of passive continental margins  
1170  
1171 623 suggests that the crust may be thinned by permanent pure shear both at the proximal and  
1172  
1173 624 distal margin (Huisman and Beaumont, 2011) (fig. 12a). This scenario can apply easily to the  
1174  
1175 625 Pyrenean case where the ductile behaviour of the middle crust is demonstrated (Asti et al.,  
1176  
1177 626 2019). The Huisman and Beaumont (2011) model produces symmetric margins associated  
1178  
1179 627 with distal domain characterized by large sheets of thinned crustal material, as discussed  
1180  
1181 628 above. The symmetrical outline is well imaged by current reconstructions of the Pyrenean  
1182  
1183 629 basins from the North Pyrenean Zone and associated examples (Parentis, Cameros and  
1184  
1185 630 Columbrets basins, fig. 1, 2 and 7).

1184  
1185 631 Brune et al. (2014) produce a different numerical model that emphasizes a rift migration  
1186  
1187 632 accomplished by sequential upper crustal faults balanced through lower crustal flow (fig.  
1188  
1189 633 12b). An interesting concept is that of 'exhumation channel', a weak locus of deformation  
1190  
1191 634 where the crust and part of the uppermost mantle are actively deformed and extremely  
1192  
1193 635 thinned during their transfer from lower to shallower levels, over a dome of upwelling  
1194  
1195 636 lithospheric mantle. This high strain volume is not a detachment fault and thus may bear  
1196  
1197 637 some affinity with the lenses of crustal material exhumed with NPZ mantle and described by  
1198  
1199 638 Asti et al. (2019). As discussed in section C above, the resulting geometry is that of areas of

1201  
1202  
1203 639 drastically thinned crust (named *crustal sheets* in the following) forming the distal margin  
1204  
1205 640 domain lying over a cooled and strengthened mantle. This mantle is exposed locally at the  
1206  
1207 641 rift axis depending on the extension rate. The final sketch derived from this model, including  
1208  
1209 642 a dome of strong mantle rimmed in its upper part by a thin layer of mylonitic crust, is a  
1210  
1211 643 reliable image for the geometry resulting from the Pyrenean rifting and associated basins at  
1212  
1213 644 a lithospheric scale.

1214 645 Jammes et al. (2015) and Jammes and Lavier (2016), introduced compositional complexities  
1215  
1216 646 in the lithosphere by using an explicit biminerale assemblage which results in the  
1217  
1218 647 development of anastomosing shear zone. In their models, the deformation appears  
1219  
1220 648 localized in the middle/lower crust and the upper lithospheric mantle and leads to the  
1221  
1222 649 preservation of almost undeformed lenses of material surrounded by localized shear zones  
1223  
1224 650 concentrating most of the deformation. Such a lenticular final geometry is also evocative of  
1225  
1226 651 the one observed in the North Pyrenean Zone as discussed in detail by Asti et al. (2019) and  
1227  
1228 652 illustrated in fig. 10.

1229 653 To unravel the dynamic evolution of the Cretaceous Pyrenean rift, Duretz et al. (2019)  
1230  
1231 654 carried out a set of thermo-mechanical numerical models of lithosphere-scale extension  
1232  
1233 655 based on the available geological constraints listed above in section I. The models were used  
1234  
1235 656 to explore the role of a km-thick basement-cover décollement layer at the base of the pre-  
1236  
1237 657 rift sediments. These numerical experiments highlight the key-role of the décollement layer  
1238  
1239 658 that can alone explain collectively: (i) salt tectonics deformation style and cover  
1240  
1241 659 décollement, (ii) high temperature metamorphism of the pre-rift cover, and (iii) ductile  
1242  
1243 660 mode of crustal thinning in the inner domain of the models. In the axis of the synclinal-  
1244  
1245 661 shaped basin (“sag” basin in the margin literature), extreme pure shear leads to the  
1246  
1247 662 development of a very thin basement layer, overlain by poorly-thinned pre-rift and syn-rift  
1248  
1249 663 sediments and underlain by exhuming mantle. These models are in good agreement with the  
1250  
1251 664 current knowledge of the architecture of the Cretaceous Pyrenean basins as exemplified by  
1252  
1253 665 reconstructions of figs. 2 and 7, as well as with the presence of large sheets of hyper thinned  
1254  
1255 666 crustal material (crustal sheets) in the distal part of numerous magma poor passive margins.

1256  
1257  
1258  
1259  
1260 667

1261  
1262  
1263 668 **E. The pre-rift salt décollement layer: a mechanical key-factor in the evolution of smooth-**  
1264  
1265 669 **slopes basins. Establishing a new link between Triassic paleogeography and rifting**  
1266  
1267 670 **mechanisms.**

1268 671

1269  
1270 672 As reported in section I and II, the common character between all pre-rift sequences of the  
1271  
1272 673 aforementioned smooth-slopes basins is the presence of the thick low-strength Late Triassic  
1273 674 evaporitic layer (Keuper). All related geological and geophysical studies highlight the  
1274  
1275 675 importance of this décollement layer in the evolution of the rift basins under study. As  
1276  
1277 676 detailed above, efficient décollement along the Keuper evaporites and clays triggers  
1278  
1279 677 mechanical decoupling and gliding of the pre-rift cover that remains in the center of the  
1280  
1281 678 basin as the crust is laterally extracted. In response to crustal hyper-thinning and horizontal  
1282  
1283 679 crustal extraction, hot mantle material approaches the detached pre-rift cover. As a  
1284  
1285 680 consequence, HT-LP metamorphism develops in the pre-rift sediments and at the base of  
1286  
1287 681 the syn-rift flysch levels as recorded in the NPZ and in the pre-rift sediments of the Cameros  
1288  
1289 682 basin. Subsequent deposition of syn-rift sediments allows preservation of the initial thermal  
1290  
1291 683 anomaly with a major consequence on the deformation regime in the pre-rift sediments and  
1292  
1293 684 crustal basement. Temperature increase in the NPZ basins center progressively leads to the  
1294  
1295 685 uprising of the brittle/ductile transition avoiding the development of prominent crustal normal  
1296  
1297 686 faults and leading to the dominantly ductile thinning of the Paleozoic basement and parts of  
1298  
1299 687 the pre-rift and syn-rift sediments (Clerc and Lagabrielle, 2014; Clerc et al., 2015b; Asti et al.,  
1300  
1301 688 2019; Duretz et al., 2019). We may now question the paleogeographic distribution of the  
1302  
1303 689 Keuper group sediments at the Europa-Iberia scale in order to evaluate a possible link  
1304  
1305 690 between modes of rift development and the occurrence of a thick Keuper layer at the base  
1306  
1307 691 of the pre-rift sequence.

1308  
1309 692 Several extensional systems interacted in the Iberia platform during the Trias, resulting in  
1310  
1311 693 the creation of intraplate basins or troughs including the Valencian, Basque-Cantabrian, and  
1312  
1313 694 Pyrenean basins (figs. 1 and 13). The sedimentary infill of these platform basins continued  
1314  
1315 695 throughout the Mesozoic. Seismic, well and field data from the Bay of Biscay region, the  
1316  
1317 696 Pyrenees and the Aquitanian Basin, suggest initial thickness of Upper Triassic formations  
1318  
1319 697 ranging from 1000 to 2700 m (James and Canérot, 1999; Biteau et al., 2006; Jammes et al.,  
1320  
698 2010a; Roca et al., 2011; Rowan, 2014; Lopez-Mir et al., 2014; Saura et al., 2016; Soto et al.,  
699 2017; Zamora et al., 2017). The salt-rich layers generally consist of shales and evaporites



1321  
1322  
1323 700 including dominant gypsum and minor halite and anhydrite (figs. 13 and 14).  
1324  
1325 701 Paleogeographic reconstructions are available for the Triassic period at the scale of the  
1326  
1327 702 Iberia-western Europa region (Dercourt et al., 1986; 1993; Ziegler, 1988; Ortí et al., 2017;  
1328  
1329 703 Soto et al., 2017). The distribution of Triassic shales and evaporites is contrasted around the  
1330  
1331 704 future Iberia plate margins. This paleogeography is confirmed by a compilation of data  
1332  
1333 705 collected independantly by D. Frizon de Lamotte (fig. 13c). Evaporites are well developed  
1334  
1335 706 along the eastern edge of Iberia (Tethys side) and in the rift opened at the place of the  
1336  
1337 707 future NPZ, the Basque-Cantabrian basin, the Bay of Biscaye basin and the southern part of  
1338  
1339 708 the Armorican margin. In the place of the future North Atlantic rift system, evaporites are  
1340  
1341 709 restricted to the Peniche, Lusitanian, Alentejo and Algarve basins along the southern half of  
1342  
1343 710 the Portugal margin and are lacking along the northern half of the Iberia Atlantic margin.  
1344  
1345 711 Along the conjugate north American margin, evaporites are known at the base of the  
1346  
1347 712 Jeanne-d'Arc basin and are of restricted extension compared to the Keuper group exposed in  
1348  
1349 713 Central Europe (fig. 13b, c).  
1350  
1351 714 Finally, along the western half of the Iberia-Newfoundland transect, evaporitic formation are  
1352  
1353 715 not reported, whereas thick evaporites are reported from areas characterized by Parentis-  
1354  
1355 716 type basins. As outlined in figures 13 and 14, this paleogeography matches the distribution  
1356  
1357 717 of the two opposite types of basins discussed in this article (Parentis type vs. Iberia-  
1358  
1359 718 Newfoundland type). Thus, we establish a link between the presence of a pre-rift salt layer  
1360  
1361 719 and the deep mechanisms of crustal stretching. Because they remain in the center of the  
1362  
1363 720 basin, evaporites contribute to the preservation of a rather high thermal gradient in the axial  
1364  
1365 721 rift allowing a dominant-ductile deformation of the basement. The lack of a major  
1366  
1367 722 décollement level at the base of the pre-rift sequence may explain by itself why pre-rift  
1368  
1369 723 sediments remain welded and coupled to the basement on the top of tilted blocks in the  
1370  
1371 724 Iberia-Newfoundland-type margins as illustrated in figure 3a, b. Indeed, in the Iberia as well as  
1372  
1373 725 in Alpine margin-types, only syn-rift sediments are deposited over the exhumed lower  
1374  
1375 726 crustal levels and subcontinental mantle (Péron-Pinvidic et al., 2007; Péron-Pinvidic and  
1376  
1377 727 Manatschal, 2009; Mohn et al., 2012), which contrasts with the evolution of the Parentis-  
1378  
1379 728 type basins.  
1380  
729  
730 In this review, on the basis of examples clustering along the Iberia-Eurasia plates boudaries,  
731 we emphasize the major role played by the Upper Triassic evaporitic layer during extensional

1381  
1382  
1383 732 processes. In the reported smooth-slopes basin examples, cover gliding occurred on a pre-  
1384  
1385 733 rift layer and thus contrasts with cases involving syn- to post-rift weak layers. The latter  
1386  
1387 734 cases have been largely documented by studies of passive margins displaying thick syn-rift  
1388  
1389 735 salt formations such as the Angola margin where the post-salt sedimentary units have glided  
1390  
1391 736 gravitationally after the margin formation (e.g. Brun and Fort, 2011, and references therein,  
1392  
1393 737 see also additional discussion relative to the pre-rift/post-rift salt effects during rifting in  
1394  
1395 738 Jammes et al., 2010c). To sum up, the specific characters emphasized in this review are  
1396  
1397 739 twofold : (i) the peri-Pyrenean salt is pre-rift allowing conservation of the pre-rift cover over  
1398  
1399 740 the high-strain axial rift. Crustal faulting has not disrupted the continuity of the Triassic  
1400  
1401 741 evaporite formation, allowing for décollement of the pre-rift sequence basinward, down to  
1402  
1403 742 the distal margin. (ii) Consequently, the axial thermal anomaly is preserved and the  
1404  
1405 743 dominant ductile mode of crustal deformation prevented the formation of faulting-related  
1406  
1407 744 steps leading to smooth-slopes basin edges.

1408  
1409 745

#### 1410 746 **F. Time-dependent rheology during the evolution of smooth-slopes basins**

1411 747

1412 748 From the statements listed at the end of section I as well as from the discussion above, we  
1413  
1414 749 first stress that the models of Pyrenean Cretaceous rifting established on the basis of  
1415  
1416 750 geological constraints from the NPZ differ significantly from the classical models of passive  
1417  
1418 751 margin formation based on the Iberia-Newfoundland margins example (Peron-Pinvidic and  
1419  
1420 752 Manatschal, 2009; Sutra et al., 2013; Osmundsen and Peron-Pinvidic, 2018, and references  
1421  
1422 753 therein). The latter models involve a dominantly brittle behavior of the crust and the  
1423  
1424 754 individualization of tilted faulted blocks bearing a concordant pre-rift cover permanently  
1425  
1426 755 welded on their back (fig. 3). In the models based on the geology of the NPZ (e.g. models of  
1427  
1428 756 Clerc et al., 2016; Teixell et al., 2016; Espurt et al., 2019), the external borders of the  
1429  
1430 757 subsiding Cretaceous flysch basins remain at low temperature and display classical faulted  
1431  
1432 758 and tilted blocks (e.g. half-grabens of Quillan basin, Camarade basin, Gensac-Bonrepos  
1433  
1434 759 basin, western border of the Mauléon basin, Arbailles basin, edges of the Gran Rieu high and  
1435  
1436 760 Lacq basin). By contrast, in the internal regions of the rift system (corresponding to the  
1437  
1438 761 future metamorphic NPZ), the basement thinned in a dominant-ductile mode because  
1439  
1440 762 temperature conditions reached 350°C to 450°C beneath the detached pre-rift cover and the  
763 syn-rift flysch.

1441  
1442  
1443 764 The peculiar evolution of the NPZ basins is depicted on figure 15 based on an original model  
1444  
1445 765 by Clerc et al., (2016). This model is strictly conceptual and was designed to account for  
1446  
1447 766 geological constraints gathered from various sites along the NPZ. The simplified system  
1448  
1449 767 includes the subcontinental mantle, a continental basement, a first decollement level in  
1450  
1451 768 Triassic evaporites, a level of layered pre-rift carbonates and a cover of syn-rift flysch. The  
1452  
1453 769 carbonates are able to deform by crystalline plasticity of calcite under HT conditions. The  
1454  
1455 770 corresponding lithologies are illustrated and briefly described in the NPZ lithostratigraphical  
1456  
1457 771 column of figure 5.

1458  
1459 772 In order to better assess the time-dependent rheological changes that necessarily affect  
1460  
1461 773 each geological layer involved during this three steps evolution, we provide synthetic  
1462  
1463 774 rheological profiles and geotherms for selected parts of the basin: in the external portion  
1464  
1465 775 representing the initial pre-extension model (fig. 15a) and in the center of the basin for the  
1466  
1467 776 following two steps (fig. 15b and c). The data used to construct these profiles derived from  
1468  
1469 777 the Duretz et al. (2019) model discussed in section D above.

1470  
1471 778 The three steps of this conceptual evolutionary model can be described as follows:

1472  
1473 779 (1) At an early rifting stage (fig. 15a) moderate extension leads to crustal thinning  
1474  
1475 780 accommodated through normal faults in the upper crust. The rheological profile consists of a  
1476  
1477 781 15 km thick, cold and brittle upper crust ( $T > 300^{\circ}\text{C}$ ) overlying a 15 km thick ductile lower  
1478  
1479 782 crust with Moho temperature around  $550^{\circ}\text{C}$ . The uppermost mantle is a strong 15 km thick  
1480  
1481 783 layer. In the inner part of the system, normal faults may pass downward to ductile shear  
1482  
1483 784 zones dipping toward the external side thus delineating a small central horst. The Triassic  
1484  
1485 785 evaporitic layers act as a décollement layer that allows the pre-rift carbonates to remain in  
1486  
1487 786 the most thinned and subsiding domains on both sides of the central horst while the syn-rift  
1488  
1489 787 flysch is being deposited above. Sliding of the pre-rift carbonates in the deep domain results  
1490  
1491 788 in the local tectonic denudation of the margins where carbonates remnants form isolated  
1492  
1493 789 rafts tilted on listric faults.

1494  
1495 790 (2) At the mid-rifting stage (fig. 15b), ductile thinning of the crust occurs in response to  
1496  
1497 791 heating due to rapid mantle uplift. The central crustal horst starts to deform ductilely and  
1498  
1499 792 progressively acquires a lens shape. Due to blanketing effect under the syn-rift sediments,  
1500  
793 the HT pre-rift carbonates suffer syn-metamorphic ductile deformation. Rheological profile

1501  
1502  
1503 794 in the center of the basin shows the Keuper weak zone at the base of the pre-rift cover and a  
1504  
1505 795 newly formed weak zone corresponding to the thinned crust which deforms at temperatures  
1506  
1507 796 between 300°C and 500°C. The lower crust has been extracted laterally and the brittle  
1508  
1509 797 mantle layer shows a decreasing thickness due to temperature increase from 400°C (step 1)  
1510  
1511 798 to 1000°C at only 20 km depth.

1512  
1513 799 (3) At the final rifting stage (fig. 15c), extreme thinning and boudinage of the crust leads to  
1514  
1515 800 local denudation of the sub-continental mantle, which is by place in tectonic contact with  
1516  
1517 801 the pre- or syn-rift sediments. The crust in the center of the basin has been cut into few  
1518  
1519 802 lenses that move independently. The crust at both edges of the proximal domain thins and  
1520  
1521 803 moves horizontally (*lateral extraction* concept of Clerc and Lagabrielle, 2014). The Triassic  
1522  
1523 804 décollement layer undergoes drastic thickness reduction leading to boudinage in response  
1524  
1525 805 to fluid-assisted tectonic brecciation and to metasomatic dissolution as observed in the  
1526  
1527 806 Urdach and Sarailé massifs in the western NPZ (Lagabrielle et al., 2019a, 2019b in press).  
1528  
1529 807 Due to their increasing plasticity, the HT marbles of the pre-rift cover progressively  
1530  
1531 808 accommodate a large part of the deformation at the base of the basin, involving calcite  
1532  
1533 809 plasticity and recrystallization, boudinage, drag folding and low angle normal shear bands. In  
1534  
1535 810 turn, the lower levels of the syn-rift flysch sequence are progressively affected by HT  
1536  
1537 811 metamorphism and ductile deformation with bedding-parallel foliation and boudinage.  
1538  
1539 812 Continuous extension of the basin floor leads also to the progressive exhumation of the  
1540  
1541 813 metamorphic pre-rift sediments, which are progressively extracted from below the syn-rift  
1542  
1543 814 cover (see complete description of this process in Clerc et al., 2016). In the thinnest crustal  
1544  
1545 815 portion, the rheological profile bears similarities with that of step 2. The crustal thickness  
1546  
1547 816 has now reduced to less than one km and the brittle/ductile transition has moved upward.  
1548  
1549 817 The pre-rift cover, salt décollement as well as the thinned basement thus deform under  
1550  
1551 818 dominant ductile deformation.

#### 1547 819 **IV. Conclusions**

1548  
1549 820

1550  
1551 821 Almost fourty years after the discovery of mantle exhumed at the foot of the north Iberia  
1552  
1553 822 passive margin (Boillot et al. 1980), this review highlights the affinities between the  
1554  
1555 823 architecture of two types of extensional basins now variously inverted in the Pyrenean  
1556  
1557 824 orogeny. These are : (i) the extensional basins that opened during the mid-Cretaceous times

1561  
1562  
1563 825 along the Iberia-Eurasia plate boundary and, (ii) the intraplate basins of northern Iberia  
1564  
1565 826 (Cameros to Columbrets basins). Taking as a reference the Parentis basin profile and on the  
1566  
1567 827 basis of geological reconstructions of NPZ rift architecture, we have designed an idealized  
1568  
1569 828 cross-section of a smooth-slopes basin shown in figure 16. The dominant features put  
1570  
1571 829 forward in this cross-section relate to the basin central region which lacks stepping normal  
1572  
1573 830 faults and large-scale tilted crustal blocks. The section shows a dominant symmetrical shape  
1574  
1575 831 with smooth-slopes that relates to a new mode of crustal stretching during continental  
1576  
1577 832 rifting characterized by a ductilely thinned crust in the central rift domain. This deformation  
1578  
1579 833 mode is typically symmetrical and contrasts drastically with stretching processes described  
1580  
1581 834 from the Iberia-Newfoundland and Alpine Tethys margins implying asymmetrical  
1582  
1583 835 architecture and extensional detachment separating upper and lower plates having  
1584  
1585 836 differential evolution.

1584 837

1586 838 The common character between all pre-rift sequences of the studied basins is the presence  
1587  
1588 839 of the thick low-strength Late Triassic evaporitic layer (Keuper facies). Geological and  
1589  
1590 840 geophysical studies point to the importance of this décollement layer in the evolution of  
1591  
1592 841 these rift basins. As established by geological studies in the NPZ, efficient décollement along  
1593  
1594 842 the Keuper evaporites and clays triggers mechanical decoupling and gliding of the pre-rift  
1595  
1596 843 cover that remains in the center of the basin as the crust is laterally extracted. Subsequent  
1597  
1598 844 deposition of syn-rift sediments allows preservation of the initial thermal anomaly with a  
1599  
1600 845 major consequence on the deformation regime in the pre-rift sediments and crustal  
1601  
1602 846 basement. The ubiquitous character of the ductilely deformed marbles in the metamorphic  
1603  
1604 847 NPZ relates to a dominant-ductile deformation regime in the pre-rift cover during the  
1605  
1606 848 Cretaceous extension. In these smooth-slopes basins, the ductilely stretched crust behaves  
1607  
1608 849 homogeneously at the regional scale and extensional allochthons are not individualized. A  
1609  
1610 850 lenticular mode of homogeneous deformation is thus defined implying interplay between  
1611  
1612 851 hectometric lenses of ductile crustal material separated by anastomosing shear zones.

1610 852

1611 853 Both laboratory and thermo-mechanical numerical models reproduce remarkably the mode  
1612  
1613 854 of deformation deduced from geophysical and geological constraints compiled in the studied  
1614  
1615 855 basins. Thus it appears that the pre-rift character of the salt layer is the key-factor of the

1621  
1622  
1623 856 rifting style in controlling the very early decoupling between the basement and the pre-rift  
1624  
1625 857 cover. This strongly contrasts with the evolution of Atlantic margins where the salt is either  
1626  
1627 858 syn-rift or post-rift. For the first time, we evidence a strong link between the occurrence of a  
1628  
1629 859 sedimentary layer covering the future rifted region (here Keuper salt and clays deposits) and  
1630  
1631 860 a mode of crustal thinning (here homogeneous bulk ductile deformation). Décollement  
1632  
1633 861 along the evaporites and clays level finally favors the formation of symmetrical basins  
1634  
1635 862 lacking numerous normal faults and related tilted blocks. This new mode of crustal  
1636  
1637 863 deformation might not be restricted to the Pyrenean region, but may apply to all regions  
1638  
1639 864 hosting thick pre-rift décollement series. It may have been active worldwide, in the distal  
1640  
1641 865 portion of continental margins devoid of typical tilted blocks and extensional allochthons  
1642  
1643 866 and where large units of extremely thinned continental crust are present.

1642 867

1643  
1644 868 To sum up, the specific characters of the smooth-slopes basins emphasized in this review are  
1645  
1646 869 twofold: (i) the peri-Pyrenean salt is pre-rift allowing conservation of the pre-rift cover over  
1647  
1648 870 the high-strain axial central region. The continuity of the Triassic evaporite formation is  
1649  
1650 871 preserved allowing for décollement of the pre-rift sequence which remain in the basin  
1651  
1652 872 center. (ii) Consequently, the axial thermal anomaly is preserved and the dominant ductile  
1653  
1654 873 mode of crustal deformation prevents the formation of faulting-related steps, thus leading  
1655  
1656 874 to smooth-slopes basin edges. Continuous sedimentation in the subsiding basin leads to  
1657  
1658 875 progressive sedimentary burial of the prerift sequence. This in turn allows the preservation  
1659  
1660 876 of the initial thermal anomaly that may grow during the rifting evolution.

1659 877

## 1660 878 **Acknowledgements**

1661  
1662 879 This work is the result of a 10 years field and laboratory research conducted in the Pyrenean  
1663  
1664 880 range with funding from various programs and institutions. We benefited of grants from the  
1665  
1666 881 French ANR Pyramid program, the Bureau de Recherche Géologique et Minière (BRGM),  
1667  
1668 882 Référentiel Géologique de la France (RGF) program and the Total/INSU/BRGM OROGEN  
1669  
1670 883 program with contributions from the CNRS and from Géosciences Montpellier and Rennes  
1671  
1672 884 research units. We thank Thierry Baudin (BRGM) and Sylvain Calassou (Total) for program  
1673  
1674 885 management and encouraging discussions. We also thank B. Azambre, P. Boulvais, M. Pujol,  
1675  
1676 886 and many others for stimulating exchanges that helped improve our ideas.

1681  
1682  
1683  
1684  
1685  
1686  
1687  
1688  
1689  
1690  
1691  
1692  
1693  
1694  
1695  
1696  
1697  
1698  
1699  
1700  
1701  
1702  
1703  
1704  
1705  
1706  
1707  
1708  
1709  
1710  
1711  
1712  
1713  
1714  
1715  
1716  
1717  
1718  
1719  
1720  
1721  
1722  
1723  
1724  
1725  
1726  
1727  
1728  
1729  
1730  
1731  
1732  
1733  
1734  
1735  
1736  
1737  
1738  
1739  
1740

1741  
1742  
1743  
1744  
1745  
1746  
1747  
1748  
1749  
1750  
1751  
1752  
1753  
1754  
1755  
1756  
1757  
1758  
1759  
1760  
1761  
1762  
1763  
1764  
1765  
1766  
1767  
1768  
1769  
1770  
1771  
1772  
1773  
1774  
1775  
1776  
1777  
1778  
1779  
1780  
1781  
1782  
1783  
1784  
1785  
1786  
1787  
1788  
1789  
1790  
1791  
1792  
1793  
1794  
1795  
1796  
1797  
1798  
1799  
1800

## 889 References

890

891 Allemand, P., Brun J.-P., Davy P., and Van Den Driessche J., 1989. Symétrie et asymétrie des  
892 rifts et mécanismes d'amincissement de la lithosphère, Bull. Soc. Géol. Fr., 5, 445–451.

893

894 Asti, R., Lagabrielle, Y., Fourcade, S., Corre, B., Monié, P., 2019. How do continents deform  
895 during mantle exhumation? Insights from the northern Iberia inverted paleopassive margin,  
896 western Pyrenees (France). *Tectonics*, 38, 1666–1693.

897 <https://doi.org/10.1029/2018TC005428>

898

899 Ayala, C., Torne, M., Roca, R., 2015. A review of the current knowledge of the crustal and  
900 lithospheric structure of the Valencia Trough Basin. *Bol. Geológico Min.* 126, 533–552.

901

902 Azambre, B., Rossy, M., 1976. Le magmatisme alcalin d'âge crétacé, dans les Pyrénées  
903 occidentales et l'Arc basque; ses relations avec le métamorphisme et la tectonique. *Bull.*  
904 *Société Géologique Fr.* 7, 1725–1728.

905

906 Bernus-Maury, C., 1984. Etude des paragéneses caractéristiques du métamorphisme  
907 mésozoïque dans la partie orientale des Pyrénées. Thèse, Pierre et Marie Curie, Paris.

908

909 Biteau, J.-J., Le Marrec, A., Le Vot, M., Masset, J.-M., 2006. The Aquitaine Basin. *Pet. Geosci.*  
910 12, 247–273.

911

912 Boillot, G., S. Grimaud, A. Mauffret, D. Mougénot, J. Kornprobst, J. Mergoïl-Daniel, and G.  
913 Torrent, 1980. Ocean-continent boundary off the Iberian margin: A serpentinite diapir west  
914 of the Galicia bank, *Earth Planet. Sci. Lett.*, 48, 23–34.

915

916 Bois, C., Gabriel, O., Lefort, J.-P., Rolet, J., Brunet, M.-F., Masse, P., Olivet, J.-L., 1997.  
917 Geologic contribution of the Bay of Biscay deep seismic survey: a summary of the main  
918 scientific results, a discussion of the open questions and suggestions for further  
919 investigation. *Mém Soc Géol Fr.* 193–309.

920

921 Brun, J. P., 1999. Narrow rifts versus wide rifts: Inferences for the mechanics of rifting from  
922 laboratory experiments, *Philos. Trans. R. Soc. London, Ser. A*, 357, 695–712.

923

924 Brun, J. P., Beslier M.O., 1996. Mantle exhumation at passive margin, *Earth Planet. Sci. Lett.*,  
925 142, 161– 173.

926

927 Brun, J.-P., and van den Driessche, J., 1994. Extensional gneiss domes and detachment fault  
928 systems; structure and kinematics. *Bull. Société Géologique Fr.* 165, 519–530.

929

930 Brun, J.P., Wenzel, F. and ECORS-DEKORP team, 1991. Crustal structure of the southern  
931 Rhine Graben from ECORS-DEKORP seismic reflection data, *Geology*, 19, 758-762. DOI:  
932 10.1130/0091-7613(1991)019<0758:CSSOTS>2.3.CO

933

934 Brun, J.-P., Fort, X., 2011. Salt tectonics at passive margins: Geology versus models. *Mar. Pet.*  
935 *Geol.* 28, 1123–1145. <https://doi.org/10.1016/j.marpetgeo.2011.03.004>



1801  
1802  
1803 936  
1804 937 Brune, S., Heine, C., Pérez-Gussinyé, M., Sobolev, S.V., 2014. Rift migration explains  
1805 938 continental margin asymmetry and crustal hyper-extension. *Nat. Commun.* 5.  
1806 939 <https://doi.org/10.1038/ncomms5014>  
1807 940  
1808 941 Buck, W. R., 1991. Modes of continental lithospheric extension, *J. Geophys. Res.*, 96, 20,161-  
1809 942 20,178.  
1810 943  
1811 944 Buck, W. R., F. Martinez, M. S. Steckler, and J. R. Cochran, 1988. Thermal consequences of  
1812 945 lithospheric extension: Pure and simple, *Tectonics*, 7, 213 - 234.  
1813 946  
1814 947 Cadenas, P., Fernández-Viejo, G., 2017. The Asturian Basin within the North Iberian margin  
1815 948 (Bay of Biscay): seismic characterisation of its geometry and its Mesozoic and Cenozoic  
1816 949 cover. *Basin Res.* 29, 521-541. <https://doi.org/10.1111/bre.12187>  
1817 950  
1818 951 Canérot, J., 1988. Manifestations de l'halocinèse dans les Chaînons Béarnais (Zone Nord-  
1819 952 Pyrénéenne) au Crétacé inférieur. *Comptes Rendus de l'Académie des Sciences de Paris* 306,  
1820 953 1099-1102.  
1821 954  
1822 955 Canérot, J., 1989. Rifting éocrétacé et halocinèse sur la marge ibérique des Pyrénées  
1823 956 Occidentales (France). Conséquences structurales. *Bull. Cent. Rech. Explor.-Prod. Elf-*  
1824 957 *Aquitaine* 13, 87-99.  
1825 958  
1826 959 Canérot, J., 2017. The pull apart-type Tardets-Mauléon Basin, a key to understand the  
1827 960 formation of the Pyrenees. *Bull. Société Géologique Fr.* 188, 35.  
1828 961 <https://doi.org/10.1051/bsgf/2017198>  
1829 962  
1830 963 Canérot, J., Hudec, M.R., Rockenbauch, K., 2005. Mesozoic diapirism in the Pyrenean orogen:  
1831 964 Salt tectonics on a transform plate boundary. *AAPG Bull.* 89, 211-229.  
1832 965 <https://doi.org/10.1306/09170404007>  
1833 966  
1834 967 Canérot, J., Lenoble, J.-L., 1989. Le diapir du Lichançumendy (Pyrénées-Atlantiques), nouvel  
1835 968 élément de la marge ibérique des Pyrénées occidentales. *Comptes Rendus Académie Sci.*  
1836 969 *Sér. 2 Mécanique Phys. Chim. Sci. Univers Sci. Terre* 308, 1467-1472.  
1837 970  
1838 971 Canérot, J., Lenoble, J.-L., 1993. Diapirisme crétacé sur la marge ibérique des Pyrénées  
1839 972 occidentales; exemple du pic de Lauriolle; comparaisons avec l'Aquitaine, les Pyrénées  
1840 973 centrales et orientales. *Bull. Société Géologique Fr.* 164, 719-726.  
1841 974  
1842 975 Capdevila, R., Boillot, G., Lepvrier, C., Malod, J.-A., Mascle, G., 1980. Les formations  
1843 976 cristallines du Banc Le Danois (marge nord ibérique). *Comptes Rendus Académie des*  
1844 977 *Sciences de Paris* 291, 317-320.  
1845 978  
1846 979 Casas-Sainz, A.M., Gil-Imaz, A., 1998. Extensional subsidence, contractional folding and  
1847 980 thrust inversion of the eastern Cameros basin, northern Spain. *Geol Rundsch* 86(4):802-818  
1848 981  
1849 982 Castanares, L.M., Robles, S., Gimeno, D. and Vicente Bravo, J.C., 2001. The Submarine  
1850  
1851  
1852  
1853  
1854  
1855  
1856  
1857  
1858  
1859  
1860

1861  
1862  
1863 983 Volcanic System of the Errigoiti Formation (Albian-Santonian of the Basque-Cantabrian  
1864 984 Basin, Northern Spain): Stratigraphic Framework, Facies, and Sequences. *Journ. Sedim.*  
1865 985 *Research.* 71 , 2, 318-333.  
1866 986  
1867 987 Chevrot, S., Sylvander, M., Díaz, J., Ruiz, M., Paul, A., PYROPE Working Group, 2015. The  
1868 988 Pyrenean architecture as revealed by teleseismic P-to-S converted waves recorded along  
1870 989 two dense transects. *Geophysical Journal International* 200, 1094-1105.  
1871 990  
1872 991 Chevrot, S., Sylvander, M., Diaz, J., Martin, R., Mouthereau, F., Manatschal, G., Masini, E.,  
1873 992 Calassou, S., Grimaud, F., Pauchet, H., Ruiz, M., 2018. The non-cylindrical crustal architecture  
1874 993 of the Pyrenees. *Sci. Rep.* 8. <https://doi.org/10.1038/s41598-018-27889-x>  
1875 994  
1876 995 Choukroune, P., 1976a. Strain patterns in the Pyrenean chain: *Philosophical Transactions of*  
1878 996 *the Royal Society of London A: Mathematical, Physical and Engineering Sciences*, v. 283, no.  
1879 997 1312, p. 271-280.  
1880 998  
1881 999 Choukroune, P., 1976b. Structure et évolution tectonique de la zone nord pyrénéenne,  
1882 1000 *Mem. Soc. Geol. Fr.*, 127, 1-116.  
1883 1001  
1884 1002 Choukroune, P., ECORS Team, 1989. The ECORS Pyrenean deep seismic profile reflection  
1886 1003 data and the overall structure of an orogenic belt. *Tectonics* 8, 23-39.  
1887 1004  
1888 1005 Choukroune, P., Mattauer, M., 1978. Tectonique des plaques et Pyrenees; sur le  
1889 1006 fonctionnement de la faille transformante nord-pyreneenne; comparaisons avec des  
1890 1007 modeles actuels. *Bull. Société Géologique Fr.* 7, 689-700.  
1891 1008  
1892 1009 Clerc, C., Lagabrielle, Y., 2014. Thermal control on the modes of crustal thinning leading to  
1894 1010 mantle exhumation: Insights from the Cretaceous Pyrenean hot paleomargins. *Tectonics* 33,  
1895 1011 1340-1359. <https://doi.org/10.1002/2013TC003471>  
1896 1012  
1897 1013 Clerc, C., Jolivet, L., Ringenbach, J.-C., 2015a. Ductile extensional shear zones in the lower  
1898 1014 crust of a passive margin. *Earth Planet. Sci. Lett.* 431, 1-7.  
1899 1015 <https://doi.org/10.1016/j.epsl.2015.08.038>  
1900 1016  
1901 1017 Clerc, C., Lahfid, A., Monié, P., Lagabrielle, Y., Chopin, C., Poujol, M., Boulvais, P.,  
1903 1018 Ringenbach, J.C., Masini, E., de St Blanquat, M., 2015b. High-temperature metamorphism  
1904 1019 during extreme thinning of the continental crust: a reappraisal of the North Pyrenean  
1905 1020 passive paleomargin. *Solid Earth* 6, 643-668.  
1906 1021  
1907 1022 Clerc, C., Lagabrielle, Y., Labaume, P., Ringenbach, J.-C., Vauchez, A., Nalpas, T., Bousquet, R.,  
1908 1023 Ballard, J.-F., Lahfid, A., Fourcade, S., 2016. Basement - Cover decoupling and progressive  
1909 1024 exhumation of metamorphic sediments at hot rifted margin. Insights from the Northeastern  
1910 1025 Pyrenean analog. *Tectonophysics* 686, 82-97. <https://doi.org/10.1016/j.tecto.2016.07.022>  
1912 1026  
1913 1027 Clerc, C., Ringenbach, J.-C., Jolivet, L., Ballard, J.-F., 2018. Rifted margins: Ductile  
1914 1028 deformation, boudinage, continentward-dipping normal faults and the role of the weak  
1915 1029 lower crust. *Gondwana Res.* 53, 20-40. <https://doi.org/10.1016/j.gr.2017.04.030>  
1916  
1917  
1918  
1919  
1920

1921  
1922  
1923 1030  
1924 1031 Corre, B., Lagabrielle, Y., Labaume, P., Fourcade, S., Clerc, C., Ballèvre, M., 2016.  
1925 1032 Deformation associated with mantle exhumation in a distal, hot passive margin  
1926 1033 environment: New constraints from the Sarailé Massif (Chaînons Béarnais, North-Pyrenean  
1927 1034 Zone). *Comptes Rendus Geosci.* 348, 279–289. <https://doi.org/10.1016/j.crte.2015.11.007>  
1928 1035  
1929 1036 Cuevas, J., Tubia, J.M., 1999. The discovery of scapolite marbles in the Biscay Synclinorium  
1930 1037 (Basque-Cantabrian basin, Western Pyrenees): geodynamic implications. *Terra Nova* 11,  
1931 1038 259–265. <https://doi.org/10.1046/j.1365-3121.1999.00255.x>  
1932 1039  
1933 1040 Damotte, B., 1998. The ECORS Pyrenean Deep Seismic Surveys, 1985–1994, *Mémoires de la*  
1934 1041 *Société géologique de France*, 173, 104 p., 8 pl.  
1935 1042  
1936 1043 Dañobeitia, J.J., Arguedas, M., Gallart, J., Banda, E., Makris, J., 1992. Deep crustal  
1937 1044 configuration of the Valencia trough and its Iberian and Balearic borders from extensive  
1938 1045 refraction and wide-angle reflection seismic profiling. *Tectonophysics* 203, 37–55.  
1939 1046  
1940 1047 Dauteuil, O., and Ricou, L.-E., 1989. Une circulation de fluides de haute-température à  
1941 1048 l’origine du métamorphisme crétacé nord-pyrénéen. *Geodin. Acta* 3, 237–249.  
1942 1049 <https://doi.org/10.1080/09853111.1989.11105190>  
1943 1050  
1944 1051 de Saint Blanquat, M., Bajolet, F., Grand’Homme, A., Proietti, A., Zanti, M., Boutin, A., Clerc,  
1945 1052 C., Lagabrielle, Y., Labaume, P., 2016. Cretaceous mantle exhumation in the central  
1946 1053 Pyrenees: New constraints from the peridotites in eastern Ariège (North Pyrenean zone,  
1947 1054 France). *Comptes Rendus Geosci.* 348, 268–278. <https://doi.org/10.1016/j.crte.2015.12.003>  
1948 1055  
1949 1056 Debroas E.-J., 1978. Evolution de la fosse du flysch ardoisier de l’Albien supérieur au  
1950 1057 Sénonien inférieur (zone interne métamorphique des Pyrénées navarro-languedociennes),  
1951 1058 *Bull. Soc. Géol. Fr.* (7), XX, p. 639-648.  
1952 1059  
1953 1060 Debroas, E.J., 1990. Le flysch noir albo-cénomanié témoin de la structuration albienne à  
1954 1061 sénonienne de la Zone nord-pyrénéenne en Bigorre (Hautes-Pyrénées, France). *Bull. Soc.*  
1955 1062 *Geol. Fr.* VI, 273–285. <https://doi.org/10.2113/gssgfbull.VI.2.273>  
1956 1063  
1957 1064 DeFelipe, I., Pedreira, D., Pulgar, J.A., Iriarte, E., Mendia, M., 2017. Mantle exhumation and  
1958 1065 metamorphism in the Basque-Cantabrian Basin (N Spain): Stable and clumped isotope  
1959 1066 analysis in carbonates and comparison with ophicalcites in the North-Pyrenean Zone  
1960 1067 (Urdach and Lherz). *Geochem. Geophys. Geosystems* 18, 631–652.  
1961 1068 <https://doi.org/10.1002/2016GC006690>  
1962 1069  
1963 1070 Deramond, J., Souquet, P., Fondécave-Wallez, M.-J., Specht, M., 1993. Relationships  
1964 1071 between thrust tectonics and sequence stratigraphy surfaces in foredeeps: model and  
1965 1072 examples from the Pyrenees (Cretaceous-Eocene, France, Spain). *Geol. Soc. Lond. Spec.*  
1966 1073 *Publ.* 71, 193–219.  
1967 1074  
1968 1075 Dercourt, J., Ricou, L. E., Vrielynck, B., 1993. Atlas Tethys Palaeoenvironmental maps Atlas  
1969 1076 and Explanatory Notes, Gauthier Villars Ed. diffusion CGMW Paris, 307 p., 14 maps  
1970  
1971  
1972  
1973  
1974  
1975  
1976  
1977  
1978  
1979  
1980

1981  
1982  
1983 1077  
1984 1078 Dercourt, J., Zonenshain, L.P., Ricou, L.E. et al., 1986. Geological evolution of the Tethys belt  
1985 1079 from the Atlantic to the Pamirs since the Lias. *Tectonophysics*, 123, 1, 241-315.  
1986 1080  
1987 1081 Ducoux, M., Jolivet, L., Cagnard, F., Gumiaux, C., Baudin, T., Masini, E., Callot, J.P., Aubourg,  
1988 1082 C., Lahfid, A., Homonnay, E., 2019. The Nappe des Marbres unit of the Basque-Cantabrian  
1989 1083 basin: the tectono-thermal evolution of a fossil hyperextended rift basin. *Tectonics*  
1990 1084 submitted.  
1991 1085  
1992 1086 Duret, T., Schmalholz, S.M., 2015. From symmetric necking to localized asymmetric  
1993 1087 shearing: the role of mechanical layering. *Geology*, 43, 8, 711-714.  
1994 1088  
1995 1089 Duret, T., Petri, B., Mohn, G., Schmalholz, S.M., Schenker, F.L., Müntener, O., 2016. The  
1996 1090 importance of structural softening for the evolution and architecture of passive margins. *Sci.*  
1997 1091 *Rep.* 6, 38704. <https://doi.org/10.1038/srep38704>  
1998 1092  
1999 1093 Duret, T., Asti, R., Lagabriele, Y., Brun, J.P., Jourdon, A., Clerc, C., Corre, B., 2019. Numerical  
2000 1094 modelling of syn-rift salt tectonics during Cretaceous Pyrenean Rifting. *Basin Research*, in  
2001 1095 press.  
2002 1096  
2003 1097 Espurt, N., Angrand, P., Teixell, A., Labaume, P., Ford, M., de Saint Blanquat, M, and Chevrot,  
2004 1098 S., 2019. Crustal-scale balanced cross-section and restorations of the Central Pyrenean belt  
2005 1099 (Nest- Cinca transect): superimposed orogenesis and Pyrenean rift system evolution.  
2006 1100 *Tectonophysics*, (to be completed)  
2007 1101  
2008 1102 Ethève, N., Mohn, G., Frizon de Lamotte, D., Roca, E., Tugend, J., Gómez-Romeu, J., 2018.  
2009 1103 Extreme Mesozoic Crustal Thinning in the Eastern Iberia Margin: The Example of the  
2010 1104 Columbrets Basin (Valencia Trough). *Tectonics* 37, 636–662.  
2011 1105  
2012 1106 Fabriès, J., Lorand, J.-P., Bodinier, J.-L., Dupuy, C., 1991. Evolution of the Upper Mantle  
2013 1107 beneath the Pyrenees: Evidence from Orogenic Spinel Lherzolite Massifs. *J. Petrol.*  
2014 1108 *Special\_Volume*, 55–76. [https://doi.org/10.1093/](https://doi.org/10.1093/petrology/Special_Volume.2.55)  
2015 1109  
2016 1110 Fabriès, J., Lorand, J.-P., Bodinier, J.-L., 1998. Petrogenetic evolution of orogenic lherzolite  
2017 1111 massifs in the central and western Pyrenees. *Tectonophysics* 292, 145–167.  
2018 1112  
2019 1113 Floquet, M., 1992. Outcrop sequence stratigraphy in a ramp setting: the Late Cretaceous  
2020 1114 Early Palaeogene deposits of the Castilian Ramp (Spain), *Field Trip Guide Book in conjunction*  
2021 1115 *with the international symposium Sequence Stratigraphy of Mesozoic- Cenozoic European*  
2022 1116 *Basins: CNRS, Institut Français du Pétrole, Dijon. 130 p.*  
2023 1117  
2024 1118 Frasca, G., Gueydan, F., Brun, J.-P., Monié, P., 2016. Deformation mechanisms in a  
2025 1119 continental rift up to mantle exhumation. Field evidence from the western Betics, Spain.  
2026 1120 *Mar. Pet. Geol.* 76, 310–328. [https://doi.org/10.1016/j.](https://doi.org/10.1016/j.marpetgeo.2016.04.020)  
2027 1121  
2028 1122 Fügenschuh, B., Froitzheim, N., Capdevila, R., & Boillot, G. (2003). Offshore granulites from  
2029 1123 the Bay of Biscay margins: Fission tracks constrain a Proterozoic to Tertiary thermal history.

2041  
2042  
2043 1124 Terra Nova, 15, 337–342, doi:10.1046/j.1365-3121.2003.00502.x.  
2044 1125  
2045 1126 Gallart, J., Rojas, H., Diaz, J., Dañobeitia, J.J., 1990. Features of deep crustal structure and the  
2046 1127 onshore-offshore transition at the Iberian flank of the Valencia Trough (Western  
2047 1128 Mediterranean). *J. Geodyn.* 12, 233–252.  
2049 1129  
2050 1130 García-Mondéjar J, Agirrezabala LM, Aranburu A, Fernández-Mendiola PA, Gómez-Pérez I,  
2051 1131 López-Horgue M, Rosales I., 1996. Aptian–Albian tectonic pattern of the Basque–Cantabrian  
2052 1132 Basin (Northern Spain). *Geol J* 31(1):13–45  
2053 1133  
2054 1134 García-Mondéjar J, Fernández-Mendiola PA, Agirrezabala LM, Aranburu A, López-Horgue  
2055 1135 MA, Iriarte E, Martínez de Rituerto S., 2004. Extensión del Aptiense-Albiense en la Cuenca  
2056 1136 Vasco-Cantábrica. SGEIGME, Madrid. Geological Society, London, Special Publications, 282,  
2057 1137 111-138, 1 January, <https://doi.org/10.1144/SP282.6>  
2059 1138  
2060 1139 Gartrell, A.P., 1997. Evolution of rift basins and low-angle detachments in multilayer analog  
2061 1140 models. *Geology* 25, 615–618. doi:10.1130/0091-7613(1997)025<0615:EORBAL>2.3.CO;2  
2062 1141  
2063 1142 Gernigon, L., Brönnner, M., Roberts, D., Olesen, O., Nasuti, A., Yamasaki, T., 2014. Crustal and  
2064 1143 basin evolution of the southwestern Barents Sea: From Caledonian orogeny to continental  
2065 1144 breakup: Evolution of the Barents Sea. *Tectonics* 33, 347–373.  
2066 1145 <https://doi.org/10.1002/2013TC003439>  
2068 1146  
2069 1147 Golberg, J.-M., Guiraud, M., Maluski, H., Séguret, M., 1988. Caractères pétrologiques et âge  
2070 1148 du métamorphisme en contexte distensif du bassin sur décrochement de Soria (Crétacé  
2071 1149 inférieur, Nord Espagne). *Comptes Rendus de l'Académie des Sciences Paris, Série* 11,307,  
2072 1150 521-527.  
2073 1151  
2074 1152 Golberg, J.M., Leyreloup, A.F., 1990. High temperature-low pressure Cretaceous  
2075 1153 metamorphism related to crustal thinning (Eastern North Pyrenean Zone, France). *Contrib.*  
2076 1154 *Mineral. Petrol.* 104, 194–207. <https://doi.org/10.1007/BF00306443>  
2077 1155  
2078 1156 Gong, Z., Langereis, C.G., Mullender, T.A.T., 2008. The rotation of Iberia during the Aptian  
2079 1157 and the opening of the Bay of Biscay. *Earth Planet. Sci. Lett.* 273, 80–93.  
2080 1158 <https://doi.org/10.1016/j.epsl.2008.06.016>  
2081 1159  
2082 1160 Grool, A. R., Ford, M., Vergés, J., Huisman, R. S., Christophoul, F., & Dielforder, A. (2018).  
2083 1161 Insights into the crustal-scale dynamics of a doubly vergent orogen from a quantitative  
2084 1162 analysis of its forelands: A case study of the Eastern Pyrenees. *Tectonics*, 37.  
2085 1163 <https://doi.org/10.1002/2017TC004731>  
2086 1164  
2087 1165 Guimerà, J., Alonso, Á., Mas, J.R., 1995. Inversion of an extensional-ramp basin by a newly  
2088 1166 formed thrust: the Cameros basin (N. Spain). ). in: *Basin Inversion* (J.G. Buchanan, P.G.  
2089 1167 Buchanan, Eds). Geological Society, Special Publication, 88, 433-453.  
2090 1168 <https://doi.org/10.1144/GSL.SP.1995.088.01.23>  
2091 1169  
2092 1170 Guiraud, M., Séguret, M., 1985. A releasing solitary overstep model for the late Jurassic–

2101  
2102  
2103 1171 early Cretaceous (Wealdian) Soria strike-slip basin (Northern Spain). In: Biddle KT, Christie-  
2104 1172 Blick N (eds) Strike slip deformation, basin formation and sedimentation, vol 37., SEPM  
2105 1173 Special Publication Society of Economic Paleontologists and Mineralogists, Tulsa, pp 159-  
2106 1174 175.  
2107  
2108 1175  
2109 1176 Hamilton, W., 1987. Crustal extension in the Basin and Range Province, southwestern United  
2110 1177 States. Geol. Soc. Lond. Spec. Publ. 28, 155-176.  
2111 1178 <https://doi.org/10.1144/GSL.SP.1987.028.01.12>  
2112 1179  
2113 1180 Huismans, R. S., Beaumont, C., 2007. Roles of lithospheric strain softening and heterogeneity  
2114 1181 in determining the geometry of rifts and continental margins  
2115  
2116 1182  
2117 1183 Huismans, R.S., Beaumont, C., 2011. Depth-dependent extension, two-stage breakup and  
2118 1184 cratonic underplating at rifted margins. Nature 473, 74-78.  
2119 1185 <https://doi.org/10.1038/nature09988>  
2120 1186  
2121 1187 Huismans, R.S., Beaumont, C., 2014. Rifted continental margins: The case for depth-  
2122 1188 dependent extension. Earth Planet. Sci. Lett. 407, 148-162. doi:10.1016/j.epsl.2014.09.032  
2123 1189  
2124 1190 James, V., Canérot, J., 1988. Diapirisme et structuration post-triasique des Pyrénées  
2125 1191 occidentales et de l'Aquitaine méridionale (France). Eclogae Geol. Helveticae 92, 63-72.  
2126 1192  
2127 1193 Jammes, S., Lavier, L., Manatschal, G., 2010a. Extreme crustal thinning in the Bay of Biscay  
2128 1194 and the Western Pyrenees: From observations to modeling. Geochem. Geophys.  
2129 1195 Geosystems 11. <https://doi.org/10.1029/2010GC003218>  
2130 1196  
2131 1197 Jammes, S., Tiberi, C., Manatschal, G., 2010b. 3D architecture of a complex transcurrent rift  
2132 1198 system: The example of the Bay of Biscay-Western Pyrenees. Tectonophysics 489, 210-226.  
2133 1199 <https://doi.org/10.1016/j.tecto.2010.04.023>  
2134 1200  
2135 1201 Jammes, S., Manatschal, G., Lavier, L., 2010c. Interaction between prerift salt and  
2136 1202 detachment faulting in hyperextended rift systems: The example of the Parentis and  
2137 1203 Mauléon basins (Bay of Biscay and western Pyrenees). AAPG Bull. 94, 957-975.  
2138 1204 <https://doi.org/10.1306/12090909116>  
2139 1205  
2140 1206 Jammes, S., Lavier, L.L., Reber, J.E., 2015. Localization and delocalization of deformation in a  
2141 1207 biminerale material. J. Geophys. Res. Solid Earth 120, 3649-3663.  
2142 1208 <https://doi.org/10.1002/2015JB011890>  
2143 1209  
2144 1210 Jammes, S., Lavier, L.L., 2016. The effect of biminerale composition on extensional processes  
2145 1211 at lithospheric scale. Geochem. Geophys. Geosystems 17, 3375-3392.  
2146 1212 <https://doi.org/10.1002/2016GC006399>  
2147 1213  
2148 1214 Jammes, S., Manatschal, G., Lavier, L., Masini, E., 2009. Tectono-sedimentary evolution  
2149 1215 related to extreme crustal thinning ahead of a propagating ocean: Example of the western  
2150 1216 Pyrenees. Tectonics 28. <https://doi.org/10.1029/2008TC002406>  
2151 1217  
2152  
2153  
2154  
2155  
2156  
2157  
2158  
2159  
2160

2161  
2162  
2163 1218 Jolivet, L., Gorini, C., Smit, J., Leroy, S., 2015. Continental breakup and the dynamics of rifting  
2164 1219 in back-arc basins: The Gulf of Lion margin: Backarc rift and lower crust extraction. *Tectonics*  
2165 1220 34, 662–679. <https://doi.org/10.1002/2014TC003570>  
2166 1221  
2167 1222 Lagabrielle, Y., Bodinier, J.-L., 2008. Submarine reworking of exhumed sub-continental  
2168 1223 mantle rocks: field evidence from the Lherz peridotites, French Pyrenees: Cretaceous  
2169 1224 exhumation of pyrenean mantle. *Terra Nova* 20, 11–21. [https://doi.org/10.1111/j.1365-](https://doi.org/10.1111/j.1365-3121.2007.00781.x)  
2170 1225 3121.2007.00781.x  
2171 1226  
2172 1227 Lagabrielle, Y., Labaume, P., de Saint Blanquat, M., 2010. Mantle exhumation, crustal  
2173 1228 denudation, and gravity tectonics during Cretaceous rifting in the Pyrenean realm (SW  
2174 1229 Europe): Insights from the geological setting of the Iherzolite bodies. *Tectonics* 29.  
2175 1230 <https://doi.org/10.1029/2009TC002588>  
2176 1231  
2177 1232 Lagabrielle, Y., Clerc, C., Vauchez, A., Lahfid, A., Labaume, P., Azambre, B., Fourcade, S.,  
2178 1233 Dautria, J.-M., 2016. Very high geothermal gradient during mantle exhumation recorded in  
2179 1234 mylonitic marbles and carbonate breccias from a Mesozoic Pyrenean palaeomargin (Lherz  
2180 1235 area, North Pyrenean Zone, France). *Comptes Rendus Geosci.* 348, 290–300.  
2181 1236 <https://doi.org/10.1016/j.crte.2015.11.004>  
2182 1237  
2183 1238 Lagabrielle Y, Asti R, Fourcade S, Corre B, Pujol M, Uzel J, Labaume P, Clerc C, Lafay R,  
2184 1239 Picazo S, Maury R. 2019. Mantle exhumation at magma-poor passive continental margins.  
2185 1240 Part I. 3D architecture and metasomatic evolution of a fossil exhumed mantle domain  
2186 1241 (Urdach Iherzolite, north-western Pyrenees, France), *BSGF - Earth Sciences Bulletin* 190: 8.  
2187 1242 <https://doi.org/10.1051/bsgf/2019007>  
2188 1243  
2189 1244  
2190 1245 Lagabrielle, Y., Asti, R., Fourcade, S., Corre, B., Uzel, J., Labaume, P., Clerc, C., Lafay, R.,  
2191 1246 Picazo, S., 2019b. The mechanisms of mantle exhumation at magma-poor passive  
2192 1247 continental margins. Part II. Insights from high-displacement, low-angle faults preserved in a  
2193 1248 fossil distal margin domain (Sarailé Iherzolites, north-western Pyrenees, France). *BSGF Earth*  
2194 1249 *Science Bull.*, in press.  
2195 1250  
2196 1251 Le Pichon, X., Bonnin, J., Francheteau, J., Sibuet, J.C., 1971. Une hypothèse d'évolution  
2197 1252 tectonique du Golfe de Gascogne. *Hist. Struct. Golfe Gasc.* 2, 11–44.  
2198 1253  
2199 1254 Lenoble, J.-L., Canérot, J., 1992. La lame extrusive de Pont Suzon (Zone Nord-Pyrénéenne en  
2200 1255 Vallée d'Aspe): reprise pyrénéenne d'une ride diapirique transverse d'âge créacé. *Comptes*  
2201 1256 *Rendus Académie Sci. Sér. 2 Mécanique Phys. Chim. Sci. Univers Sci. Terre* 314, 387–391.  
2202 1257  
2203 1258 Lister, G.S. and Davis, G.A. 1989. The origin of metamorphic core complexes and detachment  
2204 1259 faults formed during Tertiary continental extension in the northern Colorado River region,  
2205 1260 U.S.A. *Journal of Structural Geology*, Vol. 11, No. 112, pp. 65 to 94,  
2206 1261  
2207 1262 Lister, G.S., Etheridge, M.A., Symonds, P.A., 1991. Detachment models for the formation of  
2208 1263 passive continental margins. *Tectonics* 10, 1038–1064.  
2209 1264  
2210  
2211  
2212  
2213  
2214  
2215  
2216  
2217  
2218  
2219  
2220

2221  
2222  
2223 1265 Lopez-Mir, B., Muñoz, J.A., García Senz, J., 2014. Restoration of basins driven by extension  
2224 1266 and salt tectonics: Example from the Cotiella Basin in the central Pyrenees. *J. Struct. Geol.*  
2225 1267 69, Part A, 147–162. <https://doi.org/10.1016/j.jsg.2014.09.022>  
2226 1268  
2227  
2228 1269 Manatschal, G., 2004. New models for evolution of magma-poor rifted margins based on a  
2229 1270 review of data and concepts from West Iberia and the Alps. *Int. J. Earth Sci.* 93.  
2230 1271 <https://doi.org/10.1007/s00531-004-0394-7>  
2231 1272  
2232 1273 Manatschal, G., Froitzheim, N., Rubenach, M., Turrin, B.D., 2001. The role of detachment  
2233 1274 faulting in the formation of an ocean-continent transition: insights from the Iberia Abyssal  
2234 1275 Plain. *Geol. Soc. Lond. Spec. Publ.* 187, 405–428.  
2235 1276 <https://doi.org/10.1144/GSL.SP.2001.187.01.20>  
2236 1277  
2237  
2238 1278 Manatschal, G., Engström, A., Desmurs, L., Schaltegger, U., Cosca, M., Müntener, O.,  
2239 1279 Bernoulli, D., 2006. What is the tectono-metamorphic evolution of continental break-up: The  
2240 1280 example of the Tasna Ocean–Continent Transition. *J. Struct. Geol.* 28, 1849–1869.  
2241 1281 <https://doi.org/10.1016/j.jsg.2006.07.014>  
2242 1282  
2243 1283 Mas. R., Benito MI, Arribas J, Alonso A, Arribas ME, González-Acebrón L, Hernán J, Quijada E,  
2244 1284 Suárez-González P, Omodeo Salè S (2011) Evolution of an intra-plate rift basin: the Latest  
2245 1285 Jurassic-Early Cretaceous Cameros Basin (Northwest Iberian Ranges, North Spain). In: Post-  
2246 1286 Meeting field trips 28th IAS Meeting, vol Geoguías 8. Zaragoza (Spain)  
2247 1287  
2248  
2249 1288 Masini, E., Manatschal, G., Tugend, J., Mohn, G., Flament, J.-M., 2014. The tectono-  
2250 1289 sedimentary evolution of a hyper-extended rift basin: the example of the Arzacq–Mauléon  
2251 1290 rift system (Western Pyrenees, SW France). *Int. J. Earth Sci.* 103, 1569–1596.  
2252 1291 <https://doi.org/10.1007/s00531-014-1023-8>  
2253 1292  
2254 1293 McClay, K., Muñoz, J.-A., García-Senz, J., 2004. Extensional salt tectonics in a contractional  
2255 1294 orogen: A newly identified tectonic event in the Spanish Pyrenees. *Geology* 32, 737–740.  
2256 1295 <https://doi.org/10.1130/G20565.1>  
2257 1296  
2258 1297 McKenzie, D., 1978. Some remarks on the development of sedimentary basins. *Earth Planet.*  
2259 1298 *Sci. Lett.* 40, 25–32. [https://doi.org/10.1016/0012-821X\(78\)90071-7](https://doi.org/10.1016/0012-821X(78)90071-7)  
2260 1299  
2261 1300 Mendia, M., and Gil Ibarra, J. I. 1991. High-grade metamorphic rocks and peridotites  
2262 1301 along the Leiza Fault (Western Pyrenees, Spain), *Geologische Rundschau* 80/1.  
2263 1302  
2264 1303 Michon, L. and Merle, O. 2003. Mode of lithospheric extension: Conceptual models from  
2265 1304 analogue modeling. *Tectonics*, 22 (4), pp.1028. <https://doi.org/10.1029/2002TC001435>  
2266 1305  
2267 1306 Mohn, G., Karner, G.D., Manatschal, G., Johnson, C.A., 2015. Structural and stratigraphic  
2268 1307 evolution of the Iberia–Newfoundland hyper-extended rifted margin: a quantitative  
2269 1308 modelling approach. *Geol. Soc. Lond. Spec. Publ.* 413, 53–89.  
2270 1309 <https://doi.org/10.1144/SP413.9>  
2271 1310  
2272  
2273  
2274  
2275  
2276  
2277  
2278  
2279  
2280



2281  
2282  
2283  
2284  
2285  
2286  
2287  
2288  
2289  
2290  
2291  
2292  
2293  
2294  
2295  
2296  
2297  
2298  
2299  
2300  
2301  
2302  
2303  
2304  
2305  
2306  
2307  
2308  
2309  
2310  
2311  
2312  
2313  
2314  
2315  
2316  
2317  
2318  
2319  
2320  
2321  
2322  
2323  
2324  
2325  
2326  
2327  
2328  
2329  
2330  
2331  
2332  
2333  
2334  
2335  
2336  
2337  
2338  
2339  
2340

1311 Mohn, G., Manatschal, G., Beltrando, M., Masini, E., Kuznir, N., 2012. Necking of continental  
1312 crust in magma-poor rifted margins: Evidence from the fossil Alpine Tethys margins: Necking  
1313 of continental crust. *Tectonics* 31, n/a-n/a. <https://doi.org/10.1029/2011TC002961>  
1314  
1315 Mohn, G., Manatschal, G., Müntener, O., Beltrando, M., Masini, E., 2010. Unravelling the  
1316 interaction between tectonic and sedimentary processes during lithospheric thinning in the  
1317 Alpine Tethys margins. *Int. J. Earth Sci.* 99, 75–101. <https://doi.org/10.1007/s00531-010->  
1318 0566-6  
1319  
1320 Monchoux, P., 1970. Les lherzolites pyrénéennes: contribution à l'étude de leur minéralogie,  
1321 de leur genèse et de leurs transformations. Université Paul Sabatier de Toulouse (Sciences).  
1322  
1323 Muñoz, J.A., 1992. Evolution of a continental collision belt: ECORS-Pyrenees crustal balanced  
1324 cross-section, in: *Thrust Tectonics*. Springer, pp. 235–246.  
1325  
1326 Nagel, T. J. and Buck, W. R., 2004. Symmetric alternative to asymmetric rifting models.  
1327 *Geology*, 32, 11. pp 937-940 Doi 10.1130/G20785.1  
1328  
1329 Olivet, J.L., 1996. La cinématique de la plaque ibérique. *Bull Cent Rech Explor Prod Elf*  
1330 *Aquitaine* 20, 131–195.  
1331  
1332 Omodeo Salè, S., Guimerà, J., Mas, R., & Arribas, J. (2014). Tectono-stratigraphic evolution of  
1333 an inverted extensional basin: The Cameros Basin (north of Spain). *International Journal of*  
1334 *Earth Sciences*, 103(6), 1597–1620. <https://doi.org/10.1007/s00531-014-1026-5>  
1335  
1336 Ortí, F., Pérez-López, A., Salvany, J.M., 2017. Triassic evaporites of Iberia: Sedimentological  
1337 and palaeogeographical implications for the western Neotethys evolution during the Middle  
1338 Triassic–Earliest Jurassic. *Palaeogeogr. Palaeoclimatol. Palaeoecol.* 471, 157–180.  
1339 <https://doi.org/10.1016/j.palaeo.2017.01.025>  
1340  
1341 Osmundsen, P.T., Ebbing, J., 2008. Styles of extension offshore mid-Norway and implications  
1342 for mechanisms of crustal thinning at passive margins: STYLES OF EXTENSION OFFSHORE  
1343 NORWAY. *Tectonics* 27, n/a-n/a. <https://doi.org/10.1029/2007TC002242>  
1344  
1345 Osmundsen, P.T., Péron-Pinvidic, G., 2018. Crustal-Scale Fault Interaction at Rifted Margins  
1346 and the Formation of Domain-Bounding Breakaway Complexes: Insights From Offshore  
1347 Norway. *Tectonics* 37, 935–964. <https://doi.org/10.1002/2017TC004792>  
1348  
1349 Pedrera, A., García-Senz, J., Ayala, C., Ruiz-Constán, A., Rodríguez-Fernández, L. R., Robador,  
1350 A., & GonzálezMenéndez, L. (2017). Reconstruction of the exhumed mantle across the North  
1351 Iberian Margin by crustal-scale 3-D gravity inversion and geological cross section. *Tectonics*,  
1352 36. <https://doi.org/10.1002/2017TC004716>  
1353  
1354 Péron-Pinvidic, G., Manatschal, G., Minshull, T.A., Sawyer, D.S., 2007. Tectonosedimentary  
1355 evolution of the deep Iberia-Newfoundland margins: Evidence for a complex breakup  
1356 history. *Tectonics* 26, 1–19. <https://doi.org/10.1029/2006TC001970>  
1357

2341  
2342  
2343 1358 Péron-Pinvidic, G., Manatschal, G., 2009. The final rifting evolution at deep magma-poor  
2344 1359 passive margins from Iberia-Newfoundland: a new point of view. *Int. J. Earth Sci.* 98, 1581–  
2345 1360 1597. <https://doi.org/10.1007/s00531-008-0337-9>  
2346 1361  
2347  
2348 1362 Pinet, B., Montadert, L., ECORS Scientific Party, 1987. Deep seismic reflection and refraction  
2349 1363 profiling along the Aquitaine shelf (Bay of Biscay). *Geophys. J. Int.* 89, 305–312.  
2350 1364 <https://doi.org/10.1111/j.1365-246X.1987.tb04423.x>  
2351 1365  
2352 1366 Puigdefàbregas, C., Souquet, P., 1986. Tecto-sedimentary cycles and depositional sequences  
2353 1367 of the Mesozoic and Tertiary from the Pyrenees. *Tectonophysics* 129, 173–203.  
2354 1368  
2355 1369 Rat, P., 1988. The Basque–Cantabrian basin between the Iberian and European plates: some  
2356 1370 facts but still many problems. *Rev Soc Geol Esp* 1(3–4):327–348  
2357 1371  
2358  
2359 1372 Rat, P., Amiot, M., Feuillée, P., Floquet, M., Mathey, B., Pascal, A., Salomon, J., García  
2360 1373 Mondéjar, J., Pujalte, J., Lamolda, M., et al., 1983. Vue sur le Cretacé basco-cantabrique et  
2361 1374 nord-ibérique. Une marge, son arrière-pays, ses environ. sédimentaires. *Mémoires Géol.*  
2362 1375 *Univ. Dijon* 9, 191.  
2363 1376  
2364 1377 Rat, J., Mouthereau, F., Brichau, S., Crémadès, A., Bernet, M., Balvay, M., Ganne, J., Lahfid,  
2365 1378 A., Gautheron, C., 2019. Tectonothermal Evolution of the Cameros Basin: Implications for  
2366 1379 Tectonics of North Iberia. *Tectonics* 38, 440–469. <https://doi.org/10.1029/2018TC005294>  
2367 1380  
2368 1381 Ravier, J., 1959. Le métamorphisme des terrains secondaires des Pyrénées. *Mémoires de la*  
2369 1382 *Société Géologique de France*, N° 86, 250 p., 19 flg., 9 pl. phot.  
2370 1383  
2371 1384 Reston, T., McDermott, K., 2014. An assessment of the cause of the ‘extension discrepancy’  
2372 1385 with reference to the west Galicia margin. *Basin Res.* 26, 135–153.  
2373 1386 <https://doi.org/10.1111/bre.12042>  
2374 1387  
2375 1388 Reston, T.J., 1988. Evidence for shear zones in the lower crust offshore Britain. *Tectonics* 7,  
2376 1389 929–945. <https://doi.org/10.1029/TC007i005p00929>  
2377 1390  
2378 1391 Reston, T.J., Krawczyk, C.M., Hoffmann, H.-J., 1995. Detachment tectonics during Atlantic  
2379 1392 rifting: analysis and interpretation of the S reflection, the west Galicia margin. *Geol. Soc.*  
2380 1393 *Lond. Spec. Publ.* 90, 93–109. <https://doi.org/10.1144/GSL.SP.1995.090.01.05>  
2381 1394  
2382 1395 Reston, T.J., Pérez-Gussinyé, M., 2007. Lithospheric extension from rifting to continental  
2383 1396 breakup at magma-poor margins: rheology, serpentinitisation and symmetry. *Int. J. Earth Sci.*  
2384 1397 96, 1033–1046. <https://doi.org/10.1007/s00531-006-0161-z>  
2385 1398  
2386 1399 Roca, E., Muñoz, J.A., Ferrer, O., Ellouz, N., 2011. The role of the Bay of Biscay Mesozoic  
2387 1400 extensional structure in the configuration of the Pyrenean orogen: Constraints from the  
2388 1401 MARCONI deep seismic reflection survey. *Tectonics* 30.  
2389 1402 <https://doi.org/10.1029/2010TC002735>  
2390 1403  
2391  
2392  
2393  
2394  
2395  
2396  
2397  
2398  
2399  
2400

2401  
2402  
2403  
2404  
2405  
2406  
2407  
2408  
2409  
2410  
2411  
2412  
2413  
2414  
2415  
2416  
2417  
2418  
2419  
2420  
2421  
2422  
2423  
2424  
2425  
2426  
2427  
2428  
2429  
2430  
2431  
2432  
2433  
2434  
2435  
2436  
2437  
2438  
2439  
2440  
2441  
2442  
2443  
2444  
2445  
2446  
2447  
2448  
2449  
2450  
2451  
2452  
2453  
2454  
2455  
2456  
2457  
2458  
2459  
2460

1404 Roma, M., Ferrer, O., Roca, E., Pla, O., Escosa, F., Butillé, M., 2018. Formation and inversion  
1405 of salt-detached ramp-syncline basins. Results from analog modeling and application to the  
1406 Columbrets Basin (Western Mediterranean), *Tectonophysics* 10.1016/j.tecto.2018.08.012  
1407  
1408 Roure, F., Choukroune, P., 1998. Contribution of the ECORS seismic data to the Pyrenean  
1409 geology: Crustal architecture and geodynamic evolution of the Pyrenees. *Mém. Société*  
1410 *Géologique Fr.* 173, 37–52.  
1411  
1412 Rowan, M.G., 2014. Passive-margin salt basins: hyperextension, evaporite deposition, and  
1413 salt tectonics. *Basin Res.* 26, 154–182. <https://doi.org/10.1111/bre.12043>  
1414  
1415 Ruiz, M., 2007. Caracterització estructural i sismotectònica de la litosfera en el Domini  
1416 Pirenaico-Cantàbric a partir de mètodes de sísmica activa i passiva, Ph.D. thesis, Univ. of  
1417 Barcelona, Barcelona, Spain.  
1418  
1419 Salas, R., Casas, A., 1993. Mesozoic extensional tectonics, stratigraphy and crustal evolution  
1420 during the Alpine cycle of the eastern Iberian basin. *Tectonophysics* 228, 33–55.  
1421 [https://doi.org/10.1016/0040-1951\(93\)90213-4](https://doi.org/10.1016/0040-1951(93)90213-4)  
1422  
1423 Salas, R., Guimerà, J., Mas, R., Martín-Closas, C., Meléndez, A., Alonso, Á., 2001. Evolution of  
1424 the Mesozoic Central Iberian Rift System and its Cainozoic inversion (Iberian chain). In:  
1425 Ziegler PA, Cavazza W, Robertson AHF, Crasquin-Soleau S (eds), *Peri-Tethys Memoir 6: Peri-*  
1426 *Tethyan Rift/Wrench Basins and Passive Margins*, vol 186. *Mémoires du Museum National*  
1427 *d'Histoire Naturelle*, Paris, pp 145–186  
1428  
1429 Saspiturry, N., Razin, P., Baudin, T., Serrano, O., Issautier, B., Lasseur, E., Allanic, C., Thion,  
1430 I., Leleu, S., 2019. Symmetry vs. asymmetry of a hyper-thinned rift: Example of the Mauléon  
1431 Basin (Western Pyrenees, France). *Mar. Pet. Geol.* 104, 86–105.  
1432 <https://doi.org/10.1016/j.marpetgeo.2019.03.031>  
1433  
1434 Saura, E., Ardèvol i Oró, L., Teixell, A., Vergés, J., 2016. Rising and falling diapirs, shifting  
1435 depocenters, and flap overturning in the Cretaceous Sopeira and Sant Gervàs subbasins  
1436 (Ribagorça Basin, southern Pyrenees): Southern Pyrenees Cretaceous Diapirism. *Tectonics*  
1437 35, 638–662. <https://doi.org/10.1002/2015TC004001>  
1438  
1439 Scotese, C.R. and Schettino, A., 2017. Late Permian-Early Jurassic paleogeography of  
1440 Western Tethys and the world. In Soto et al., eds, *Permo-Triassic salt provinces of Europe,*  
1441 *North Africa and the Atlantic margins. Tectonics and Hydrocarbon potential.* Elsevier, pp. 57-  
1442 91.  
1443  
1444 Sibuet, J.-C., Srivastava, S.P., Spakman, W., 2004. Pyrenean orogeny and plate kinematics. *J.*  
1445 *Geophys. Res. Solid Earth* 109, B08104. <https://doi.org/10.1029/2003JB002514>  
1446  
1447 Soto, J.I, Flinch, J.F. and Tari, G., 2017. Permo-Triassic salt provinces of Europe, North Africa  
1448 and the Atlantic margins: A synthesis. In Soto et al., eds, *Permo-Triassic salt provinces of*  
1449 *Europe, North Africa and the Atlantic margins. Tectonics and Hydrocarbon potential.*  
1450 Elsevier, pp. 3-41.

2461  
2462  
2463 1451  
2464 1452 Sutra, E., Manatschal, G., Mohn, G., Unternehr, P., 2013. Quantification and restoration of  
2465 1453 extensional deformation along the Western Iberia and Newfoundland rifted margins. *Geoch.*  
2466 1454 *Geoph. Geosys.* 14 (8), 2575e2597.  
2467 1455  
2468 1456 Teixell, A., 1998. Crustal structure and orogenic material budget in the west central  
2469 1457 Pyrenees. *Tectonics* 17, 395–406. <https://doi.org/10.1029/98TC00561>  
2470 1458  
2471 1459 Teixell, A., Labaume, P., Lagabrielle, Y., 2016. The crustal evolution of the west-central  
2472 1460 Pyrenees revisited: Inferences from a new kinematic scenario. *Comptes Rendus Geosci.* 348,  
2473 1461 257–267. <https://doi.org/10.1016/j.crte.2015.10.010>  
2474 1462  
2475 1463 Teixell, A., Labaume, P., Ayarza, P., Espurt, N., de Saint Blanquat, M., Lagabrielle, Y., 2018.  
2476 1464 Crustal structure and evolution of the Pyrenean-Cantabrian belt: A review and new  
2477 1465 interpretations from recent concepts and data. *Tectonophysics* 724, 146–170.  
2478 1466 <https://doi.org/10.1016/j.tecto.2018.01.009>  
2479 1467  
2480 1468 Thiébault J., Durand-Wackenheim C., Debeaux M. and Souquet P., 1992. Métamorphisme  
2481 1469 des évaporites triasiques du versant nord des Pyrénées centrales et occidentales. *Bull. Soc.*  
2482 1470 *Hist. Nat. Toulouse.* 128, 77-84.  
2483 1471  
2484 1472 Thinon, I., Matias, L., Réhault, J.P., Hirn, A., Fidalgo-González, L., Avedik, F., 2003. Deep  
2485 1473 structure of the Armorican Basin (Bay of Biscay): a review of Norgasis seismic reflection and  
2486 1474 refraction data. *J. Geol. Soc.* 160, 99–116. <https://doi.org/10.1144/0016-764901-103>  
2487 1475  
2488 1476 Tirel, C., Brun, J.-P. and Burov, E., 2008. Dynamics and structural development of  
2489 1477 metamorphic core complexes. *Journal of Geophysical Research*, 113(B4): B04403.  
2490 1478  
2491 1479 Tomassimo, A., Marillier, F., 1997. Processing and interpretation in the tau-p domain of the  
2492 1480 ECORS Bay of Biscay expanding spread profiles. *Mém. Société Géologique Fr.* 171, 31–43.  
2493 1481  
2494 1482 Tugend, J., Manatschal, G. and Kuszniir, N.J., 2015. Spatial and temporal evolution of  
2495 1483 hyperextended rift systems: Implication for the nature, kinematics, and timing of the  
2496 1484 Iberian-European plate boundary, *Geology*, 43(1), 15–18, doi:10.1130/G36072.1.  
2497 1485  
2498 1486 Tugend, J., Manatschal, G., Kuszniir, N.J., Masini, E., Mohn, G., Thinon, I., 2014. Formation  
2499 1487 and deformation of hyperextended rift systems: Insights from rift domain mapping in the  
2500 1488 Bay of Biscay-Pyrenees. *Tectonics* 33, 1239–1276. <https://doi.org/10.1002/2014TC003529>  
2501 1489  
2502 1490 Vergés, J., García-Senz, J., 2001. Mesozoic evolution and Cainozoic inversion of the Pyrenean  
2503 1491 rift. *Mém. Muséum Natl. Hist. Nat.* 186, 187–212.  
2504 1492  
2505 1493 Vielzeuf, D., Kornprobst, J., 1984. Crustal splitting and the emplacement of Pyrenean  
2506 1494 Iherzolites and granulites. *Earth Planet. Sci. Lett.* 67, 87–96. [https://doi.org/10.1016/0012-](https://doi.org/10.1016/0012-821X(84)90041-4)  
2507 1495 [821X\(84\)90041-4](https://doi.org/10.1016/0012-821X(84)90041-4)  
2508 1496  
2509 1497 Vissers, R.L.M., Drury, M.R., Newman, J. and Fliervoet, T.F., 1997. Mylonitic deformation in  
2510  
2511  
2512  
2513  
2514  
2515  
2516  
2517  
2518  
2519  
2520

2521  
2522  
2523 1498 upper mantle peridotites of the North Pyrenean Zone (France) : implications for strength  
2524 1499 and strain localization in the lithosphere. *Tectonophysics*, 279, 303-325.  
2525 1500  
2526 1501 Wang, Y., Chevrot, S., Monteiller, V., Komatitsch, D., Mouthereau, F., Manatschal, G.,  
2527 1502 Sylvander, M., Diaz, J., Ruiz, M., Grimaud, F., Benahmed, S., Pauchet, H., Martin, R., 2016.  
2528 1503 The deep roots of the western Pyrenees revealed by full waveform inversion of teleseismic P  
2529 1504 waves. *Geology* 44, 475–478. <https://doi.org/10.1130/G37812.1>  
2530 1505  
2531 1506 Wernicke, B., 1981. Low-angle normal faults in the Basin and Range Province: nappe  
2532 1507 tectonics in an extending orogen. *Nature* 291, 645–648. <https://doi.org/10.1038/291645a0>  
2533 1508  
2534 1509 Wernicke, B., 1985. Uniform-sense normal simple shear of the continental lithosphere. *Can.*  
2535 1510 *J. Earth Sci.* 22, 108–125. <https://doi.org/10.1139/e85-009>  
2536 1511  
2537 1512 Ziegler, 1988. Evolution of Arctic-North Atlantic and western Tethys. Tulsa. AAPG Memoir,  
2538 1513 43, 198 pp.  
2539 1514  
2540 1515 Zamora, G., Fleming, M., Gallastegui, J., 2017. Salt Tectonics Within the Offshore Asturian  
2541 1516 Basin: North Iberian Margin, in Soto, J.I, Flinch, J.F. and Tari, G., 2017. Permo-Triassic salt  
2542 1517 provinces of Europe, North Africa and the Atlantic margins: A synthesis. In Soto et al., eds,  
2543 1518 Permo-Triassic salt provinces of Europe, North Africa and the Atlantic margins. *Tectonics and*  
2544 1519 *Hydrocarbon potential*. Elsevier, pp. 353-367.  
2545 1520  
2546 1521  
2547 1522  
2548  
2549  
2550  
2551  
2552  
2553  
2554  
2555  
2556  
2557  
2558  
2559  
2560  
2561  
2562  
2563  
2564  
2565  
2566  
2567  
2568  
2569  
2570  
2571  
2572  
2573  
2574  
2575  
2576  
2577  
2578  
2579  
2580

2581  
2582  
2583 **1523 Figure captions**  
2584

2585 1524

2587 **1525 Figure 1. Location of the studied basins and their paleogeographic position during the**  
2588  
2589 **1526 Cretaceous at the onset of the Iberia drift.**

2590 1527 (a) Simplified structural map of the Cantabrian-Pyrenean orogenic system and adjoining  
2592 Iberia showing Eurasia deformed and undeformed domain (modified from Verges and Garcia-  
2593 Senz, 2001 and Teixell et al., 2018). (b) Hypothetical reconstruction at the onset of the Iberia  
2594 drift (modified after Tugend et al., 2014).  
2596

2597 1531

2599 **1532 Figure 2. A compilation of Cretaceous basins architecture from the Cantabrian-Pyrenean**  
2600 **1533 belt.**

2602 1534 Reconstructions from field and geophysical data collected by various authors in the Basque-  
2603 Cantabrian basin (a, b, c) and in the North Pyrenean Zone (NPZ): Mauléon basin (d),  
2605 Chainons Béarnais (e, f), Baronnies basin (g) and Agly massif-Boucheville basin (h).  
2606

2607 1537

2609 **1538 Figure 3. Structure and evolution of Iberia-Newfoundland-type and Alpine-type passive**  
2611 **1539 margins** (modified from Péron-Pinvidic and Manatschal, 2009 and Mohn et al., 2012).

2613 1540 (a): two sketches showing the main concepts linked to Iberia-Newfoundland-type margin  
2614 evolution, namely: (i) strong final asymmetry with upper and lower plates separated by a  
2615 single detachment fault (HHD, Hobby High detachment), (ii) emplacement of extensional  
2616 allochthons as rigid crustal blocks over the exhumed mantle. (b): strain distribution and  
2617 strain partitioning during lithospheric thinning at magma-poor rifted margin, with example  
2618 from the fossil Alpine Tethys margin. In this model, the pre-rift cover remains welded on the  
2619 tilted crustal blocks; the middle crust is thinned to zero and the upper crust and upper  
2620 mantle are juxtaposed at the break up stage. The concepts shown in (a) and (b) contrast with  
2621 the concepts attached to the smooth-slopes basins evolution developed in this paper.  
2622

2623 1549

2630 **1550 Figure 4. The geological record of the Cretaceous extension in the Paleozoic basement and**  
2631 **1551 exhumed mantle of the North Pyrenean Zone (NPZ).**

2633 1552 The map shows the location of mantle bodies and crustal units illustrated in photographs a  
2634 to k. (a): dated crustal mylonites associated with the Urdach Iherzolites; thin section  
2635

2641  
2642  
2643 1554 microphotograph (natural light) of the leucocratic gneissic mylonite exposed at Col d'Urdach  
2644  
2645 1555 and containing numerous micafishes (dating by the Ar/Ar method at 105 Ma; after Asti et al.,  
2646  
2647 1556 2019). (b): thin section of typical ultramylonite from the lenses of Paleozoic material welded  
2648  
2649 1557 on the exhumed mantle rocks of the Sarailé lherzolite (Asti et al., 2019). (c): phacoidal fabric  
2650  
2651 1558 defined by anastomosing shear zones in the mantle body of Bestiac. This fabric is typical of  
2652  
2653 1559 the lenticular layer as defined by Lagabrielle et al. (2019a, 2019b). (d): phacoidal fabric in the  
2654  
2655 1560 lenticular layer of the lherzolite body of Moncaup. (e): phacoidal fabric in the lenticular layer  
2656  
2657 1561 of the lherzolite body of Sarailé (Lagabrielle et al., 2019b). (f): curved shear zones and  
2658  
2659 1562 elongated tectonic lenses in serpentinized lherzolites of the lenticular layer in the Moncaut  
2660  
2661 1563 peridotite body. (g and h): phacoidal fabric in the lenticular layer of the lherzolite body of  
2662  
2663 1564 Urdach: h shows pervasive carbonation (Lagabrielle et al., 2019a). (i and j): thin section and  
2664  
2665 1565 outcrop of anastomosing serpentinized shear bands in the lherzolites of Etang de Lers  
2666  
2667 1566 (Lherz). (k): anastomosing serpentinized shear bands in the lherzolites of Avezac.

2668  
2669 1567  
2670  
2671 1568 **Figure 5. The geological record of the Cretaceous extension in the pre-rift cover of the**  
2672  
2673 1569 **metamorphic North Pyrenean Zone (NPZ). Some field view of outcrops showing the layer**  
2674  
2675 1570 **perpendicular flattening and the S0/S1 syn-metamorphic foliation.**

2676  
2677 1571 (a): layer-parallel boudinage in the Calce quarry (Jurassic dolostones of the Agly massif  
2678  
2679 1572 cover, Eastern NPZ). (b): layer-parallel ductile stretching of the meta-laterite and carbonate  
2680  
2681 1573 breccia in the Benou quarry near Turon de la Tecouère lherzolite body (Chainons Béarnais,  
2682  
2683 1574 Western NPZ). (c): flattened fossils in the Jurassic meta-dolostones of the Saleix valley (Aulus  
2684  
2685 1575 basin, Central NPZ). (d): extreme stretching of a rudist-rich Urgonian marbles at Sarrance  
2686  
2687 1576 (Chainons Béarnais, Western NPZ) (see also fig. 6c). (e): tight normal faults affecting the  
2688  
2689 1577 early S0/S1 syn-metamorphic foliation in the pre-rift cover marbles of the Agly massif. These  
2690  
2691 1578 features characterize the ductile-brittle transition that occurred at the end of the rifting  
2692  
2693 1579 history. (f): same features as (e) but in the marbles of the detached Lherz body cover  
2694  
2695 1580 (southern side). (g): recumbent folds associated with the early ductile foliation in marbles  
2696  
2697 1581 from the detached cover of the Pays de Sault Paleozoic basement (Eastern NPZ). (h): tectonic  
2698  
2699 1582 brecciation with calcite veining marking the ductile-brittle transition in the marbles of the  
2700  
2701 1583 Lherz body cover (western side).

2702  
2703 1584  
2704  
2705 1585 **Figure 6 . A theoretical log of the lithological succession in the internal domain of the**

2701  
2702  
2703 **1586 Cretaceous NPZ rift basins.**  
2704

2705 1587 The photographs illustrate the various rock-types forming the basin basement (crust and  
2706 1588 mantle) and the pre-rift and syn-rift series. (a): Chaînons Béarnais (Saraillé massif, western  
2707 1589 NPZ). (b): Boucheville basin (eastern NPZ). (c): Urgonian at Sarrance (western NPZ) (see also  
2710 1590 fig. 5d). (d): Jurassic dolomites at Calce (eastern NPZ). (e): base of pre-rift series (Bestiac,  
2711 1591 eastern NPZ). (f): base of pre-rift series (Moncaup, central NPZ). (g): crustal lenses of Saraillé  
2713 1592 massif (western NPZ). (h): lenticular layer (Urdach mantle body, western NPZ).  
2714

2715 1593

2716  
2717 **1594 Figure 7. Interpreted and reconstructed profiles of peri-Pyrenean Cretaceous basins**  
2718 **1595 architecture.**

2719  
2720 1596 (a): Parentis basin. (b): Columbrets basin. (c and d): Cameros basin. See location of basins in  
2721 1597 fig. 1.  
2722

2723 1598

2724  
2725 **1599 Figure 8. A compilation of model results and conceptual representations of extended to**  
2726 **1600 hyper-extended continental crust.**

2727  
2728 1601 This compilation aims enhancing the main mechanical concepts involved in the processes of  
2729 1602 crustal extension and how they apply or not apply to the genesis and evolution of the  
2730 1603 smooth-slopes basins defined in this article (see text for discussion).  
2731  
2732

2733 1604

2734  
2735 **1605 Figure 9. A compilation of reconstructed architecture of Pyrenean Cretaceous basins and a**  
2736 **1606 Basque-Parentis transect.**

2737  
2738 1607 All represented sections are based on the activation of a restricted number of detachment  
2739 1608 faults. As discussed in text, such representations do not match the newly defined smooth-  
2740 1609 slopes architecture that characterize the Pyrenean and peri-Pyrenean Cretaceous basins.  
2741  
2742

2743 1610

2744  
2745 **1611 Figure 10. Deformation regimes of the various units composing a typical smooth-slopes**  
2746 **1612 basin.**

2747  
2748 1613 (a): distribution of pure shear and simple shear regimes in a simplified smooth-slopes basin  
2749 1614 system. (b): Detail of the very distal part of the hyper-extended crust (area shown in a). (b1):  
2750 1615 simplified log showing the association of metric to hectometric crustal lenses separated  
2751 1616 from the mantle rocks by the crust-mantle detachment and from the detached pre-rift cover  
2752 1617 by the cover décollement (see definition in Lagabrielle et al., 2019a, 2019b). (b2): field view  
2753  
2754  
2755  
2756  
2757  
2758  
2759  
2760



2761  
2762  
2763 1618 of crustal sheets from the base of the Saraillé massif (western NPZ). (b3): field view of  
2764  
2765 1619 anastomosing shear zones cutting through the serpentinitized peridotite of the Saraillé body  
2766  
2767 1620 and forming the lenticular layer of the crust-mantle detachment (see also fig. 4c to k).

2768  
2769 1621

2770 1622 **Figure 11. A compilation of schematic architecture of selected Atlantic and Mediterranean**  
2771  
2772 1623 **passive margins.**

2773 1624 These margin profiles are selected because they offer architectures which do not fit with  
2774  
2775 1625 the Iberia-Newfoundland-type margin (see fig. 2). In particular, they show large scale crustal  
2776  
2777 1626 boudinage and lenticulation that are consistent with a ductile regime of extensional  
2778  
2779 1627 deformation. Sheets of hyper thinned crustal material is indicated by the orange arrow (see  
2780  
2781 1628 comments in text). Note that scale is similar in all profiles.

2782  
2783 1629

2784 1630 **Figure 12. Three numerical models of rift development compared to the Angola-Brazil and**  
2785  
2786 1631 **Iberia transects.**

2787 1632 All models highlight a mode of deformation that leads to the development of very thin and  
2788  
2789 1633 long sheets of crustal material also observed in the Angola-Campos transect but not in the  
2790  
2791 1634 Iberia transect. Such deformation necessarily imply a ductile behaviour of the crust  
2792  
2793 1635 consistent with processes acting in the central part of the smooth-slopes basins studied in  
2794  
2795 1636 this paper (see text for further comments).

2796  
2797 1637

2798 1638 **Figure 13. Paleogeography of Triassic deposits and Cretaceous rifting around the Iberia**  
2799  
2800 1639 **plate.**

2801 1640 (a): paleogeographic maps for the Triassic period (modified from Orti et al., 2017) and  
2802  
2803 1641 location of some further Cretaceous rifted regions. Note that by contrast to the area where  
2804  
2805 1642 Cretaceous smooth-slopes basins will open, the area corresponding to the future Iberia-  
2806  
2807 1643 Newfoundland conjugate margins are devoid of thick evaporitic series. (b): paleogeographic  
2808  
2809 1644 maps for the Ladinian and Carnian (Middle-early Late Triassic times, 242-227 Ma) modified  
2810  
2811 1645 after Scotese and Schettino (2017). (c): paleogeography of Upper Triassic deposits prepared  
2812  
2813 1646 after a compilation of unpublished data by D. Frizon de Lamotte (pers. com.) superimposed  
2814  
2815 1647 on a plate reconstruction by Olivet (1996).

2816  
2817 1648

2821  
2822  
2823 **1649 Figure 14. Correlation between the paleogeography of Triassic deposits and the mode of**  
2824  
2825 **1650 rifting around the Iberia plate.**

2826  
2827 1651 (a): cartoons (a1 and a2) illustrating the contrasted rifting modes between the Iberia-  
2828  
2829 1652 Newfoundland-type and the Parentis-type margins (modified from Clerc and Lagabrielle,  
2830  
2831 1653 2014). (b): paleogeography of Triassic (Late Norian) deposits according to Marcoux et al. in  
2832  
2833 1654 the Dercourt et al. (1993) map atlas. As paleogeographic maps in fig. 13, this reconstruction  
2834  
2835 1655 points to the lack of thick evaporites deposits in the future Iberia-Newfoundland rifting  
2836  
2837 1656 domain (see text for discussion).

2838  
2839  
2840  
2841  
2842  
2843  
2844  
2845  
2846  
2847  
2848  
2849  
2850  
2851  
2852  
2853  
2854  
2855  
2856  
2857  
2858  
2859  
2860  
2861  
2862  
2863  
2864  
2865  
2866  
2867  
2868  
2869  
2870  
2871  
2872  
2873  
2874  
2875  
2876  
2877  
2878  
2879  
2880

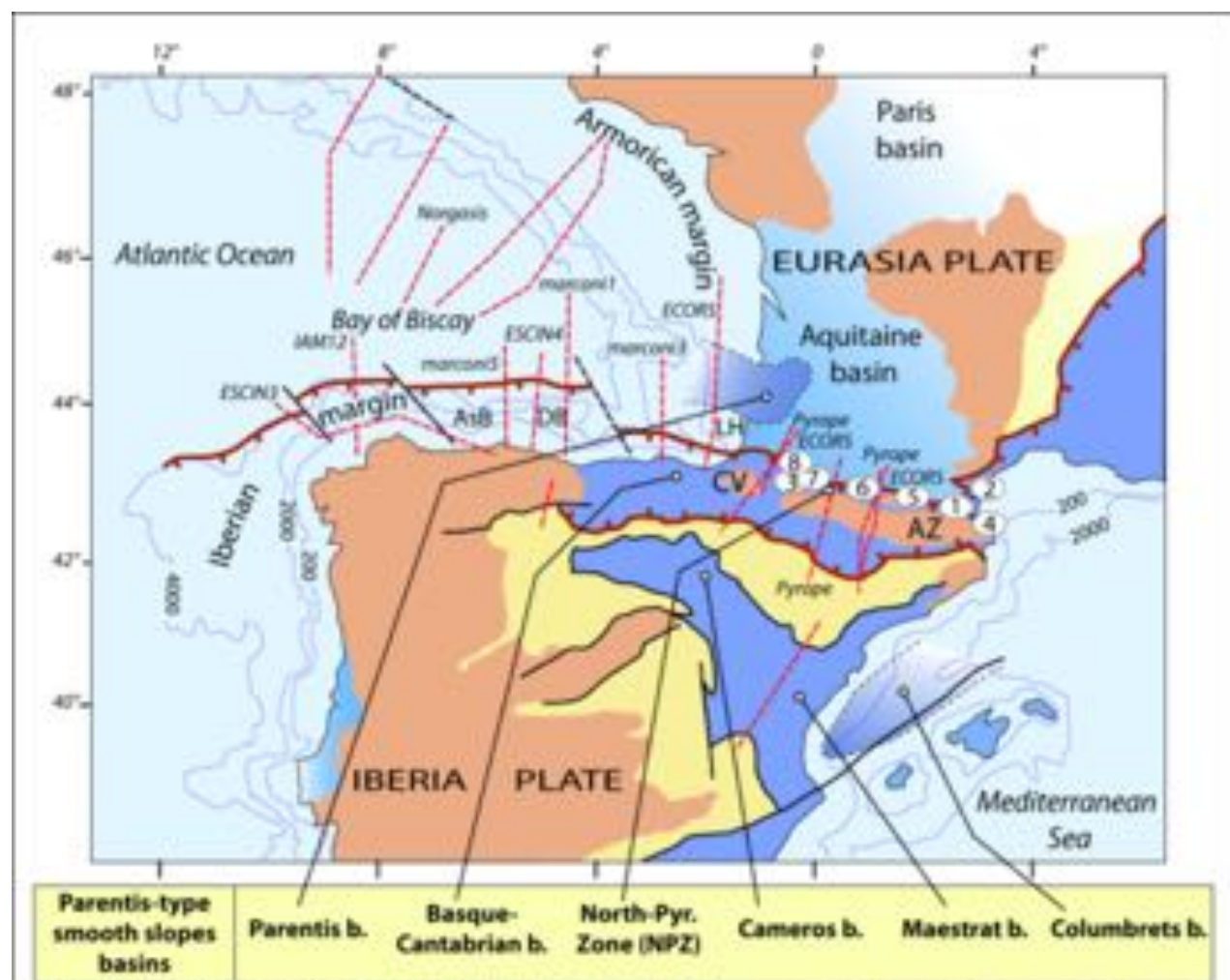
2838  
2839 **1658 Figure 15. Time-dependent rheological evolution of the Pyrenean rifting based on**  
2840  
2841 **1659 geological constraints from the North Pyrenean Zone and numerical results from a thermo-**  
2842  
2843 **1660 mechanical numerical modeling.**

2844 1661 Sketches depicting the geological evolution are extracted from the Clerc et al. (2016) model.  
2845  
2846 1662 Rheological profiles derive from the Duretz et al., (2019) model. They are placed at critical  
2847  
2848 1663 locations (1, 2 and 3) of the rift in order to emphasize the drastic changes in the mechanical  
2849  
2850 1664 behaviour during its evolution from limited crustal extension to local mantle exhumation  
2851  
2852 1665 (see detailed description in text).

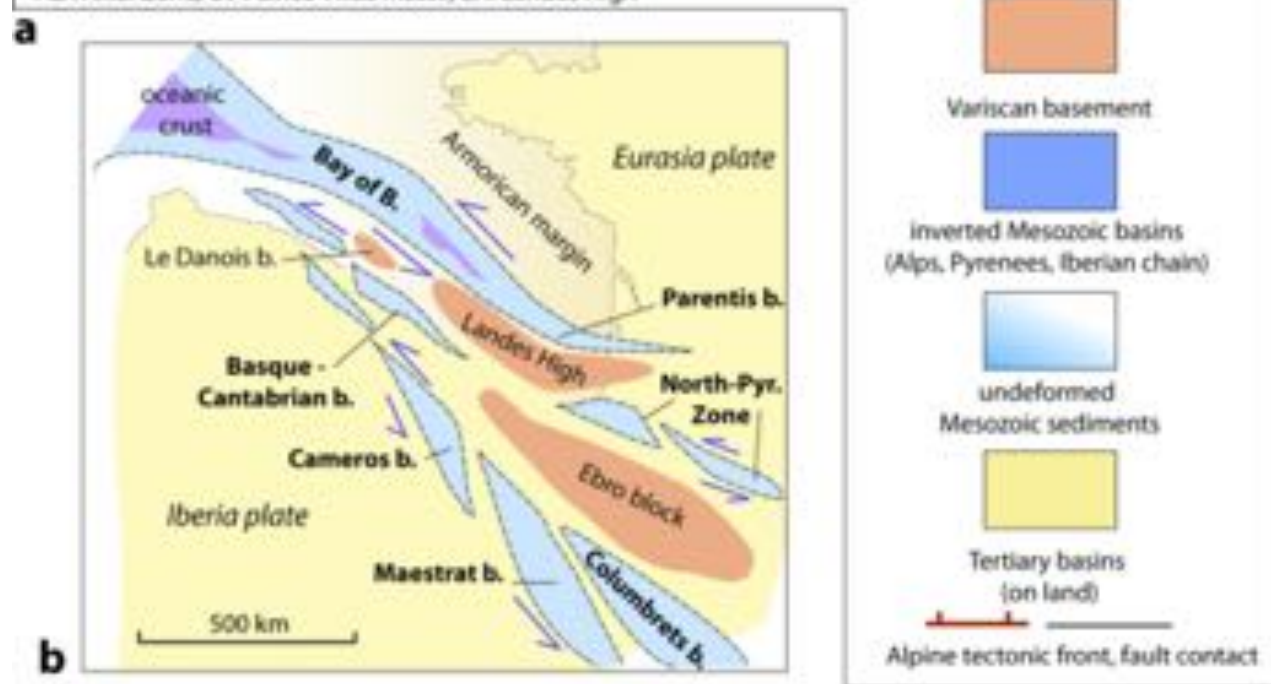
2853  
2854  
2855  
2856  
2857  
2858  
2859  
2860  
2861  
2862  
2863  
2864  
2865  
2866  
2867  
2868  
2869  
2870  
2871  
2872  
2873  
2874  
2875  
2876  
2877  
2878  
2879  
2880

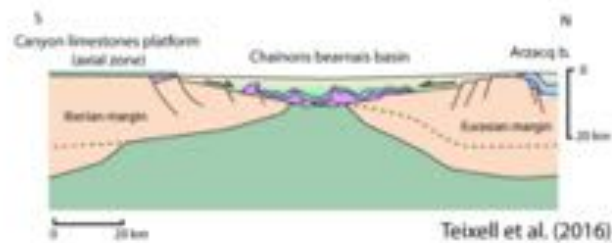
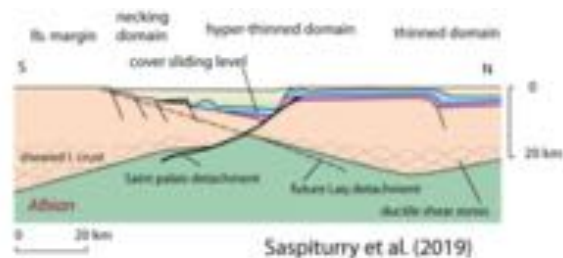
2854 **1667 Figure 16. A theoretical structural model for the Cantabrian, Pyrenean and Iberian**  
2855  
2856 **1668 symmetrical smooth-slopes basins based on the features and concepts discussed in this**  
2857  
2858 **1669 article.**

2859  
2860  
2861  
2862  
2863  
2864  
2865  
2866  
2867  
2868  
2869  
2870  
2871  
2872  
2873  
2874  
2875  
2876  
2877  
2878  
2879  
2880



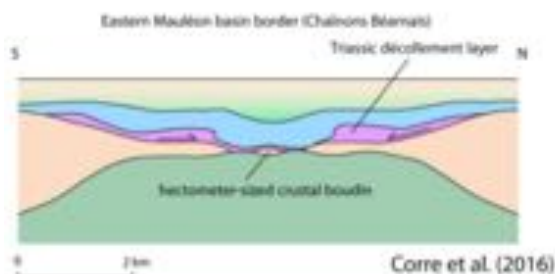
① location of photographs in figure 6



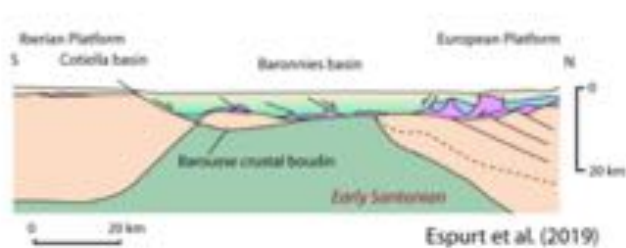


**a. Western North Pyrenean Zone (1)**

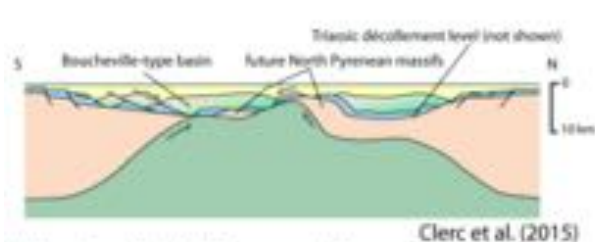
**b. Western North Pyrenean Zone (2)**



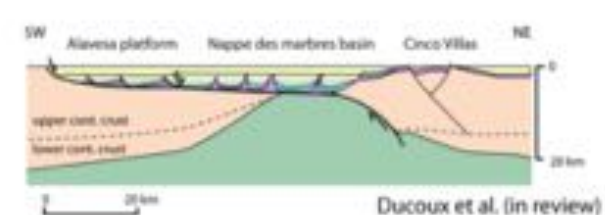
**c. Western North Pyrenean Zone (3)**



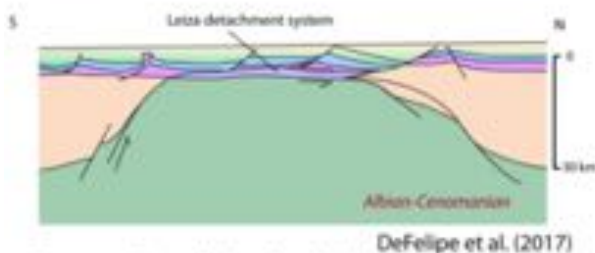
**e. Central North Pyrenean Zone**



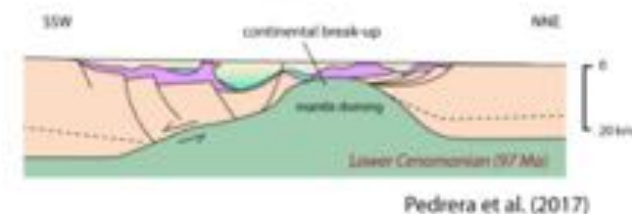
**h. Eastern North Pyrenean Zone**



**f. Basque-Cantabrian basin (1)**



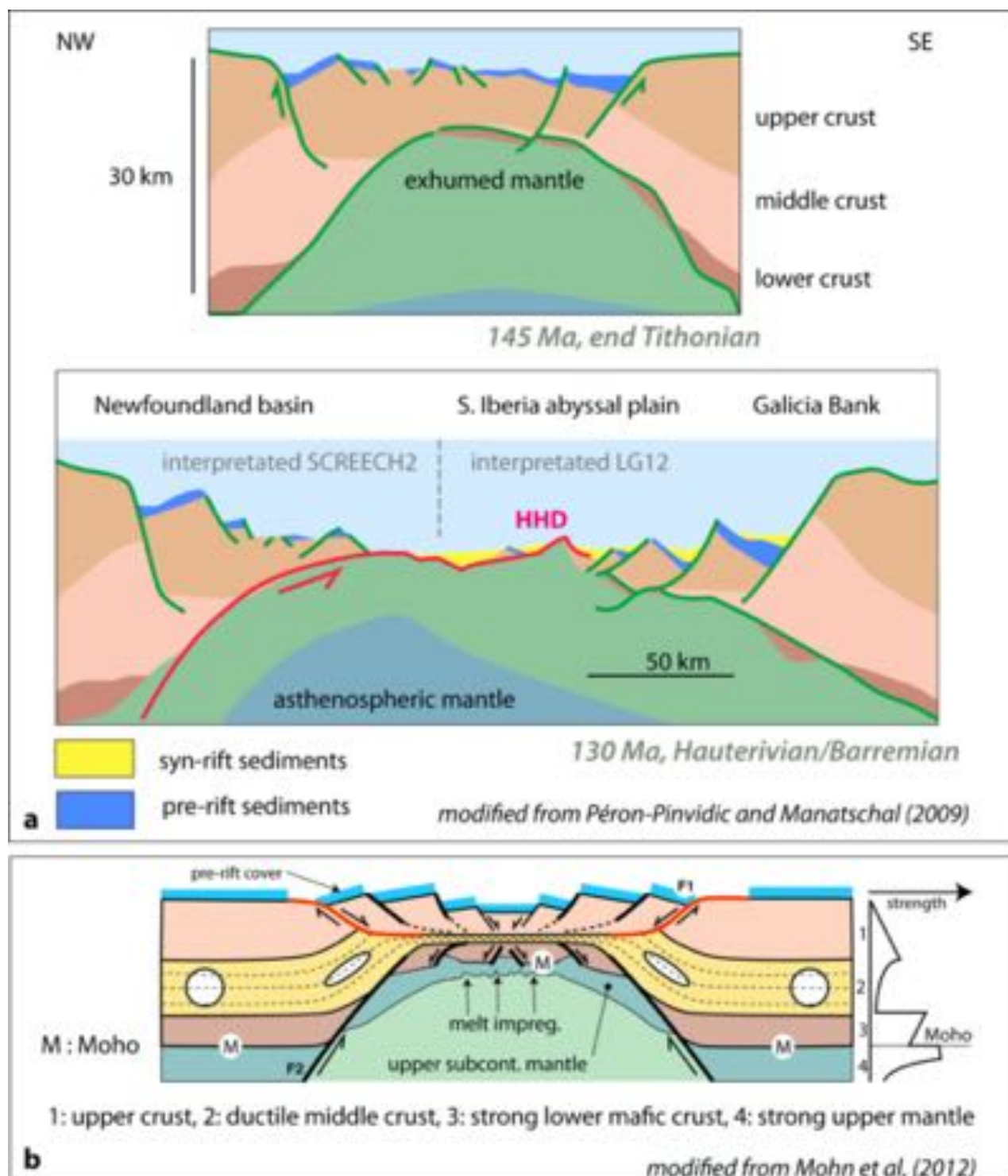
**g. Basque-Cantabrian basin (2)**



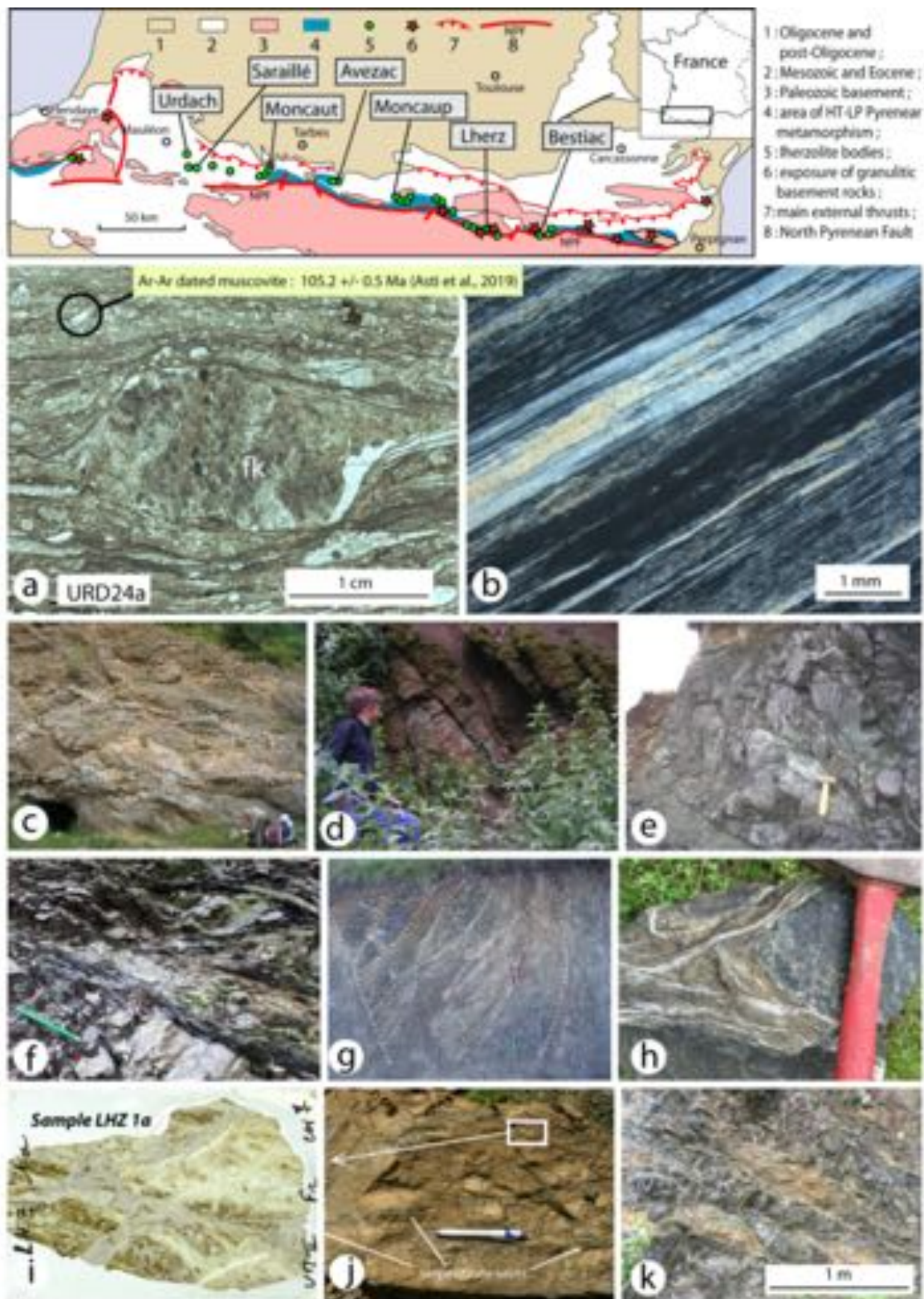
**h. Basque-Cantabrian basin (3)**



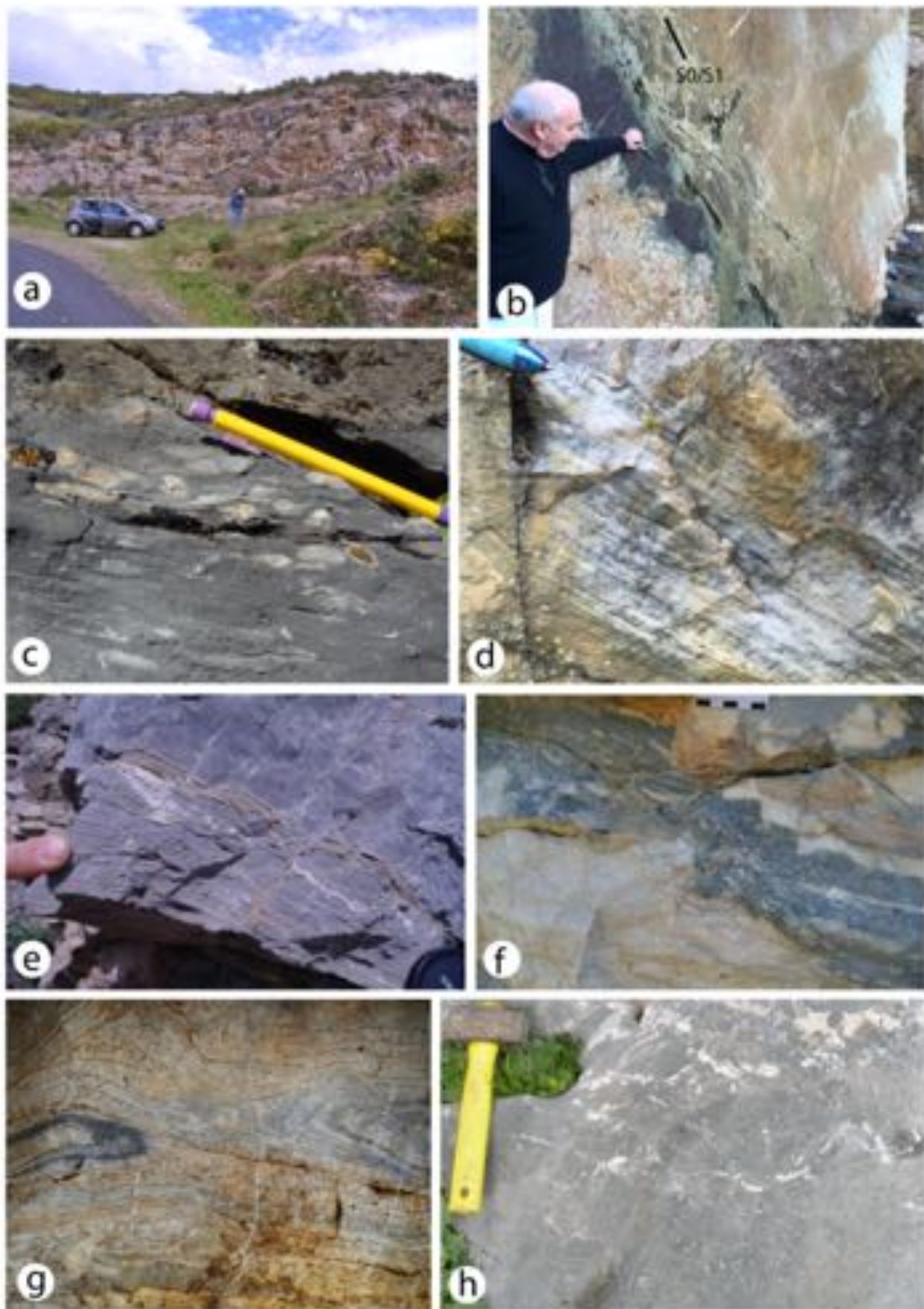
Lagabrielle et al., fig. 2, ESR, submitted



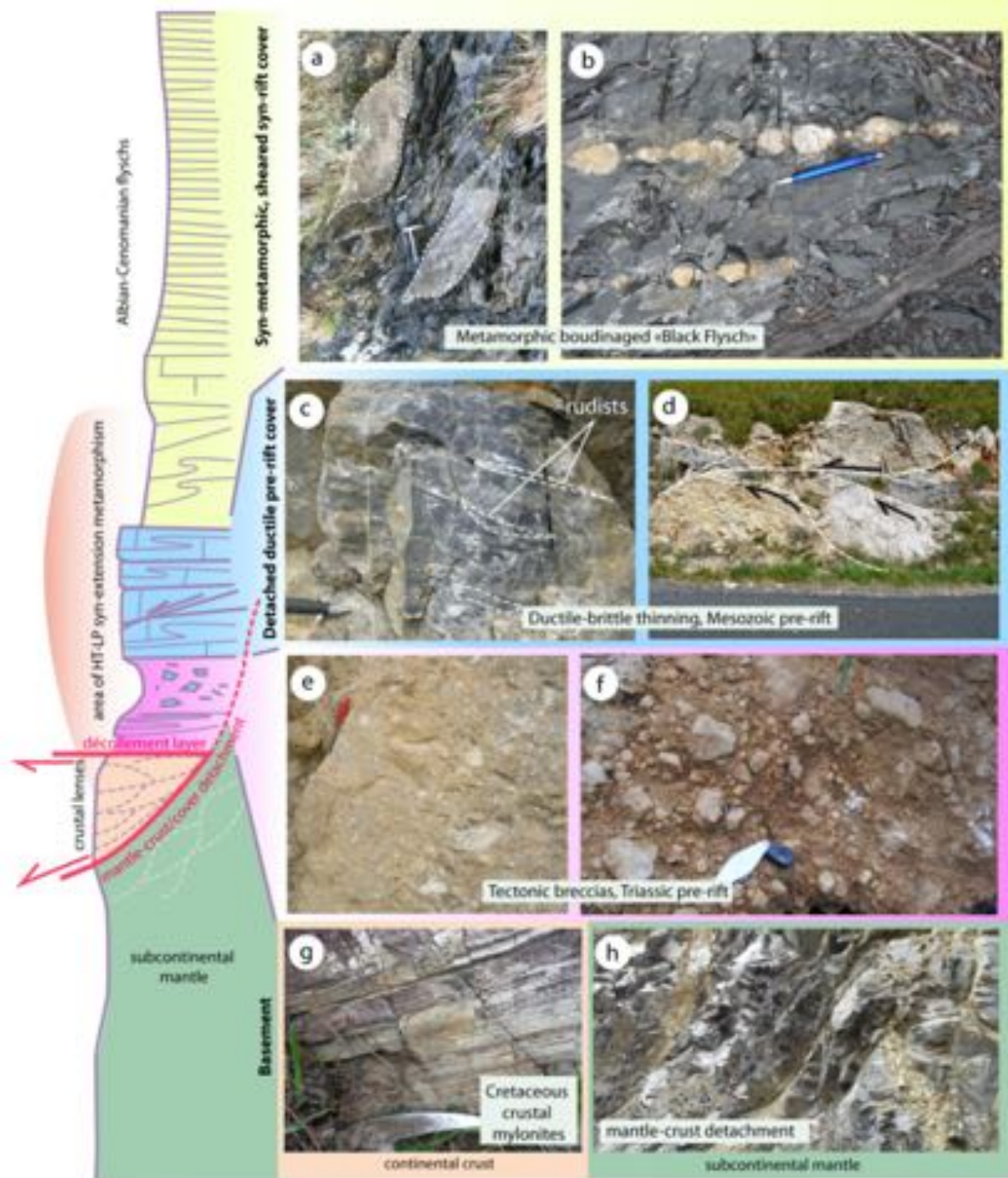
Lagabrielle et al., fig. 3, ESR, submitted



Lagabrielle et al., fig. 4, ESR, submitted

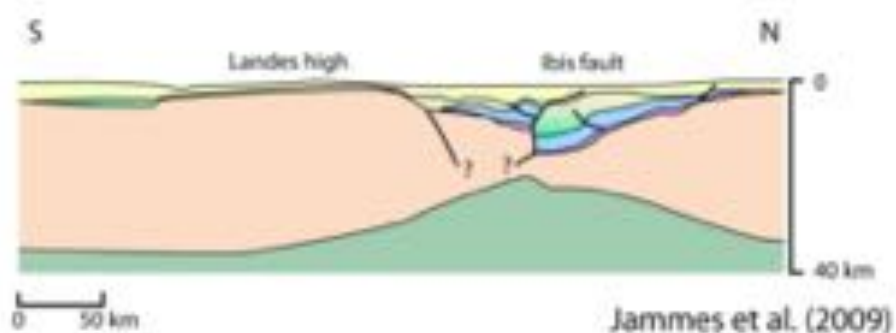


Lagabrielle et al., fig. 5, ESR, submitted

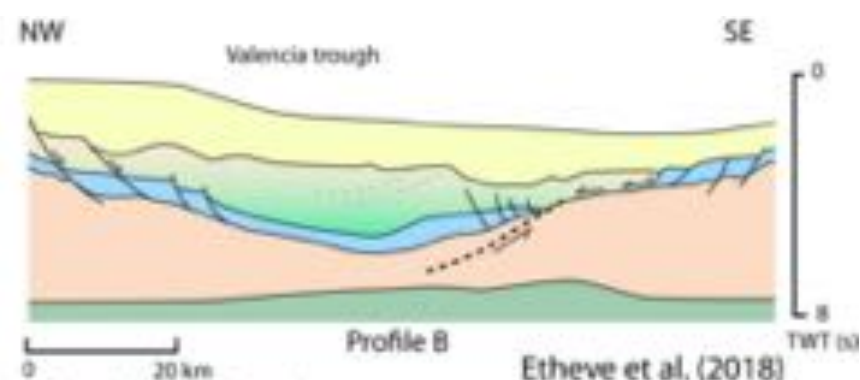


Lagabrielle et al., fig. 6, ESR, submitted

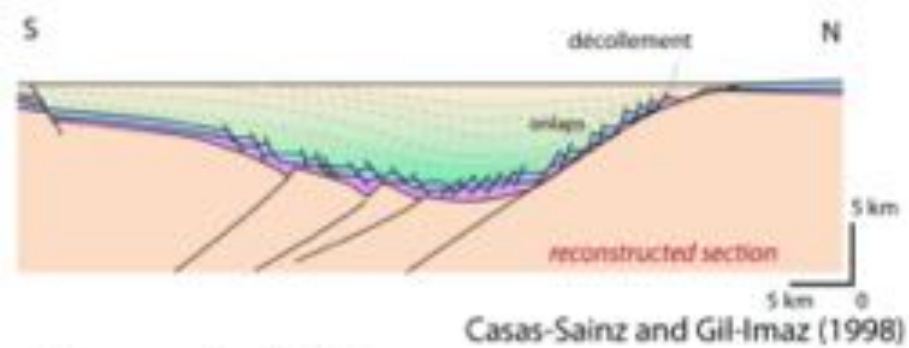




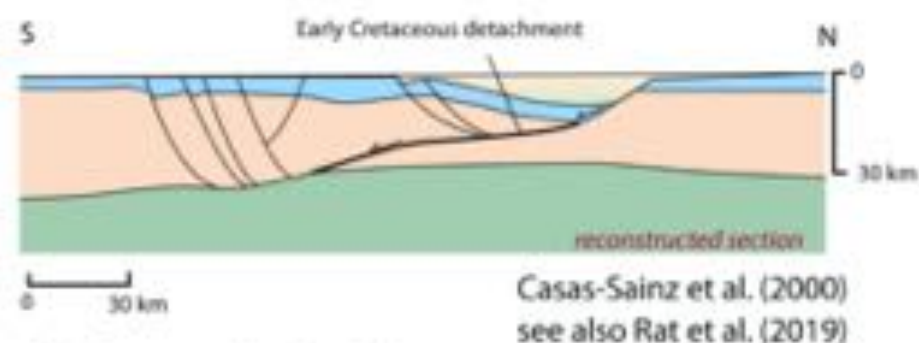
**a. Parentis basin**



**b. Columbrets basin**

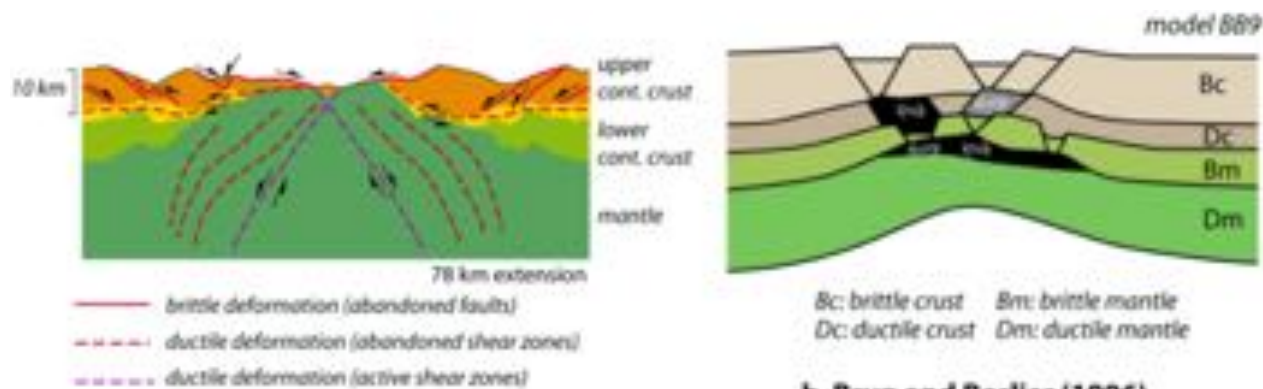


**c. Cameros basin (1)**



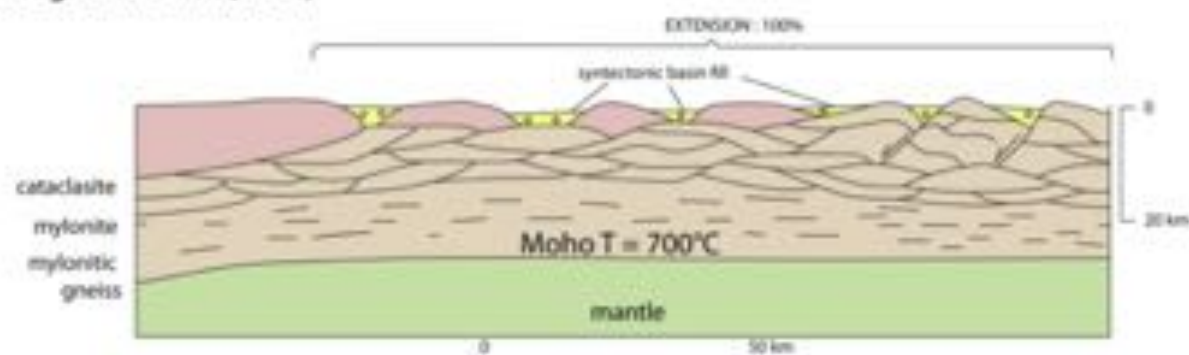
**d. Cameros basin (2)**



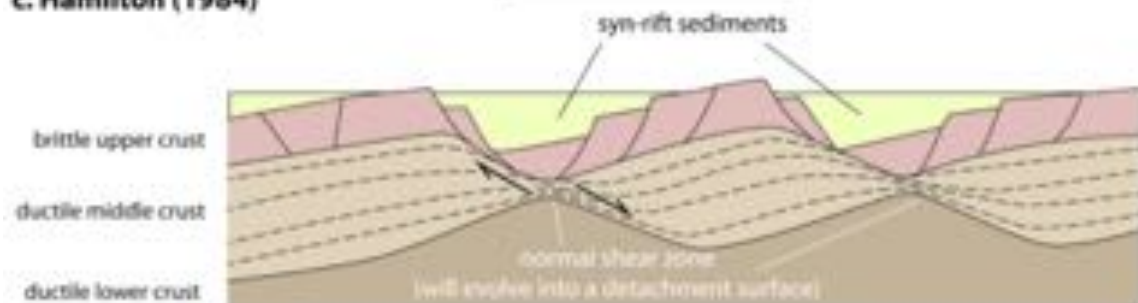


**a. Nagel and Buck (2004)**

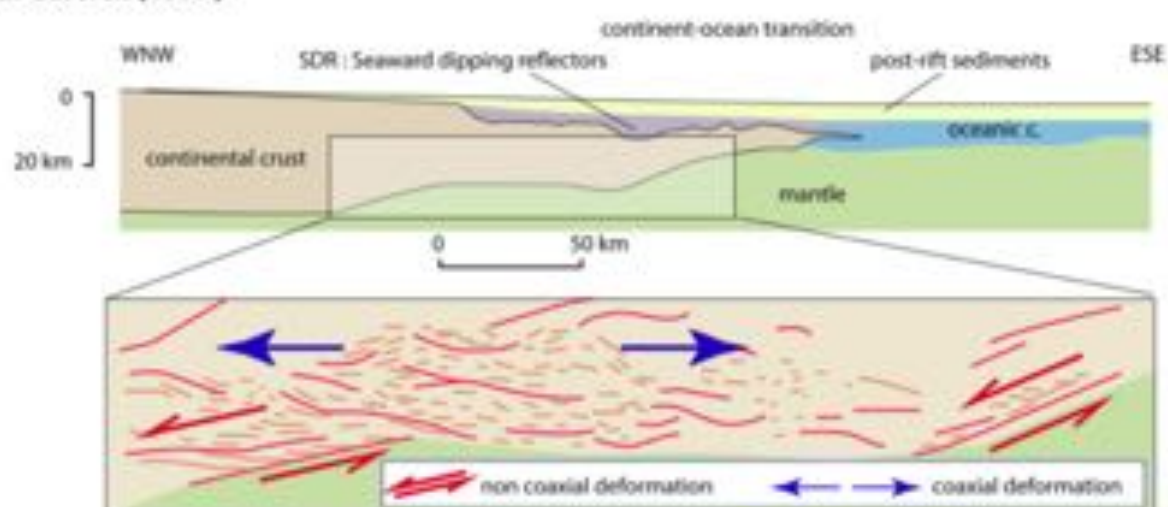
**b. Brun and Beslier (1996)**



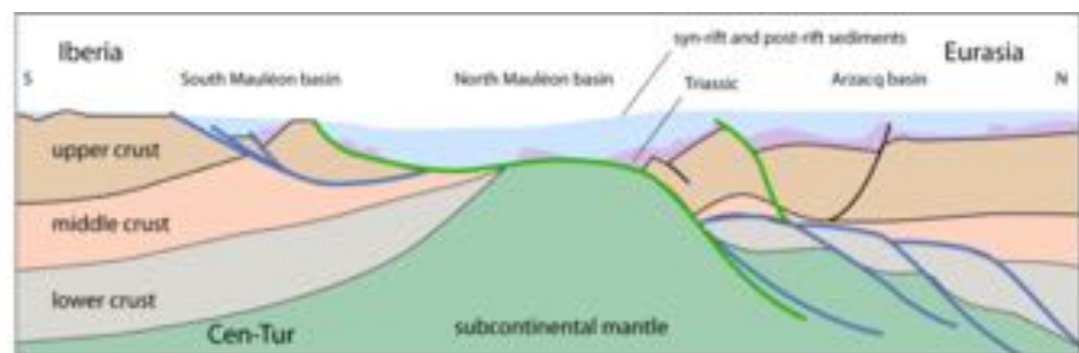
**c. Hamilton (1984)**



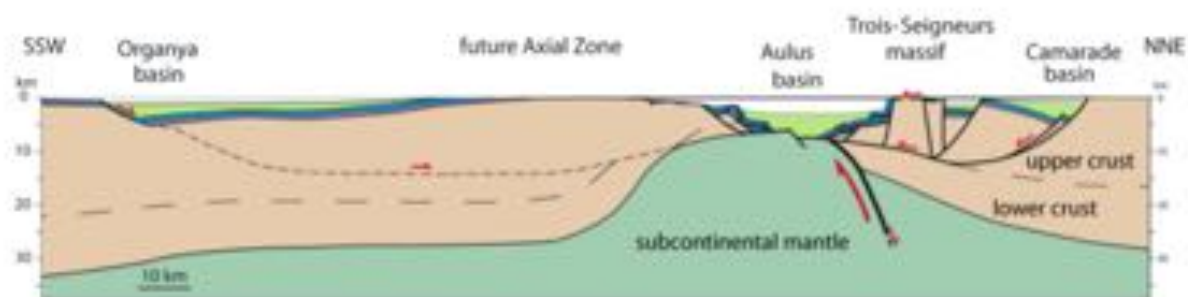
**d. Gartrell (1997)**



**e. Clerc et al. (2018)**



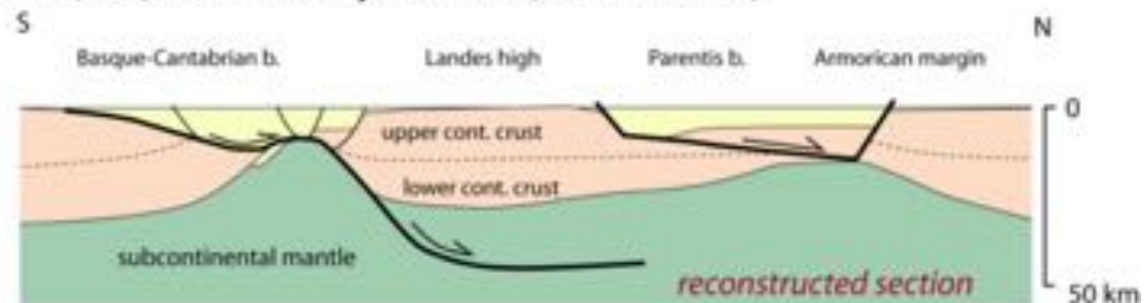
a. Masini et al. (2014): Mauléon basin



b. Lagabrielle et al. (2010): Central North Pyrenean Zone (Aulus basin, Etang de Lers)



c. Vauchez et al. (2013): Eastern North Pyrenean Zone (Boucheville basin)



d. Roca et al. (2011) : Basque-Parentis transect

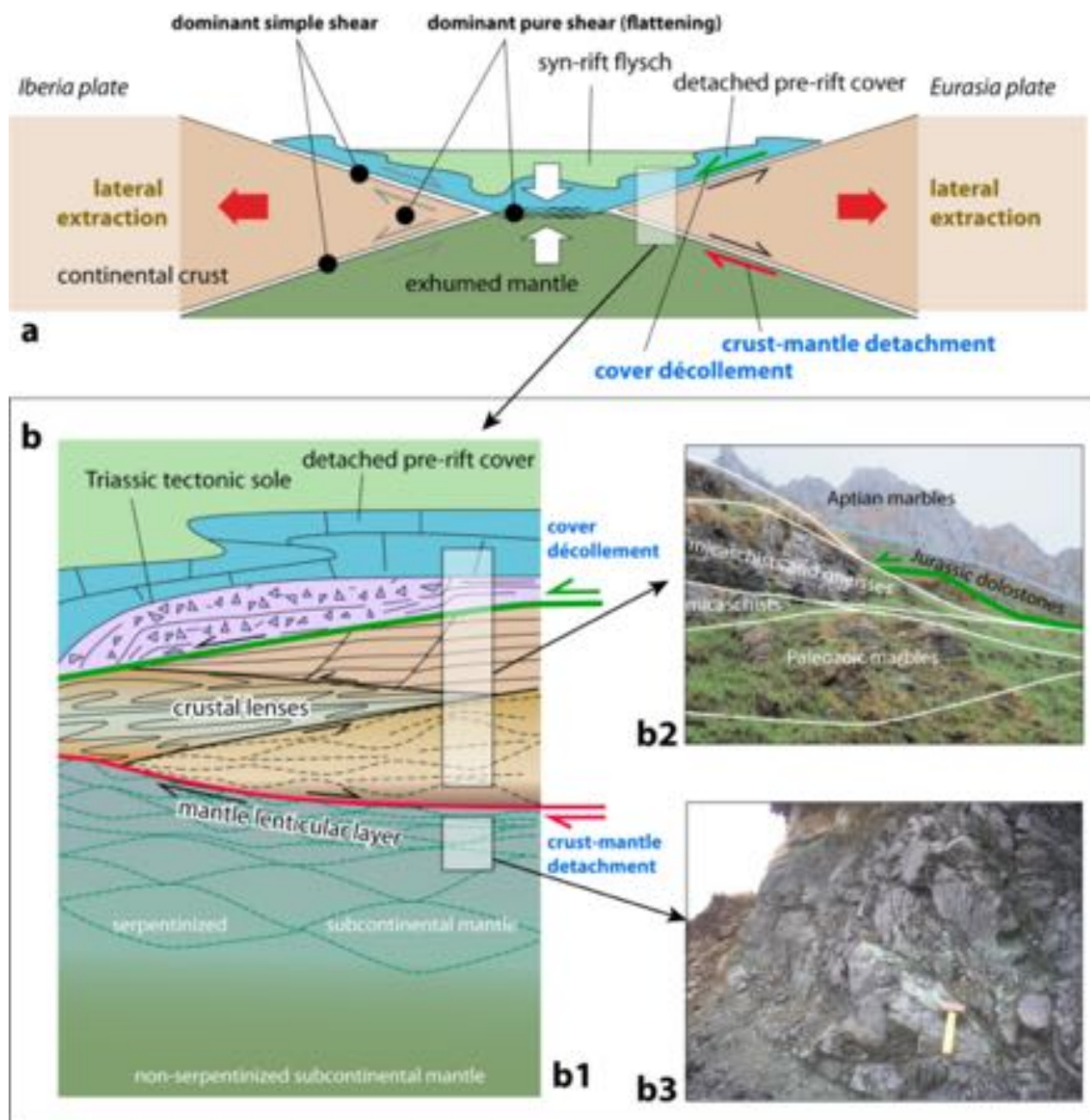
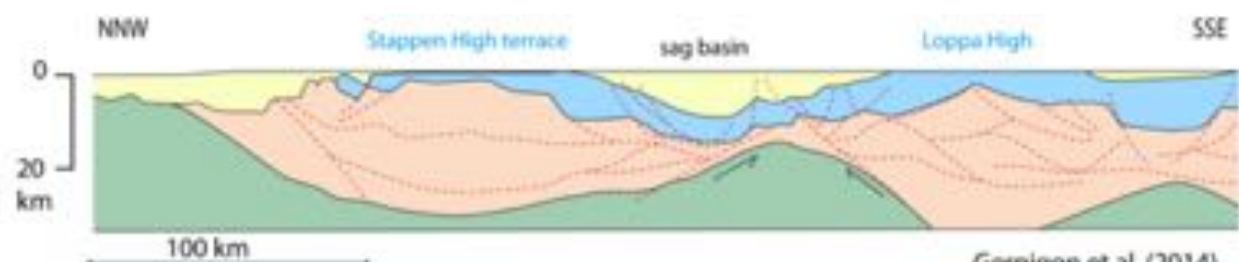
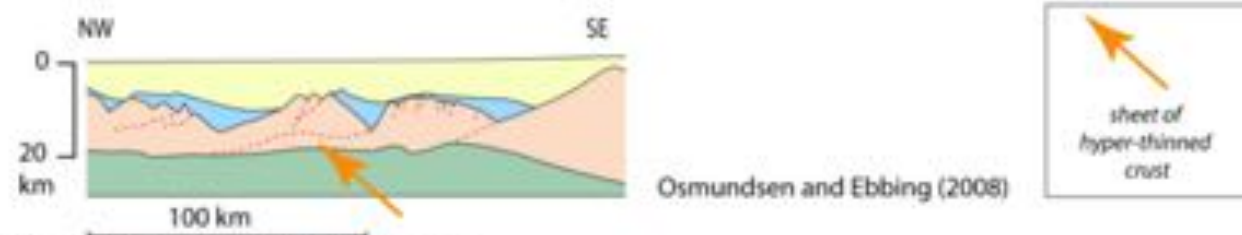


fig. 10

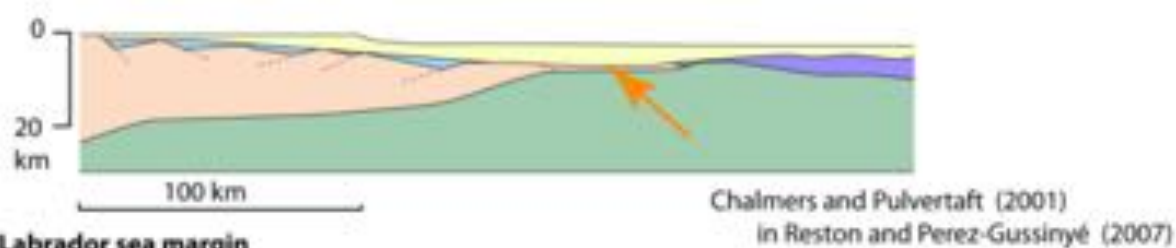
Lagabrielle et al., smooth slopes basins, submitted



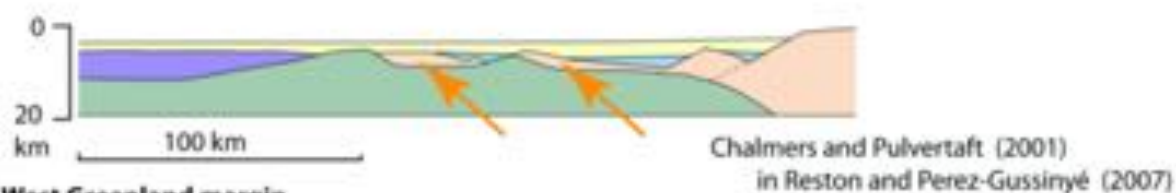
**a. Barents margin**



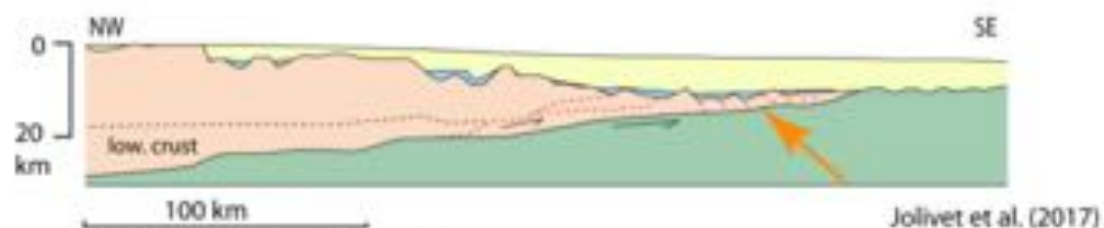
**b. Northern More basin, Norway margin**



**c. Labrador sea margin**

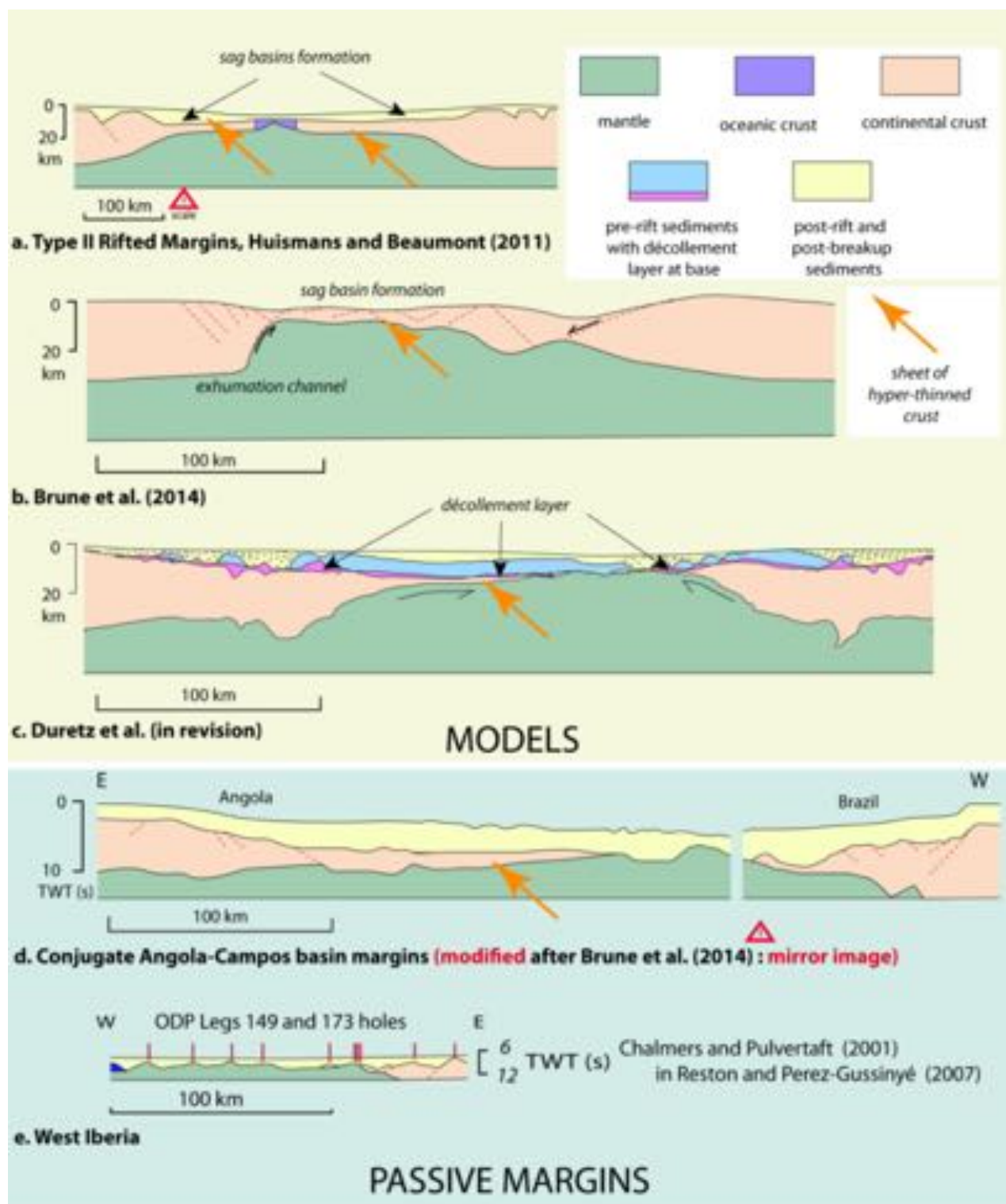


**d. West Greenland margin**

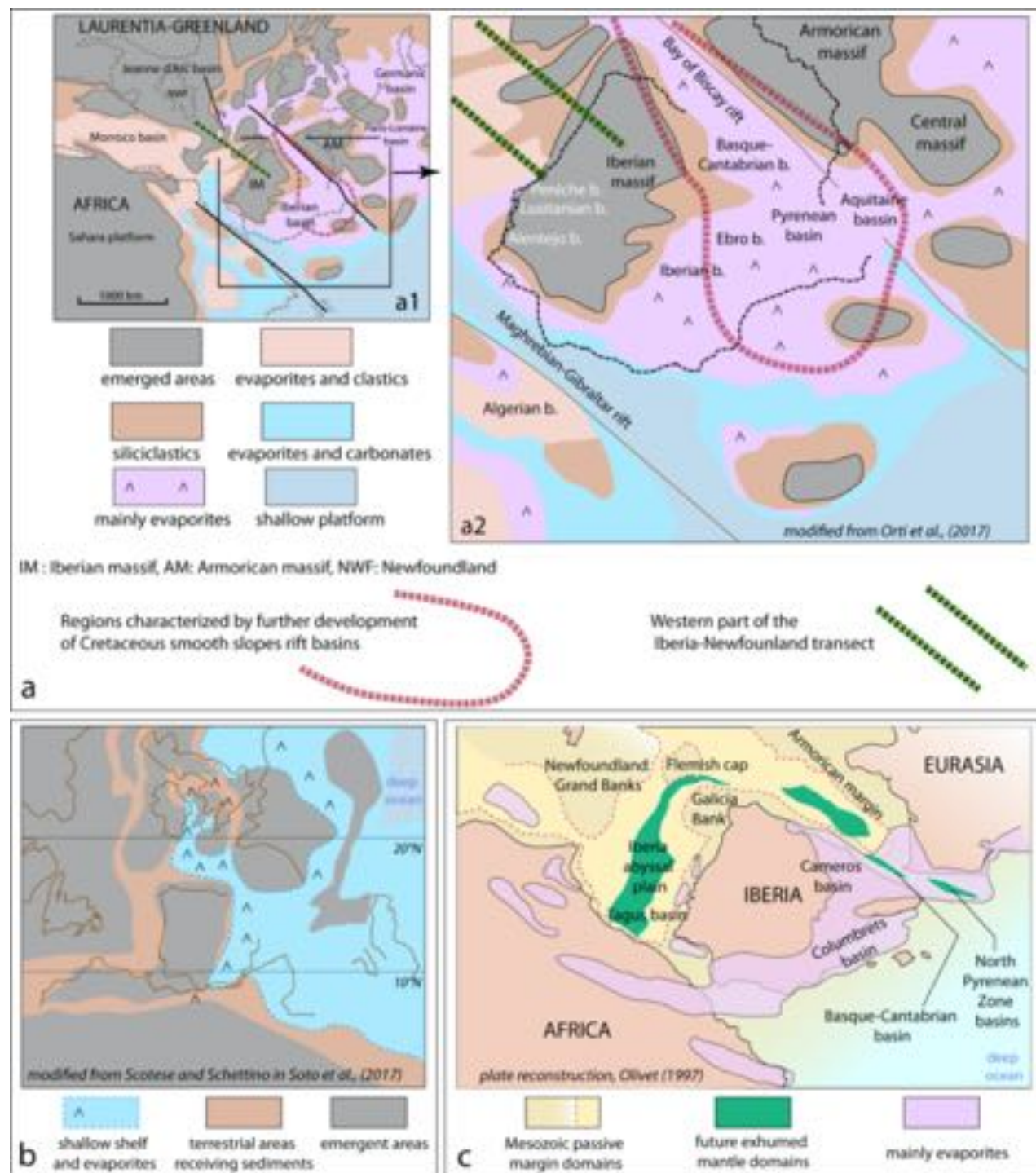


**e. Western Mediterranean, Gulf of Lion**

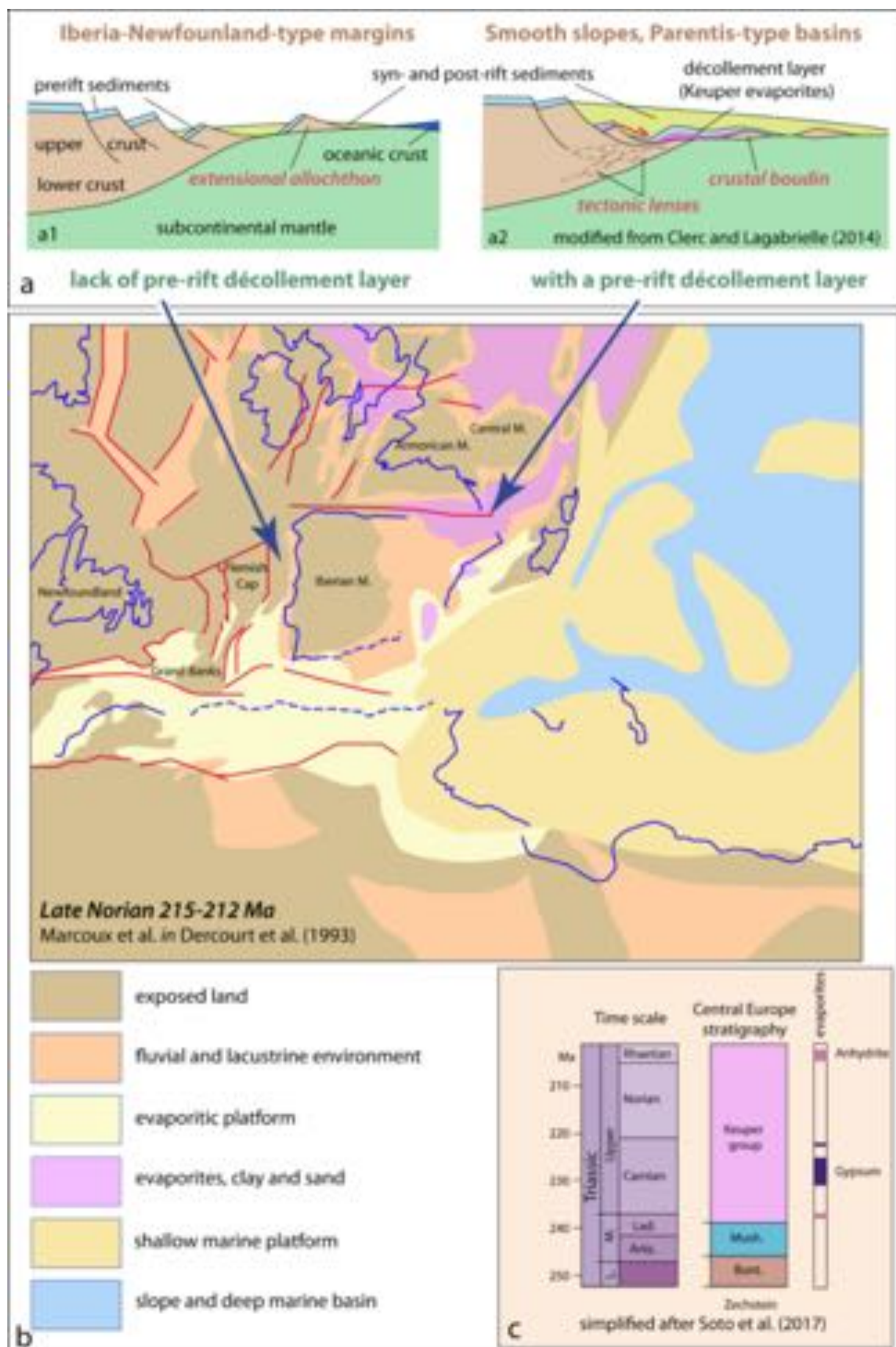




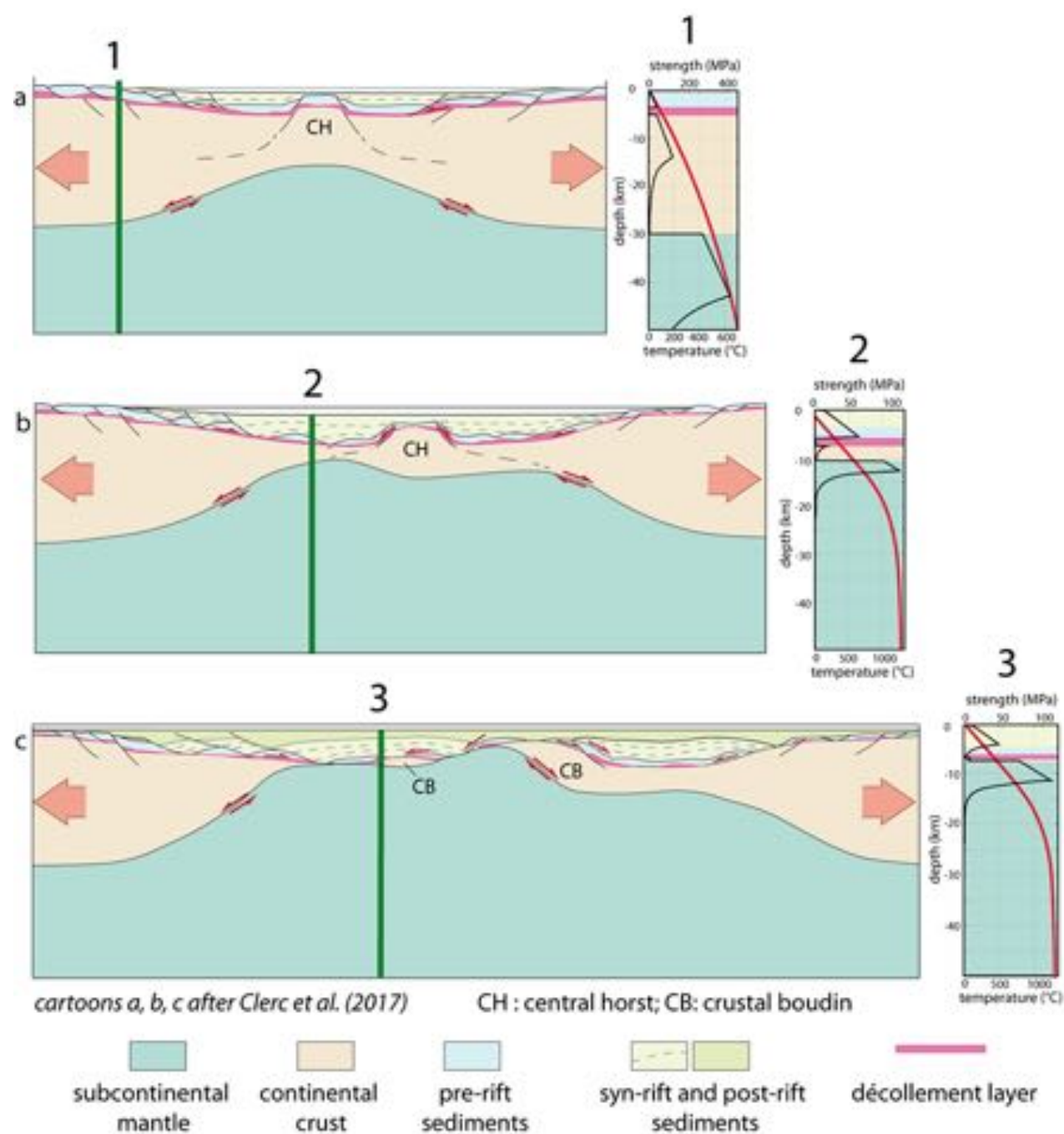
Lagabrielle et al., fig. 12, ESR, submitted



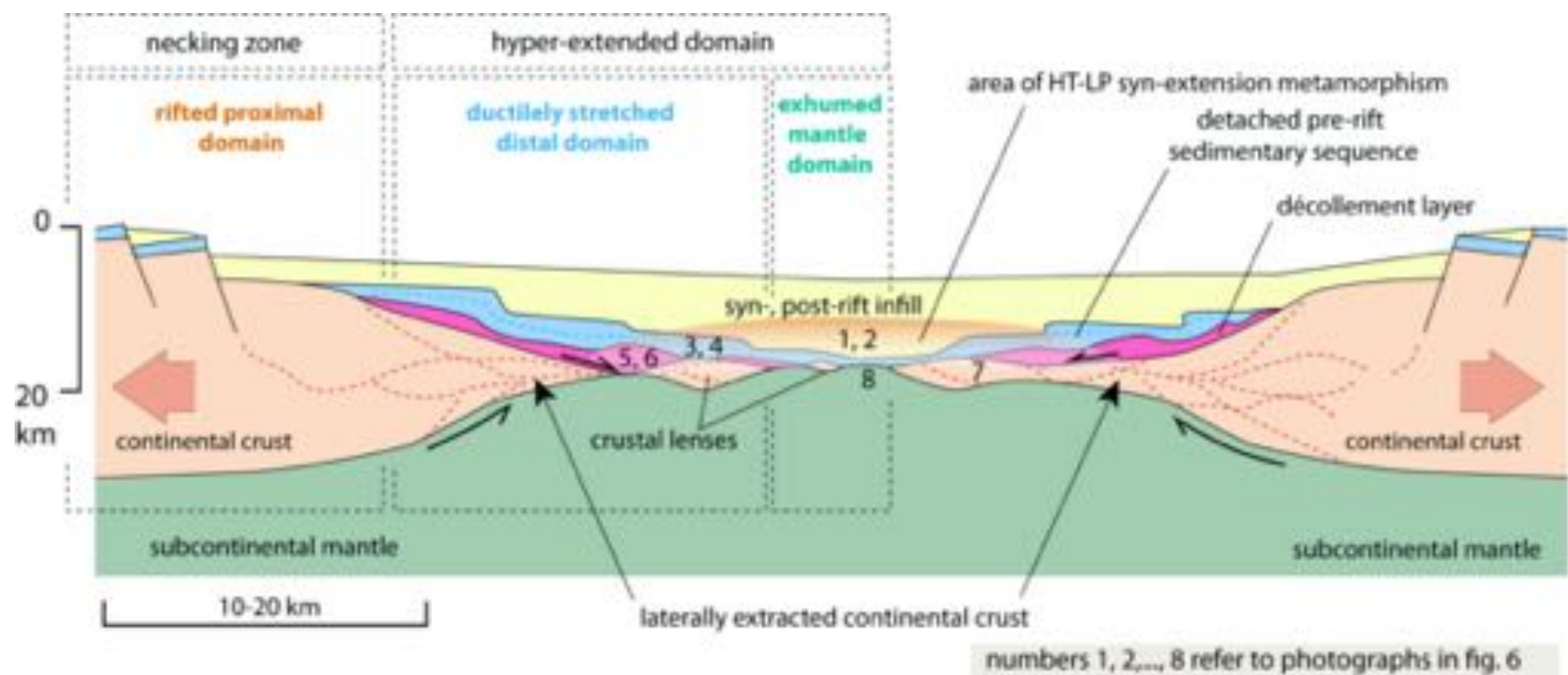
Lagabrielle et al., fig. 13, ESR, submitted







Lagabrielle et al., fig. 15, ESR, submitted



Lagabrielle et al., fig. 16, ESR, submitted